Spatiotemporal analysis of cell wall synthesis related enzymes and the influence of cell wall stress factors

Dissertation

zur Erlangung des Grades eines

Doktor der Naturwissenschaften

(Dr. rer.nat.)

des Fachbereichs Chemie der Philipps-Universität Marburg

Vorgelegt von

Lisa Stuckenschneider

aus Hamburg

Marburg, September 2021

Die vorliegende Dissertation wurde von 04/2017 bis 09/2021 am Fachbereich Chemie und Zentrum für synthetische Mikrobiologie, SYNMIKRO der Philipps-Universität Marburg unter Leitung von Prof. Dr. Peter Ludwig Graumann angefertigt.

Vom Fachbereich Chemie der Philipps-Universität Marburg (Hochschulkennziffer 1180) als Dissertation angenommen am ___08.11.2021_____

Erstgutachter: Prof. Dr. Peter Ludwig Graumann

Fachbereich Chemie, Philipps-Universität Marburg

Zweitgutachter: Prof. Dr. Lars-Oliver Essen

Fachbereich Chemie, Philipps-Universität Marburg

Tag der Disputation: ___09.11.2021_____

Eidesstaatliche Erklärung

Ich erkläre, dass eine Promotion noch an keiner anderen Hochschule als der Philipps-Universität Marburg, Fachbereich Chemie, versucht wurde.

Hiermit versichere ich, dass ich die vorliegende Dissertation

"**Spatiotemporal analysis of cell wall synthesis related enzymes and the influence of cell wall stress factors**"

selbstständig, ohne unerlaubte Hilfe Dritter angefertigt und andere als die in der Dissertation angegebenen Hilfsmittel nicht benutzt habe. Alle Stellen, die wörtlich oder sinngemäß aus veröffentlichten oder unveröffentlichten Schriften entnommen sind, habe ich als solche kenntlich gemacht. Dritte waren an der inhaltlich-materiellen Erstellung der Dissertation nicht beteiligt; insbesondere habe ich hierfür nicht die Hilfe eines Promotionsberaters in Anspruch genommen. Kein Teil dieser Arbeit ist in einem anderen Promotions- oder Habilitationsverfahren verwendet worden. Mit dem Einsatz von Software zur Erkennung von Plagiaten bin ich einverstanden.

Marburg,

_____ _____

Ort/Datum Unterschrift (Lisa Stuckenschneider)

Abstract

Bacteria have a highly varied appearance and shape, which is primarily affected by the cell wall and other components that give shape to the cells. Despite decades of research in the field of cell wall synthesis there are still many open questions regarding the organisation of the bacterial peptidoglycan sacculus, but also regarding the spatiotemporal distribution of proteins that are involved in peptidoglycan synthesis. An essential class of these, the so-called Penicillin Binding Proteins, or PBPs for short, are all performing the last steps and some additional steps of the peptidoglycan synthesis. The *Bacillus subtilis* genome codes for a large number of different PBPs, which have different enzymatic properties, and it is not yet clear for all of these proteins, when – or under which conditions – they become active. Some of the PBPs are known to interact with cell wall synthesis machineries, the so called elongasome or divisome, both being partly organised by cytoskeletal elements like MreB or FtsZ.

To better understand their localisation and function, different PBPs and MreB were used in this thesis as indicators for the location of cell wall synthesis. They were investigated under different conditions, where the main focus was the spatiotemporal distribution of these proteins. Five different PBPs from different classes were selected, and n-terminally tagged with an mVenus fluorophore. These were then investigated with the help of a high-resolution microscopy method called single-molecule tracking, and the diffusion coefficients of the molecules were determined. Two different dynamic molecular populations could be discovered, one a slow-diffusing, likely enzymatically active population, and the other a fast-moving inactive population. Most PBPs demonstrate a 50% slow diffusing population, which means that roughly half of the molecules are bound to their substrate. Additionally, the reactions involving the PBPs were tested in the presence of different environmental conditions – to achieve this, the cells were treated with osmotic stressors (NaCl and sorbitol), as well as antibiotics (vancomycin, penicillin G, nisin, fosfomycin, bacitracin). Through these experiments, changes in the diffusion coefficients of the proteins were observed. Particularly the availability of peptidoglycan building blocks was altered by the presence of antibiotics. MreB also reacts to the available amounts of peptidoglycan building blocks through a change in its dynamic populations, but not as strongly as most studied PBPs.

Additionally, this thesis builds on the results of a previous doctoral thesis from the same research group (written by Dr. Simon Dersch). Therefore, this thesis (written by Lisa Stuckenschneider) also investigated the elongasome components PbpH, Pbp2a and MreB through corresponding deletion *(*Δ*pbpA* and Δ*pbpH*) and depletion genetic backgrounds (MreB levels were strongly reduced in the cell by a Cas9 system), with the

same antibiotics. The dynamics of both of the redundant transpeptidases PbpH and Pbp2a change strongly in the corresponding deletion strains and under the influence of antibiotics. Although the decreased MreB levels in the cell had only a minor effect on the diffusion constants of PbpH or Pbp2a. The absence of MreB made the diffusion of PbpH more susceptible to antibiotic treatment, and to a similar degree as in the Δ*pbpA* background.

Zusammenfassung

Bakterien haben ein vielseitiges Erscheinungsbild, welches größtenteils durch die Zellwand und andere formgebende Komponenten beeinflusst wird. Trotz jahrzehntelanger Forschung auf dem Gebiet der Zellwandsynthese gibt es immer noch viele offene und ungeklärte Fragen zur Organisation des bakteriellen Peptidoglykan Sacculus, aber auch zur räumlichen und zeitlichen Verteilung der an der Peptidoglykan Synthese beteiligten Proteinen, die sogenannten Penicillin Binde Proteine oder kurz PBPs, welche die letzten Reaktionen der Peptidoglykansynthese katalysieren. Das *Bacillus subtilis* Genom kodiert für eine große Anzahl von verschiedenen PBPs mit verschiedenen enzymatischen Eigenschaften bei denen jedoch nicht immer bekannt ist, wann oder unter welchen Bedingungen diese aktiviert werden. Einige PBPs sind dafür bekannt mit Proteinkomplexen, Elongasom and Divisom genannt, zu interagieren, welche für die Zellwandsynthese zuständig sind und meiste durch Zytoskelettelemente wie MreB und FtsZ organisiert werden.

Um die Lokalisation und Funktion besser zu verstehen, wurden in dieser Arbeit verschiedene PBPs und MreB, als Indikatoren für den Ort der Zellwandsynthese, unter verschiedenen Bedingungen untersucht, wobei der Fokus auf der zeitlichen und räumlichen Verteilung dieser Proteine lag. Fünf PBPs wurden exemplarisch aus den verschiedenen Klassen ausgewählt und n-Terminal mit einem mVenus-Fluorophor fusioniert. Diese wurden mit Hilfe einer hochauflösende zeitliche und räumliche Mikroskopie Technik die Einzel-Molekül Verfolgung („Single-molecule-tracking“ genannt) untersucht und der Diffusionskoeffizient der Moleküle wurde bestimmt. Zwei verschiedene dynamische Populationen wurden entdeckt und nachgewiesen: eine langsam diffundierende, wahrscheinlich enzymatisch aktive, und eine schnelle, frei bewegliche inaktive Molekül-Population. Wobei die meisten PBPs 50% langsame Moleküle aufweisen und damit ungefähr die Hälfte der Moleküle an Substrat gebunden ist. Darüber hinaus sollte die Reaktion der PBPs auf verschiedene Umweltfaktoren getestet werden, dazu wurden die Zellen mit osmotischen Stressoren (NaCl und Sorbitol) sowie mit Antibiotika (Vancomycin, Penicillin G, Nisin, Fosfomycin und Bacitracin) behandelt. Hierbei konnten Veränderungen des Diffusionskoeffizienten der Proteine festgestellt werden. Vor allem wenn die Verfügbarkeit der Peptidoglykanbausteine durch die Anwesenheit der Antibiotika abweicht. Auch MreB reagiert auf die verfügbare Menge von Peptidoglykanbausteinen mit einer Veränderung der dynamischen Populationen, allerdings nicht so stark wie die meisten untersuchten PBPs.
Des Weiteren wurde an die Ergebnisse einer vorherigen Doktorarbeit der Arbeitsgruppe angeknüpft (geschrieben von Dr. Simon Dersch). Die Reaktionen von am Elongasom

beteiligten Proteinen (PbpH, Pbp2a und MreB) und jeweiligen Deletionen (Δ*pbpA und* Δ*pbpH*) bzw. Depletion (MreB wurde durch ein Cas9 System in der Zelle auf ein niedriges Niveau gebracht) wurden im genetischen Hintergrund mit denselben Antibiotika untersucht. Die Dynamiken der beiden redundanten Transpeptidasen PbpH und Pbp2a veränderten sich merkbar im korrespondierenden Deletionsstamm unter dem Einfluss der Antibiotika. Während das niedrige Niveau von MreB in der Zelle nur einen geringen Einfluss auf die Diffusionskonstanten von PbpH oder Pbp2a hat, verändert sich das Verhalten von PbpH doch stark unter dem Einfluss von Antibiotika.

Table of contents

Table of Figures

Abbreviations

amp	Ampicillin
APS	Ammoniumperoxodisulfate
bp	base pair
cm	Chloramphenicol
DMSO	Dimethyl sulfoxide
DNA	deoxyribonucleic acid
dNTP	Deoxynucleotide
EDTA	Disodiumethylendiamintetraacidic acid
EtOH	Ethanol
ery	erythromycin
GFP	Green fluorescent protein
GlcNAc	N-Acetylglucosamine acid
GMM	Gaussian Mixture Model
h	hour
HCl	hydrochloric acid
IPTG	Isopropyl-β-galactopyranosid
kan	kanamycin
kb	kilobase pair
LB	Lysogeny Broth
λ	Wavelength
min	minutes
ms	millisecond
MurNAc	N-Acetylmuramic acid
MW	molecular weight
NA	numerical aperture
OD	Optical density
PAGE	polyacrylamide gel electrophoresis
PBS	phosphate buffered saline
PCR	Polymerase chain reaction
PG	Peptidoglycan
pH	potential of hydrogen
rpm	revolutions per minute
RT	room temperature
sd	standard deviation
SDS	sodiumdodecylsulfate

sec /s	second
SMT	Single Molecule Tracking
spec	spectinomycin
TAE	Tris-Acetat-EDTA
TEMED	N,N,N‘,N‘-Tetramethylethylendiamin
tet	tetracycline
(v/v)	volume per volume
(w/v)	weight per volume
xyl	xylose
YFP	yellow fluorescent protein

1 Introduction

1.1 Bacterial cell wall

Looking at the bacterial kingdom, a huge variety in size and shape of the bacterial cell can be observed. Most of the time this can be seen as an adaptation to their natural environment, such as the nutrient level, pH, environmental stress factors and various other conditions (Csonka, 1989; Hoffmann et al., 2013; Jiang et al., 2015; Young, 2007). But how can so many different shapes exist and what makes them keep that specific shape?

One of the key factors is the structure surrounding the bacterial cell, the so-called bacterial cell wall , which is commonly present in most bacteria with some exclusions (small group of obligate intracellular bacteria (Otten et al., 2018) and L-forms (Kawai et al., 2019)). The bacterial cell wall is composed of peptidoglycan (or murein) and builds a rigid sacculus to protect the bacterial cell and counters the internal pressure of the cell (turgor) (Pazos et al., 2017; Vollmer et al., 2008). The bacterial cell wall is an important factor for the identification and comparison of bacteria within the bacterial kingdom. They are separated into two large groups, based on the staining method developed by Christian Gram – Gram-staining. While Gram-positive bacteria keep the crystal violet staining dye, the Gram-negative one's loss of the staining dye indicates a different structure of the cell envelope that Gram-positive and Gram-negative bacteria have (Moyes et al., 2009).

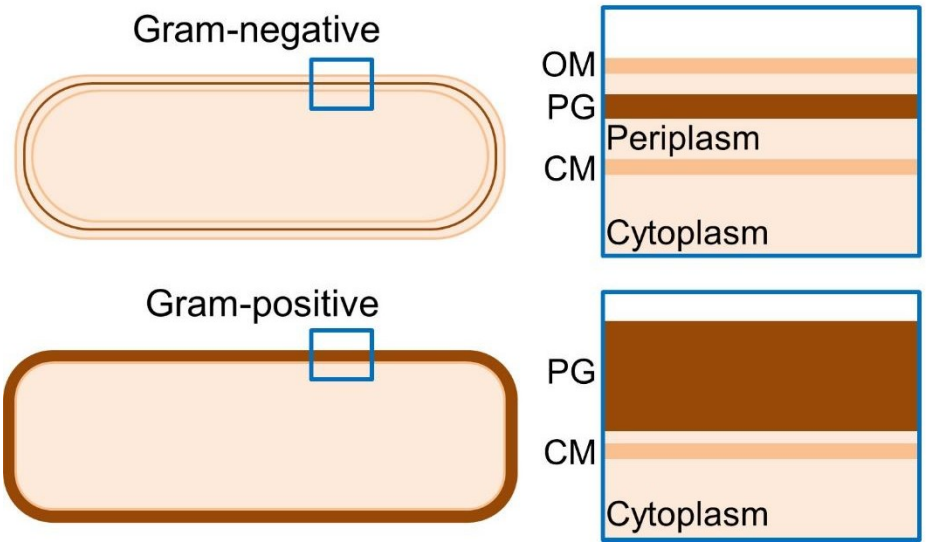

Figure 1: schematic of the differences between Gram-positive and Gram-negative bacteria, published by Egan et al., 2017.

Gram-negative bacteria have an inner membrane enclosed by a single thin layer of peptidoglycan with a thickness of about 6 nm, which is covered by another outer membrane. In contrast, the bacteria of the gram-positive group just have one membrane, corresponding to the inner membrane of gram-negative bacteria, and are surrounded by a thick cell wall containing multiple layers of peptidoglycan, which can reach a diameter of 30-100 nm (Fig. 1) (Beeby et al., 2013; Egan et al., 2017; Pasquina-Lemonche et al., 2020; Vollmer et al., 2008; Vollmer & Seligman, 2010).

1.1.1 Structure of the bacterial cell wall

A mesh of interconnected peptidoglycan (PG) strands forms the bacterial cell wall. PG strands are composed of alternating N - acetylglucosamine (GlcNAc) and N - acetylmuramic acid (MurNAc) glycopeptides linked by β – 1,4 bonds (Fig. 2A). A short pentapeptide side chain is replacing the lactyl group of MurNAc, commonly following the amino acid sequence: L-Ala-D-Glu-m-DAP-D-Ala-D-Ala. Alternatively, the m-DAP (meso-diaminopimelic acid) can be exchanged by a L-Lys, which is common in most Gram-positive bacteria (except the model organism *Bacillus subtilis*) (Fig. 2A). The peptide side chain is needed for the crosslinking between the PG strands, which is achieved by a transpeptidation reaction. This takes place between the carboxyl group of D-Ala at position 4 of one strand and the amino group of m-DAP or L-Lys at position 3 of another strand. This forms a short peptide bridge between two side chains of PG strands (Fig. 2B). The energy to generate this covalent bond is supplied by the cleavage of the fifth positioned D-Ala of the donor side chain (Egan et al., 2017; Hayhurst et al., 2008; Höltje, 1998; Macheboeuf et al., 2006; Typas et al., 2012).

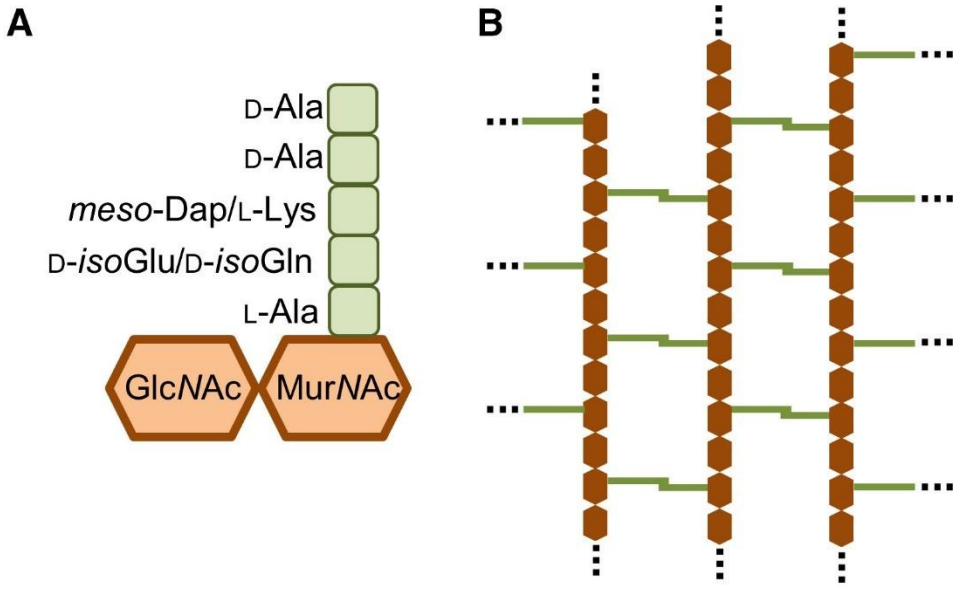

Figure 2: structural details of peptidoglycan organization A showing the peptidoglycan monomer with the possible alteration of the 2nd and 3rd amino acid in the peptide side chain. **B** showing a simplified model of the crosslinked peptidoglycan layer, published by Egan et al., 2017.

The bacterial cell wall is a very variable structure, and can differ strongly between bacterial species. As already discussed, the PG layers can differ between bacterial species and depending on whether the organism is Gram-positive or -negative. Gram-negative bacteria like *E. coli* only have 1 to 3 individual layers of PG, whereas Gram-positive bacteria like *Bacillus subtilis* can have up to 30 (Fig. 1). The PG strands themselves can also be composed of a variable number of disaccharides depending on the bacterial species (*E. coli* 25 to 80 and *B. subtilis* around 96), and on the growth phase of the bacteria. Similarly, the amount of crosslinking can also vary between organisms, and also depend on the growth phase or environmental conditions. In *B. subtilis*, for example, the degree of crosslinking reaches 56% during exponential growth and it can be higher during the stationary phase (Beeby et al., 2013; Egan et al., 2017; Hayhurst et al., 2008; Typas et al., 2012; Vollmer et al., 2008; Vollmer & Seligman, 2010). Despite the existing findings regarding cell wall thickness, degree of crosslinking and length of strands, the overall structure of the cell wall and especially the organisation of the PG strands is still under debate.

1.1.2 Biosynthesis of the bacterial cell wall

The synthesis of peptidoglycan can be divided up into three different stages separated by location in the cell (Fig. 3). The first stage is taking place in the cytoplasm of the bacterial cell and is covering the synthesis of the precursors of peptidoglycan mainly involving the Mur enzymes. The first step is the transformation of UDP-GlcNAc to UDP-MurNAc catalysed by MurAA and MurAB in *B. subtilis* or MurA and MurB in *E. coli*. UDP-GlcNAc is generated by three enzymes GlmS, GlmM and GlmU and those are catalysing four reactions starting with Fructose-6-phosphate. Subsequently, the pentapeptide side chain is added residue-by-residue to UDP-MurNAc via the ligases MurC, MurD, MurE and MurF, which are hydrolysing ATP to power the reaction (Barreteau et al., 2008; Egan et al., 2017; Höltje, 1998; Laddomada et al., 2016).

The second stage is linked to the cytoplasmic membrane. On the inner leaflet of the membrane, the UDP-MurNAc-L-Ala-D-Glu-m-DAP-D-Ala-D-Ala (UDP-MurNAc-pentapeptide) gets linked to undecaprenol-phosphate by MraY, an integral membrane protein, to form undecaprenyl-MurNAc-pentapetide, which is alternatively called lipid I. The glycosyltranferase MurG is connecting lipid I with UDP-GlcNAc to generate lipid II (undecaprenyl-pyrophosphoryl-MurNAc-pentapetide-GlcNAc). Afterwards lipid II needs to get transported on the external side of the cell and flipped across the hydrophobic membrane to then get integrated into the growing peptidoglycan network (Laddomada et al., 2016; Szwedziak & Löwe, 2013; Typas et al., 2012; Zhao et al., 2017)

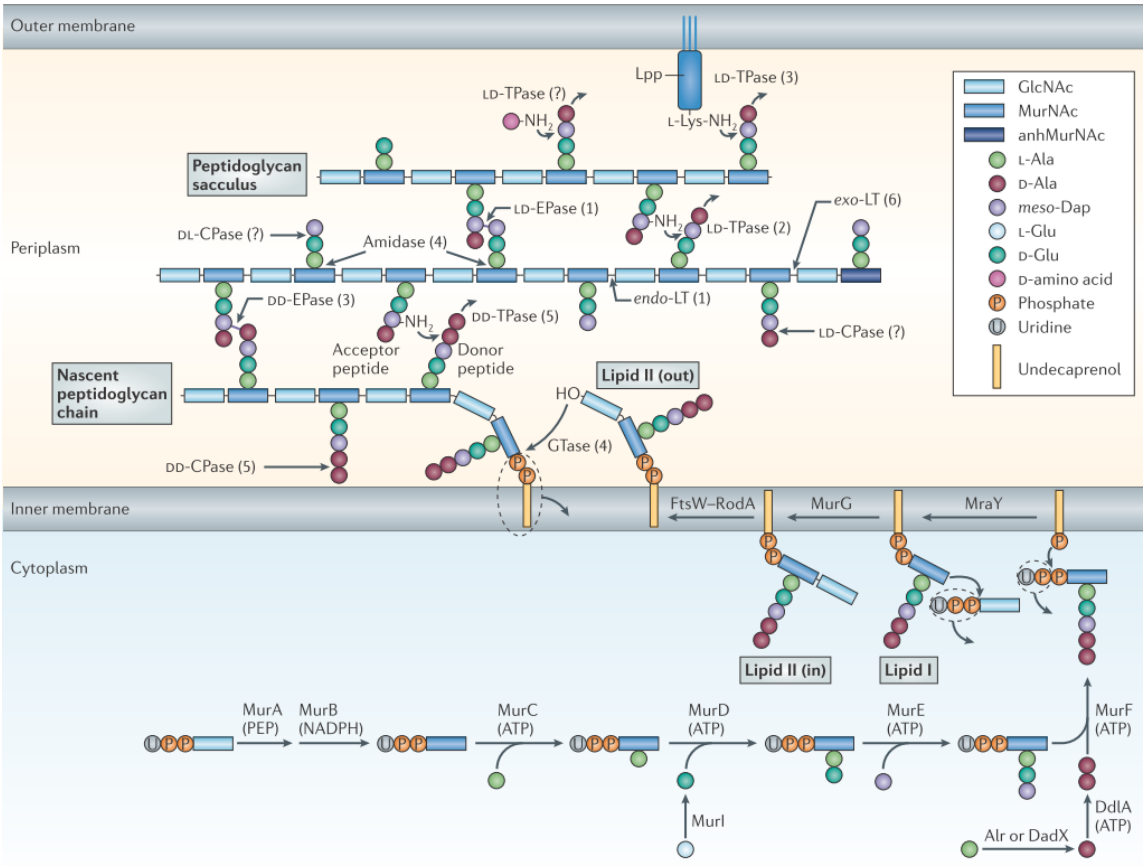

Figure 3: Peptidoglycan synthesis pathway; illustrating the most important steps of the cell wall synthesis of a gram-negative bacterium with some additional details not mentioned in the section 1.1.2, published by Typas et al., 2012.

How the translocation of lipid II is achieved and which enzymes are involved in this process, was long unclear. Recently, several potential flippases were discovered, among other members of the SEDS (Shape, Elongation, Division, Sporulation) protein family (Emami et al., 2017; Leclercq et al., 2017; Mohammadi et al., 2011; Pazos et al., 2017; Ruiz, 2016; Sjodt et al., 2018; Zhao et al., 2017). These proteins were found to have a GTPase activity and an involvement in the cell wall synthesis pathway. *E. coli* and *B. subtilis* were both found to possess at least two SEDS each: RodA and FtsW are both considered to be able to flip lipid II to the outside of the cell (Ruiz, 2016; Zhao et al., 2017). Even though it was already disproved for RodA, which definitely has a function as a glycosyltransferase (Emami et al., 2017; Meeske et al., 2016; Sjodt et al., 2018). FtsW is also considered a glycosyltransferase and to be involved at the divison process of the bacterial cells (Leclercq et al., 2017). MurJ was additionally identified as an integral membrane protein with an essential function for the peptidoglycan synthesis. The accumulation of lipid II in the cytoplasm of the bacterial cell can be achieved by depletion of MurJ, indicating its importance for the process (Kuk et al., 2019; Meeske et al., 2015, 2016). The loss of MurJ can be partially replaced by the function of Amj in *B. subtilis* and Wzk in *E. coli* (Kumar et al., 2019; Meeske et al., 2015; Ruiz, 2016; Zhao et al., 2017).

Even though the process of flipping lipid II through the membrane is now clearer, it is still not known which of these proteins are essential for this process, or if MurJ and the SEDS RodA and FtsW are working alongside each other to reach a stable translocation of lipid II and PG synthesis (Meeske et al., 2016; Zhao et al., 2017).

The last stage of peptidoglycan synthesis takes place outside of the bacterial cell membrane and deals with the assembly of the mature PG sacculus. The maturation is reached by two reactions, transglycosylation and transpeptidation, which are performed by two families of proteins: the SEDS and the penicillin-binding proteins (PBP) (Bhavsar & Brown, 2006; Egan et al., 2017, 2020; Höltje, 1998; Laddomada et al., 2016; Szwedziak & Löwe, 2013; Typas et al., 2012; Zhao et al., 2017). First, the lipid II precursor is transferring its glycan residue to the GlcNAc to the already existing PG strand and the undecaprenol-phosphate is getting recycled via transportation to the cytoplasm, where it can get reloaded again. The transglycosylation is catalysed either by the SEDS proteins RodA or FtsW or by a class A PBP (further discussed in the chapter 1.2.) and leads to an elongation of the synthesised PG strand (Bhavsar & Brown, 2006; Egan et al., 2017, 2020; Emami et al., 2017; Höltje, 1998; Laddomada et al., 2016; Leclercq et al., 2017; Szwedziak & Löwe, 2013; Typas et al., 2012; Zhao et al., 2017). The last step in the generation of the mesh-like network of PG strands is the transpeptidation of the PG strand side chain. For this reaction the D-Ala of a pentapeptide side chain is removed to provide the energy for the following 4,3 crosslinking reaction between D-Ala and m-DAP or L-Lys (Bhavsar & Brown, 2006; Egan et al., 2017, 2020; Höltje, 1998; Laddomada et al., 2016; Macheboeuf et al., 2006; Sauvage et al., 2008; Scheffers et al., 2004; Szwedziak & Löwe, 2013; Typas et al., 2012; Zhao et al., 2017).

To be able to insert new PG strands and allow cell growth, the PG synthesis machinery needs to get coordinated by hydrolytic reactions performed by PG hydrolases, which cleave the covalent bonds of the existing PG network to create space for new insertions. This is most likely carried out by a multiprotein complex of hydrolases and synthases, where hydrolysis ensures PG insertion and leads the cell wall synthesis machinery to the site of action. Several models have been suggested in the past, and only the “three for one” model by Höltje, 1998 was highly accepted (Fig. 4A and B) for a long time. In this model, a multienzyme complex is composed out of PBPs and hydrolases. It is inserting three already crosslinked PG strands into the sacculus. During the elongation step, the complex interacts with the leading PG strand, which is getting hydrolysed, and simultaneously, the new trimer glycan strand is inserted into the cell wall. For *B. subtilis* a new model was proposed, called the “three under two” model, which suggests that

three new PG strands are inserted under the innermost pre-existing PG layer and get crosslinked with the old glycan strands. The newly synthesised PG layer becomes the new innermost one and is now the stress-bearing layer. This growth pattern is also called the “inside to outside” model (Fig. 4B), because the innermost layer is pushing the older layers outwards (Billaudeau et al., 2017).

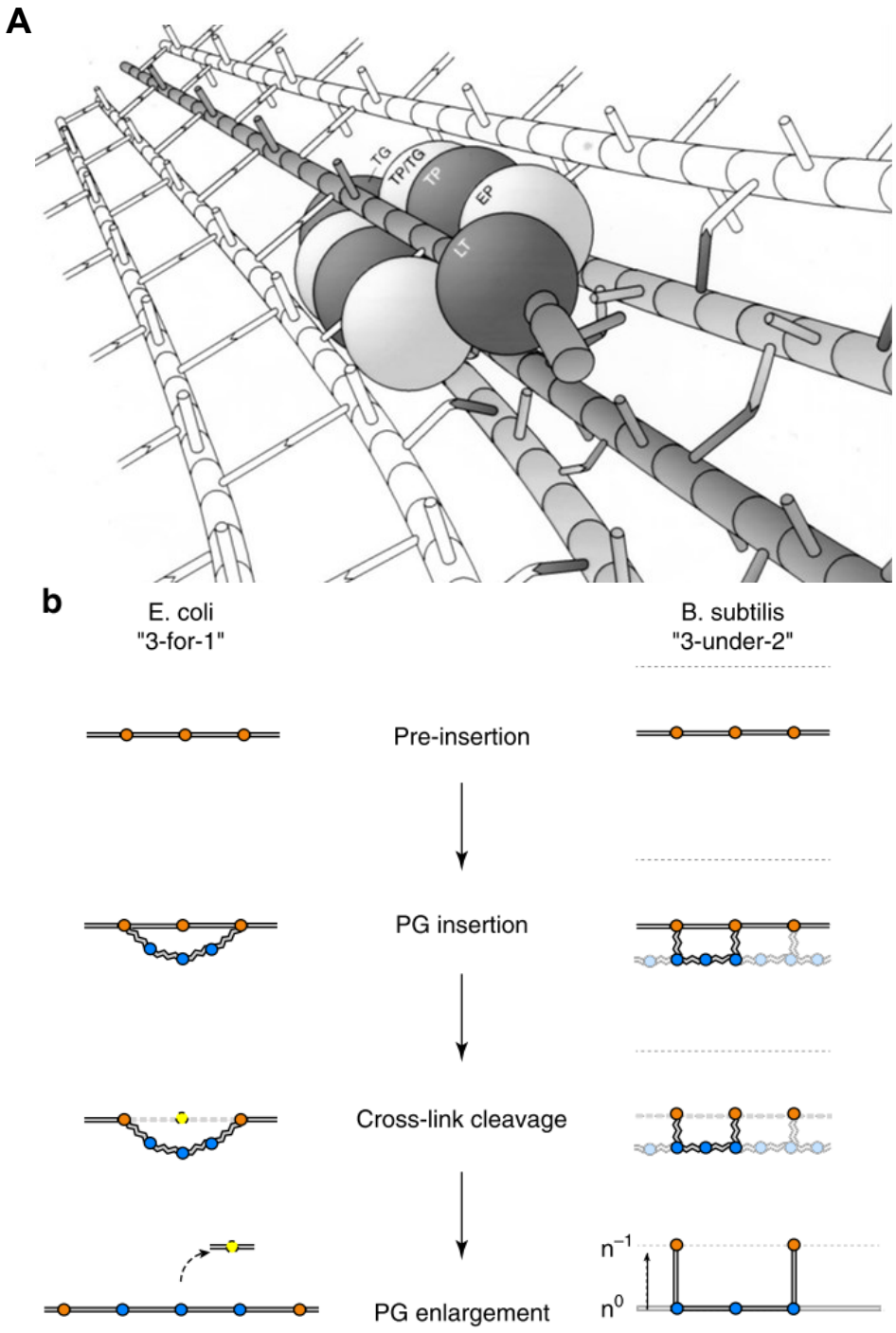

Figure 4: Two models of the PG insertion pattern A is showing the protein complex inserting new PG by the Three for One model published by Höltje, 1998. **B** compares the two different proposed peptidoglycan insertion models for the two model organisms (*E. coli* and *B. subtilis*) published by Billaudeau et al., 2017.

1.2 Penicillin-Binding Proteins (PBPs)

As the name Penicillin-Binding Proteins (PBPs) implies, these proteins can get targeted by β-lactam antibiotics, which penicillin is a part of. The structure of β-lactam antibiotics is mimicking the D-Ala-D-Ala terminus of the pentapeptide side chain of PG and therefore forms a covalent bond with the active site of the transpeptidase domain of PBPs, leading to an inactivation of the protein (Kohanski et al., 2010; Raynor, 1997; Strominger et al., 1971). Since bacteria have several PBPs for the transglycosylation and transpeptidation of PG, a classification for PBPs was needed. The PBPs have been divided into two groups by their molecular weight, High Molecular Weight (HMW) or Low Molecular Weight (LMW) and the HMW are further differentiated into two different classes by their enzymatic functions (Egan et al., 2017; Höltje, 1998; Macheboeuf et al., 2006; Sauvage et al., 2008; Scheffers et al., 2004).

The HMW PBPs are generally composed of a short cytoplasmic N-terminal domain, one transmembrane helix and a periplasmic enzymatically active domain. The periplasmic domain of the HMW PBPs can either be bifunctional (class A) or monofunctional (class B). The bifunctional PBPs or class A PBPs have an additional transglycosylation activity on top of transpeptidation activity. Whereas the class B PPBs just have transpeptidase enzymatic activity. The LMW PBPs, on the other hand, are hydrolytic enzymes with a carboxypeptidase or endopeptidase activity (Macheboeuf et al., 2006; Sauvage et al., 2008; Scheffers et al., 2004). Since the genome of *Bacillus subtilis,* for example, codes for 16 so far identified PBPs, a great redundancy must exist between different proteins, but it is still unclear at which stage which individual protein becomes important and essential for the cell wall growth (Scheffers et al., 2004).

Having a closer look at the different PBPs of *Bacillus subtilis*, the model organism used in this thesis, it is known that *B. subtilis* harbours ten HMW PBPs (four class A PBPs, six class B PBPs) and six LMW PBPs (Scheffers et al., 2004). In contrast to *E. coli* (Yousif et al., 1985), it is possible to delete all four class A bifunctional PBPs (Pbp1, 2c, 2d and 4) in *B. subtilis*, which leads to an abnormal morphology and a strong non-lethal growth defect. Thus, the effect of all four class A PBPs deleted might be strongly influenced by the absence of Pbp1, which alone leads to a reduced cell growth and an abnormal morphology of the formed colonies (McPherson & Popham, 2003; D. L. Popham & Setlow, 1995; David L. Popham & Setlow, 1996). Another functional redundancy between the two class B PBPs Pbp2a and PbpH is known. Both proteins are involved in the elongation of the bacterial cell wall, and if one of them is deleted, the cells are still viable. A deletion of both is not possible and is lethal for the cell (Wei et al., 2003). The

only essential PBP so far known for *Bacillus subtilis* is Pbp2b, an important cell division protein. Interestingly a depletion of it leads to a lethal effect on the cell; on the other hand, a mutation leading to an inactivation of Pbp2b is not lethal and another PBP, Pbp3, then becomes more important for the cell division and partly compensates for the lost function of Pbp2b (Daniel et al., 1996; Sassine et al., 2017). This would likely mean that PBP2b and Pbp3 are partly functionally redundant.

1.3 The elongasome and divisome

As discussed in 1.1.2, the peptidoglycan synthesis is performed by multiprotein complexes, which are strongly involved in the shape maintenance of bacteria. Thus, the cell requires longitudinal growth and needs to get divided, which two big proteins complexes are responsible for, the elongasome and the divisome.

The elongasome is known as the Rod complex or the peptidoglycan elongation machinery (PGEM). Its main function is to carry out peptidoglycan synthesis along the cell periphery to make the cell grow longer. It is a complex composed of several enzymes and is thought to move circumferentially around the cell. This movement is guided by the cytoskeletal element MreB, which provides a scaffold for the PGEM coordinating the insertion and crosslinking of the PG strands during the elongation of the cell wall. Generally, the rod complex is composed out of MreB at the cytoplasmic side, RodZ, MreD, MreC and RodA as transmembrane proteins and Pbp2 (or Pbp2a and PbpH for *B. subtilis*) as the involved transpeptidases on the external cell side, which each is linked to the membrane via one transmembrane helix (Fig. 5) (Divakaruni et al., 2005; Egan et al., 2017, 2020; Wei et al., 2003; Zhao et al., 2017). For the elongation stage, the class A PBP Pbp1 can act as an additional path of insertion and crosslinking of PG strands into the cell wall, in a more random and unorganized pattern (Dion et al., 2019).

As the PBPs were already discussed in 1.2 and the function of RodA in 1.1.2, the other components of the PGEM will shortly be discussed here starting with RodZ. RodZ is an integral membrane protein and is thought to have an anchoring function for MreB, since it has been shown to interact with MreB and to have a similar circumferential movement around the cells like MreB (Bendezú et al., 2009; Morgenstein et al., 2015; Van Den Ent et al., 2010), thus has an important role in the cell shape maintenance (Van Den Ent et al., 2010). MreC and MreD are both transmembrane proteins encoded in the same operon as MreB. They have been shown to interact with MreB and to have a similar localization pattern in long circumferential structures as MreB in the cell (Leaver & Errington, 2005; Soufo & Graumann, 2005; Wang et al., 2012) as well as having a regulating effect on the rod complex (Divakaruni et al., 2007; Van Den Ent et al., 2006).

They were also shown to interact with each other and several other PBPs (Van Den Ent et al., 2006). Recently, Liu et al., 2020 showed that MreC is mediating a reduction in the interaction between RodA and Pbp2 in *E. coli* and MreD is a negative regulator of the Pbp2 and MreC interaction, hence both proteins together are needed to get a normal Pbp2 RodA interaction level.

One of the most important components of the PGEM is the cytoskeletal filamentous proteins MreB. MreB has been found to be essential protein for the cell shape maintenance in most bacteria and its depletion leads to a loss of cell shape and eventually lysis of the bacterial cell. In *B. subtilis* two paralogous and partly functional redundant proteins (MreBH and Mbl) of MreB exist, showing a similar localization pattern as MreB, as well as some other proteins named before PbpH/Pbp2a and RodA (Defeu Soufo & Graumann, 2006, 2010; Jones et al., 2001; Kawai, Asai, et al., 2009; Reimold et al., 2013). MreB was found to be localized in rather short filaments or forming so-called “patches”. It demonstrates a movement around the circumference of the bacterial cell, potentially driven by the rod complex components and is dependent on the active synthesis of PG (Daniel & Errington, 2003; Graumann, 2007, 2009; Van Teeffelen et al., 2011; van Teeffelen & Renner, 2018; Wickstead & Gull, 2011). Other studies suggest that the localization of MreB might be dependent on the cell wall precursor and their abundance in the cell (Schirner et al., 2015), or alternatively, the curvature of the cell (Hussain et al., 2018). Overall, a more recent study also suggests that the rod complex is not as rigid as previously considered, and that its regulation and localization are more complex (Dersch et al., 2020; Dion et al., 2019; Özbaykal et al., 2020).

Another important protein complex for normal bacterial growth is the divisome, which is assembled in two different stages, the “early” and “late” stage, to the site of division and is triggering the separation of the mother and daughter cell (Aarsman et al., 2005; Egan & Vollmer, 2013, 2015; Gamba et al., 2009). The cell division is strongly dependent on the essential PBP Pbp2b in *B. subtilis* (or PBP3 in *E. coli*), which is responsible for the modification of the freshly synthesised peptidoglycan in the newly generated cell poles (Aarsman et al., 2005; Botta & Park, 1981).

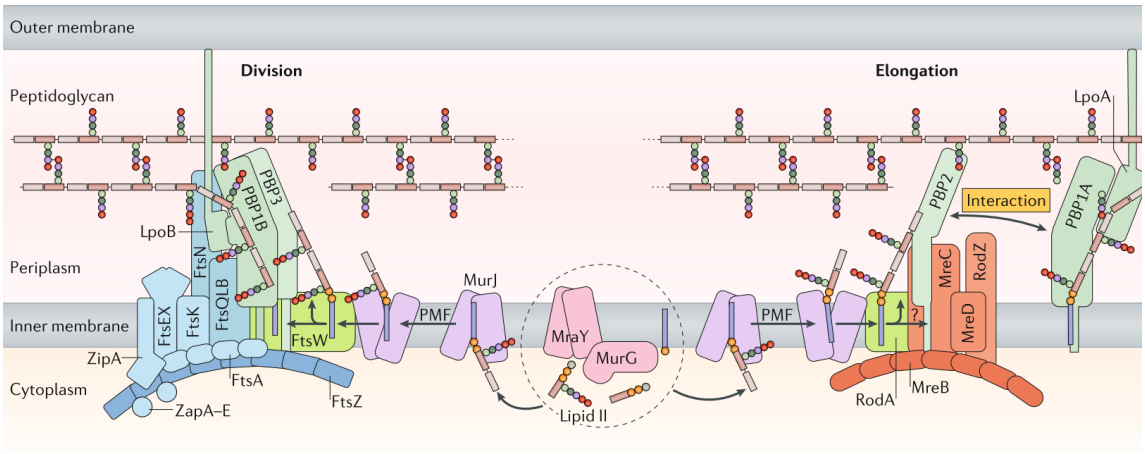

Figure 5: Elongasome and divisome complex; graphic showing the division and elongation process of a gram-negative bacterium next to each other for better comparison published by Egan et al., 2020.

The early stage of cell division is normally initiated by a mid-cell localization and polymerization of the protein FtsZ in a GTP-dependent manner. FtsZ is a protein that can polymerize to form filamentous structures in the cell. The FtsZ filaments are bundled to protofilaments forming the Z-ring at the septum and were found to have a dynamic behaviour via directional “treadmilling” (Barrows & Goley, 2021; Bisson-Filho et al., 2017; Graumann, 2007, 2009; McCausland et al., 2021; Söderström et al., 2018; Wickstead & Gull, 2011). FtsZ is a crucial component of the division process since it recruits the early stage divisome proteins FtsA, ZapA, SepF and EzrA in *Bacillus subtilis*. While FtsA, SepF and ZapA are responsible for building a functional Z-ring and anchoring it to the membrane, EzrA possesses a regulatory function in regard to FtsZ and can modulate the localization and number of Z-rings (Chung et al., 2004; Duman et al., 2013; Gamba et al., 2009; Jensen et al., 2005; Singh et al., 2007). During the early stage of divisome assembly in *E. coli*, additional proteins are involved, which are shown in Figure 5 (Egan et al., 2020; Egan & Vollmer, 2013).

The “late” stage of the assembly of the divisome is marked by the appearance of Pbp2b, FtsL, DivIB, DivIC, FstW and GpsB in *B. subtilis*. Since the functions of Pbp2b and FtsW were already discussed before in this chapter, the focus will be on the remaining late stage divisome components. FtsL has been found to have a regulatory role in cell division, while DivIB and DivIC seem to have a stabilising and turnover-controlling effect on FtsL (Bramkamp et al., 2006; Daniel & Errington, 2000). GpsB is involved in the regulation of the localisation of Pbp1 and it has an antagonistic effect to EzrA in regard of the positioning of Pbp1 (Claessen et al., 2008). The last protein involved in the localization of the septum and regulation of the Min inhibitory system is called DivIVA. DivIVA is normally localized at positions with a high negative curvature, in this case the freshly constructed cell pole, forming a ring like structure and by this, it is positioning the

division inhibitor MinCD (earlier referred to as the Min inhibitory system) to keep FtsZ from immediately assembling into another Z-ring (Edwards & Errington, 1997; Eswaramoorthy et al., 2011).

1.4 The bacterial cell wall as a target for antibiotic treatment

The bacterial cell wall is still one of the most common targets for antibiotics; these inhibit the normal cell wall synthesis at several stages of the process (Fig. 6). In this section, some mechanisms and antibiotic groups important for the understanding of this thesis will be discussed. The most important group of such antibiotics are the β-lactams, from which the designation for penicillin binding proteins is derived – it comes from the antibiotic penicillin, which binds to a conserved active site within the PBPs. The natural product penicillin was first discovered in 1928 by Alexander Fleming, but decades later it was found that penicillin was inhibiting the last step of the cell wall synthesis - the crosslinking (Raynor, 1997; Strominger et al., 1971). Penicillin and all related antibiotics have a similar structure, which contains a thiazolidine ring with a β-lactam ring with an attached variable rest depending on the antibiotic, while the thiazolidine and the β-lactam ring are building the central structure. The inhibition is caused by the binding of the penicillin to the active site of the penicillin binding domain (in different PBPs) and subsequent hydrolysis of the β-lactam ring, which is opened, thus mimicking the D-Ala-D-Ala of the side chain of a single peptidoglycan building block (Josephine et al., 2004, 2006; Kohanski et al., 2010). The active site of the penicillin binding domain, which is also catalysing the crosslinking of the PG strands, has an acyl serine transferase activity with a SxxK motif in the centre of the active site and two additional motifs ((S/Y)XN and (K/H)(T/S)G) (Angeles & Scheffers, 2020; Goffin & Ghuysen, 1998).

A second group of important antibiotics are the glycopeptide antibiotics. An especially prominent compound of this group is vancomycin. Vancomycin was first discovered and purified from a soil bacterium in 1956. As well as with penicillin, the D-Ala-D-Ala of the pentapeptide peptidoglycan precursor has important implications for its activity. Vancomycin is not mimicking the terminal part of the pentapeptide, but rather detecting it and interacting with the cell wall precursor lipid II (Breukink & de Kruijff, 2006; Münch & Sahl, 2015; Reynolds, 1989; Sheldrick et al., 1978). By doing so, it is indirectly inhibiting the transglycosylation and transpeptidation as the last steps of the PG synthesis.

Staying with the antibiotics interacting with lipid II, the lantibiotic nisin needs to get discussed. Nisin belong to the family of the lantibiotics and was the first of this group to

be discovered in the 1920s. In contrast to the other antibiotics interacting with lipid II, nisin is not simply binding it and thereby inhibiting the cell wall synthesis, it is also perturbing the cell membrane by building a pore like complex with lipid II (Breukink & de Kruijff, 2006; de Kruijff et al., 2008; Münch & Sahl, 2015; Oppedijk et al., 2016; Scherer et al., 2015).

Since lipid II is believed to be the main bottleneck of the cell wall synthesis, perturbation of the process of flipping the carrier lipid back to the cytoplasm can interfere with the entire process. Bacitracin is an antibiotic interfering exactly with this critical part of the cell wall synthesis and interacts with the UndPP by covering it in a dome-like manner, in a metal ion dependent fashion, preventing it from getting dephosphorylated and flipped back into the cell to get reloaded with a MurNAc-pentapetide. Bacitracin is a dodecapeptide and is binding the carrier lipid to form a 1:1:1 bacitracin- bivalent metal-carrier lipid complex (Economou et al., 2013; Radeck et al., 2017).

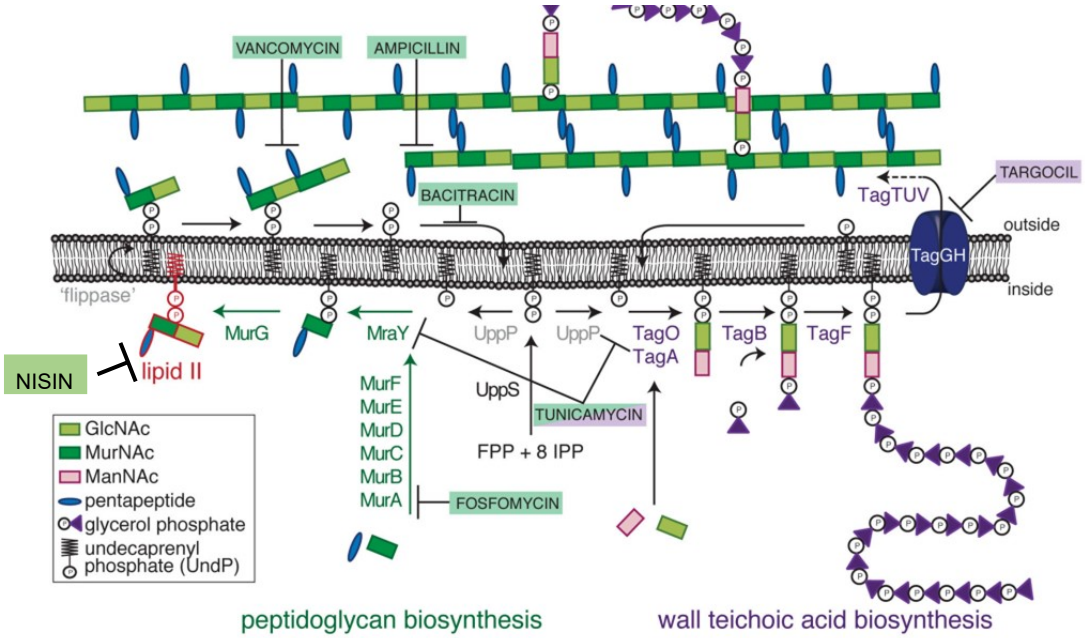

Figure 6: schematic of the peptidoglycan synthesis with indication where specific antibiotics inhibit the cell wall synthesis process, modified after Schirner et al., 2015.

The last antibiotic important for this thesis is fosfomycin, which is the only antibiotic tested that inhibits a reaction step in the early, cytoplasmic stage of the cell wall synthesis, and it therefore needs to get transported into the cytoplasm of the cell by the widely spread α-glycerophosphate permease. In the cytoplasm it is interacting with, and inhibiting the first step catalysed by MurA. MurA performs the reaction to form UDP-GlcNAc-enoylpyruvate by reacting UDP-GlcNAc with phosphoenolpyruvate (PEP). Fosfomycin is inhibiting this reaction by mimicking PEP and covalently binding to the active site of MurA (Jordan et al., 2008; Kahan et al., 1974b; Silver, 2017).

1.5 Thesis aims

The aim of this thesis was to obtain a more detailed insight into the organization of the synthesis machinery of the bacterial cell wall in the model organism *Bacillus subtilis*, with particular interest in localization, protein-protein interactions and dynamics, also building on previous findings presented in the doctoral thesis of Dr. Simon Dersch. Of special interest was the peptidoglycan elongation machinery (PGEM). Therefore, several Penicillin Binding Proteins (PBPs) were chosen and studied *in vivo* under cell wall challenging conditions (osmotic stress and antibiotic treatment) to understand the adaptation of those PBPs with the help of a single molecule tracking (SMT) approach. SMT was used because of its high spatiotemporal resolution for faster acquisition of molecule diffusion. Before starting the experimental work presented in this thesis, the PBPs PbpH and Pbp2a (Murray et al., 1997; Wei et al., 2003), as well as Pbp3 (Murray et al., 1996; Sassine et al., 2017) as transpeptidases (class B PBPs), Pbp4 as a bifunctional class A PBP (McPherson & Popham, 2003; D. L. Popham & Setlow, 1995; David L. Popham & Setlow, 1996) and Pbp4a as a LMW carboxypeptidase (Duez et al., 2001; Pedersen et al., 1998; Sauvage et al., 2007) were chosen.

The high functional redundancy of the PBPs has for years been a topic lacking full understanding in the research field, and due to this fact, this thesis also aimed to get a better impression at which conditions different PBPs react differently to stress and to potentially find a hint as to when a PBP is particularly affected. Additionally, the cytoskeletal filament component MreB was included in the study to deepen the knowledge of its diffusive behaviour with an antibiotic treatment at a high spatiotemporal level. Since the effects of antibiotics on MreB is quite controversial and the different applied time scale in studies, MreB should also get investigated with this thesis SMT setup to get better comparable results of MreB to previously shown stress conditions shown by this group.

2. Materials and Methods

2.1 Reagents and kits

Chemicals used for this work were purchased from Sigma-Aldrich (USA), Carl Roth GmbH & Co. KG (Germany), VWR (Germany) or AppliChem (Germany). Molecular cloning and genetic manipulation were performed with the help of DNA endonucleases, DNA polymerases and other reagents like dNTPs or Gibson Assembly Master Mix from New England Biolabs (England). Size standards for DNA and protein molecular weight standards were supplied by New England Biolabs (England) or Thermo Fisher Scientific (USA). Plasmid and gel extraction were performed using the GenJET Plasmid Miniprep Kit (Thermo Fisher Scientific, USA) or GenElute^{TM} HP Plasmid Miniprep Kit (Sigma Aldrich, USA). PCR and DNA purification were used from Omega (E.N.Z.A. Cycle Pure Kit) and Analytic Jena (innuPREP Bacteria DNA Kit) respectively.

2.2 Growth media, supplements and buffers

Table 1: cultivating media and included media components

Media	**Ingredients**
LB medium (autoclaved)	10g/l trypton 5 g/l yeast extract 10 g/l sodium chloride Add ddH_2O
LB agar (autoclaved)	10g/l trypton 5 g/l yeast extract 10 g/l sodium chloride 15 g/l Add ddH_2O
10 x $S7_{50}$ salt solution (pH 7,0, autoclaved)	10 mM ammonium sulfate 50 mM potassium dihydrogenphosphate 214 mM potassium hydroxide 500 mM MOPS add ddH_2O

100 x Metal solution (sterile filtered)	7 mM calcium chloride 0.05 mM iron(III) chloride 200 mM magnesium chloride 0.5 mM manganese chloride 0.034 mM hydrochloric acid 0.03 mM thiaminhydrochloride 0.1 mM zinc chloride add ddH_2O
$S7_{50}$ medium	1x $S7_{50}$ salt solution 1x metal solution 1% fructose (w/v) 0.1% glutamate (w/v) 0.004% casamino acids (w/v) add ddH_2O
TSB medium (sterile filtered, store at -20°C)	10 % (w/v) PEG4000 5% (v/v) DMSO 2% (v/v) 1M $MgCl_2$ 1% (w/v) bacto tryptone 0.5% (w/v) yeast extract 0.5% (w/v) NaCl add ddH_2O
10 x MC-medium (sterile filtered)	0,17 mM ammonium ferric (III)citrate 1% (w/v) casamino acids 12.31 mM dipotassium hydrogenphosphate 20.18 mM glucose 7.72 mM potassium dihydrogenphosphate 2.16 mM potassium glutamate 0.6 mM sodium citrate add ddH_2O

MC-medium (sterile filtered)	10% (v/v) 10 x MC-medium 0.333 mM magnesium sulfate add ddH_2O
10x T-base (autoclaved)	150 mM ammonium sulfate 800 mM dipotassium hydrogenphosphate 44 mM potassium dihydrogenphosphate 3,4 mM trisodium citrate add H_2O
SpC-medium (sterile filtered)	1x T-base 0.0025% (w/v) casaminoacids 0.5 mM glucose 4% (w/v) yeast extract 0.0146 mM magnesium sulfate add ddH_2O
SpII-medium (sterile filtered)	1x T-base 0.1 mM calcium chloride 0.0025% (w/v) casamino acids 5 mM glucose 20% yeast extract 0.682 mM magnesium sulfate add ddH_2O
SOC-medium (autoclaved)	20 mM glucose 0.5% (w/v) yeast extract 2.5 m potassium chloride 10 mM magnesium chloride 10 mM magnesium sulfate 10 mM sodium chloride 2 % (w/v) tryptone add ddH_2O

Table 2: Antibiotics and other media supplements

Supplement	Stock concentration	Working concentration
Ampicillin (amp)	100 mg/ml in ddH_2O	100 µg/ml
Chloramphenicol (cm)	50 mg/ml in 50% EtOH	5 µg/ml
Kanamycin (kan)	25 mg/ml in ddH_2O	50 µg/ml
Xylose	50% (w/v) in ddH_2O	0,01% (v/v)
IPTG	1 M in ddH_2O	1 mM
Tetracycline (tet)	10 mg/ml in 50% EtOH	20 µg/ml
Erythromycin (ery)	4 mg/ml in EtOH	1 µg/ml
Spectinomycin (spec)	25 mg/ml in 50% EtOH	100 µg/ml
Vancomycin	40 mg/ml in ddH_2O	4 µg/ml
Penicillin G	40 mg/ml in ddH_2O	4 µg/ml
Nisin	30 mg/ml in ddH_2O	30 µg/ml
Bacitracin	100 mg/ml in ddH_2O	200 µg/ml
Fosfomycin	300 mg/ml in ddH_2O	300 µg/ml
Sorbitol	3M	1M
NaCl	5M	0.5M

Table 3: Buffers for gel electrophoresis and SDS-PAGE

Buffers	**Ingredients**
6 x DNA-loading dye	0.149 mM bromphenolblue 20% (v/v) glycerine 60% (v/v) 10 x TAE-Puffer add ddH_2O
50 x TAE-buffer	1 M acetic acid. 50 mM Na_2EDTA 2 M Tris/ HCl add ddH_2O
Lysis buffer (pH 7,5)	50 mM sodium chloride 5 mM Na_2EDTA 50 mM Tris-HCl add ddH_2O
SDS-loading dye	0.6% (w/v) bromphenolblue 600 mM DTT 10% (w/v) SDS 300 mM Tris-HCl pH 6.8 add ddH_2O
Stacking gel (5% acrylamide)	16,49% (v/v) Rotiphorese Gel 30 4,4 mM Tris pH 6,8 0,1% (w/v) SDS 0,1% (v/v) TEMED 0,004% (v/v) APS add ddH_2O

Running gel (10% acrylamide)	27.5% (v/v) Rotiphorese Gel 30 0.16 M Tris (pH 8,8) 0.08% (w/v) SDS 0.8% (v/v) TEMED 0.08% (v/v) APS add ddH_2O
SDS-running buffer	383,6 mM glycine 69,35 mM SDS 50 mM Tris add ddH_2O
Western blot transfer buffer (pH 9,8)	48 mM Tris 39 mM glycine 1.3 mM SDS 20% (v/v) ethanol add ddH_2O
PBST	8,1 mM disodiumhydrogenphosphate 21,74 mM sodiumdihydrogenphosphat 100 mM sodiumchlorid 0,1% (v/v) Tween 20 add ddH_2O

2.3 Vectors and oligonucleotides

All oligonucleotides were ordered from Sigma Aldrich (Germany). Their final concentrations were adjusted to 100 pmol/µl with ddH_2O and they were stored at -20°C. A list containing all oligonucleotides can be found under S2.

For this work, different vectors were used to manipulate *Bacillus subtilis* (list of generated plasmids table S1). For generating a n-terminal fusion to a mVenus fluorophore, the vector pHJDS (Defeu Soufo & Graumann, 2004) was modified to have a mVenus instead of a YFP. Additionally, a vector was used to exchange a cm to tet resistance and a vector for markerless deletion of gene in strains generated by the Bacillus genetic stock centre (Koo et al., 2017).

2.4 Bacterial strains

Several bacterial strains were used to create the strains used in this work and all bacterial strains are listed in table S3. The *E. coli* strain *DH5alpha* (Woodcock et al., 1989) was used to generate the modified plasmid, which was subsequently used for transforming *B. subtilis.* The domesticated laboratory strains PY79 (Schroeder & Simmons, 2013; Youngman et al., 1984; Zeigler et al., 2008) and 168 (Albertini & Galizzi, 1999; Burkholder & Giles, 1947; Zeigler et al., 2008) were used to obtain mVenus fusion strains with different genetical backgrounds analysed with single molecule tracking.

2.5 Microbiological methods

2.5.1 Growth conditions of *E. coli* cells

E. coli cultures were generally cultivated at 37°C and 200 rpm in LB medium or at 37°C on LB agar plates if not differently explained in the methods. All bacterial growth was followed and measured at OD_{600} with a spectrophotometer.

2.5.2 Preparation and transformation of chemically competent E. coli cells

For the chemically competent *E. coli* cells, an overnight culture was inoculated into fresh LB medium in a ratio of 1:40. The culture was incubated at 30°C until an OD_{600} of 0.5 was reached, and was afterwards centrifuged for 10 min at 3200xg and 4°C. The cell pellet was carefully resuspended in 5 ml ice-cold TSB medium and the resuspended cells were split into 100 µl aliquots prior to flash-freezing in liquid nitrogen. The cells were then stored at -80°C.

Frozen *E. coli* cells were slowly thawed on ice. The thawed cells were mixed with 100 µl of ligation or Gibson assembly reaction mix, incubated on ice for 20 min, followed by a heat shock for 45 sec at 42°C. The cells were mixed with prewarmed 900µl of SOC (table 3) and were incubated for 1h at 37°C. Afterwards 100 µl of the cultures was plated on a LB agar plate with the corresponding antibiotic, the rest was concentrated by centrifugation and 800 µl of the supernatant was discarded. The cell pellet was resuspended and plated out as well. The plates were incubated at 37°C overnight.

2.5.3 Growth conditions of *B. subtilis* cells

B. subtilis cultures were grown at 30°C and 200 rpm in LB or at 30°C on LB agar with the exception of cells grown for microscopy (when the cells got cultivated in $S7_{50}$ minimal medium, Table 1), or for reaching their competence to take up DNA molecules (see 2.2.4). Like with *E. coli* cultures, the growth was measured at OD_{600}.

2.5.4 Preparation and transformation of competent *B. subtilis* cells

B. subtilis was prepared for transformation with two different methods: In the first case SpC and SpII, and in the second case, MC medium were used. *B. subtilis* is naturally competent and is able to take DNA fragments up in the stationary phase and incorporate the taken up DNA.

2.5.4.1 MC medium method

For this method, the 10 ml of MC medium (components in Table 1) were freshly prepared and an overnight culture was inoculated into the MC medium to an OD_{600} of 0.1. This culture was then incubated at 37°C for about 3h, or until an OD_{600} of 1.4 was reached. For this method, fresh medium should be prepared every time and used up immediately after preparation.

2.5.4.2 SpC and SpII method

For the preparation of *B. subtilis* competent cells with the help of an SpC and an SpII medium, an overnight culture was inoculated into 20 ml of SpC medium (Table 1) to reach an OD_{600} of 0.1. The inoculated SpC culture was incubated at 37°C until an exponential growth was reached (OD_{600} of ~ 0.3- 0.6). Subsequently, this culture was diluted 1:10 into prewarmed SpII (Table 1, 20 ml into 200ml) and incubated for another 90 min at 37°C. The culture was centrifuged at room temperature, 4200 rpm for 15 min (Centrifuge Beckman Rotor 16.25). 18 ml of the supernatant was kept in a sterile tube for resuspending the cell pellet, the rest of the supernatant was discarded. If the competent cells needed to be prepared for later, 2 ml of sterile 50% glycerol was mixed into the cell resuspension and 200 µl aliquots were frozen.

2.5.4.3 Transformation of *B. subtilis* cells

For transforming *B. subtilis*, 3 sterile tubes were filled with 200 µl of competent cells and either 3 µl and 6µl of the relevant plasmid, or 0.3 µl and 0.6 µl of chromosomal DNA were added. The cultures were incubated at 37°C for 30 min up to 2h, afterwards the cultures were plated out onto solid LB plates with the corresponding antibiotic and incubated at 30°C until colonies became visible.

2.5.4.4 Markerless deletion of genes and exchange of resistance cassette in *Bacillus subtilis*

Exchanging the resistance cassette was achieved by transforming a *Bacillus subtilis* strain containing an mVenus fusion at the original locus with a cm resistance cassette with the plasmid RL1848. The transformants were selected on tet LB agar plates and were subsequently validated by streaking the transformants on tet or cm LB agar plates to check the complete replacement of the cm resistance cassette to the tet resistance cassette.

The deletion strains were obtained from the Bacillus genetic stock centre, thus the plasmid pDR244 can be used to create a markerless deletion by removing the kanamycin or erythromycin resistance cassette from the strains (Koo et al., 2017). The temperature-sensitive plasmid pDR244 contains a Cre recombinase exciting the resistance cassette flanked by DNA recognition site for the recombinase. *Bacillus subtilis* transformants containing the pDR244 plasmid were selected for a spectinomycin resistance cassette at 30°C and were afterwards streaked on a LB agar plate not supplemented by an antibiotic. Those plates were incubated at 42°C and the transformants were restreaked on LB agar plates supplemented with spectinomycin, kanamycin and a plate without an antibiotic supplement. In the end, transformants were observed to have lost the pDR244 and the antibiotic resistance cassette if they were growing on the LB agar plate without the antibiotics and not on the LB agar plates complemented with spectinomycin or kanamycin.

2.5.5 Determination of cell density

The optical density is a way of determining the number of cells per ml of culture. For obtaining the density, 1 ml of a cell culture was measured either undiluted or diluted (1:100) in a microcuvette with the help of a cell density meter.

2.5.6 Long-term storage of bacteria

All generated bacterial strains were grown to the late exponential phase and were supplemented with glycerol to reach a final glycerol concentration of 30% (v/v). Subsequently, bacterial stocks were then long term stored at -80°C.

2.6 Molecular biology methods

2.6.1 Polymerase chain reaction (PCR)

PCRs were used to amplify the wished-for DNA fragment (Mullis et al., 1986) with a Phusion DNA Polymerase or to look for positive transformants with a Colony PCR and a Taq Polymerase. A commonly used PCR reaction mix contained the ingredients listed below (Table 4) and the reactions were performed in a Thermocycler with the setting recommended by the manufacturer (New England Biolabs, England, Table 5).

Table 4: PCR Reaction Mix for Phusion high fidelity DNA polymerase and Taq Polymerase for 50 µl

Phusion reaction mix	**components**	**Taq polymerase reaction mix**
~ 100ng	DNA	~ 100ng
10 µl	manufacturer-specific supplied polymerase buffer	10 µl
1 µl	10mM dNTPs	1 µl
2.5 µl	10 µM primer forward	1 µl
2.5 µl	10 µM primer reverse	1 µl
0.5 µl	Polymerase	0.25 µl
1.5 µl	DMSO	/
Add to 50 µl	ddH_2O	Add to 50 µl

Table 5: PCR program for Phusion DNA Polymerase and Taq Polymerase, T_M is dependent on the oligonucleotide (primer)

Phusion	**temperature**	**time**	**Taq Polymerase**	**temperature**	**time**
Initial denaturation	98°C	30 sec	Initial denaturation	95°C	30 sec
	98°C	10 sec		95°C	30 sec
25-35 cycles	T_M	30 sec	25-30 cycles	T_M	60 sec
	72°C	30 sec per kb		68°C	60 sec per kb
Final extension	72°C	10 min	Final extension	68°C	5 min
	10°C	∞		10°C	∞

All PCR products were analysed by agarose gel electrophoresis and cleaned up by QIAquick Gel Extraction Kit (QIAGEN) before subsequently being used for endonuclease digestion or Gibson assembly.

2.6.2 Agarose gel electrophoresis and gel extraction

To separate DNA fragments by size, agarose gel electrophoresis was performed. A 1% agarose gel was generated by mixing 1% (w/v) of agarose (Carl Roth GmbH & Co. KG, Germany) with the desired volume of TAE- Buffer (Table 3). This mixture was heated up, mixed with 1µl per 100 ml of Midori Green DNA staining solution (Nippon Genetics Europe GmbH) and was poured into the fitting cast. After the gel was solidified, it was moved into the agarose gel electrophoresis chamber filled with TAE buffer. The DNA samples were mixed with 6x DNA Loading Dye (New England Biolabs, England). The gel electrophoresis was carried out at ~100V and subsequent was visualised by UV light.

2.6.3 Digestion of DNA molecules by restriction endonucleases

All digestions of linear PCR products or plasmid DNA were carried out with buffers and restriction endonucleases from New England Biolabs (England) and the manufacturer instructions were taken into account. To prevent re-ligation of the linearized plasmid DNA, 1 µl of a calf intestinal phosphatase (CIP) was added to the reaction mix. Afterwards, the DNA was purified either by gel extraction or by PCR product purification.

Table 6: Restriction digest reaction mixes

Vector		**Insert**	
1.5 µg	Plasmid DNA	1 µg	PCR product
1 µl	per restriction enzyme	0.5 µl	per restriction enzyme
5 µl	10x buffer	5 µl	10x buffer
add to 50 µl	ddH_2O	add to 50 µl	ddH_2O

2.6.4 Ligation of DNA fragments

In this thesis, two different types of ligations were performed, either using the T4 Ligase or a Gibson Assembly reaction mix already containing all necessary enzymes.

2.6.4.1 Gibson assembly

For the Gibson assembly (Gibson et al., 2009), the digested vector and undigested PCR product were mixed in a ratio 1:3 or 1:5 with the Gibson Assembly Mix and incubated for 60 min at 50°C prior to a transformation in *E. coli* as previously explained in 2.3.2.2.

2.6.4.2 T4 ligase approach

For the T4 Ligase approach, the digested vector and PCR product were mixed in either a ratio 1:5 or 1:3 with 1 µl of T4 ligase and 2 µl T4 DNA ligase buffer added for a 20 µl reaction. The reaction mixes were incubated at 30°C for 2h or 37°C for 1h prior to transformation (2.3.2.2)

2.6.5 Isolation of Plasmid DNA from *E. coli* and chromosomal DNA from *B. subtilis*

Plasmid DNA from *E. coli* was isolated with a plasmid purification kit based on alkaline lysis and was performed by the manufacturer´s manual. To isolate chromosomal DNA from *B. subtilis*, the innuPREP Bacteria DNA Kit (Analytic Jena, Germany) was used. The concentrations of the purified DNA were determined by the NanoDrop™-Spectrometer (Thermo Scientific, USA).

2.6.6 DNA sequencing

Subsequently, the constructed plasmids were verified via Sanger sequencing (GATC, Germany and Eurofins Genomics, Germany).

2.7 Biochemical methods

2.7.1 Western blot analysis of *B. subtilis* strains

To confirm that the full-length strains were intact and functional, cell lysate of the corresponding strain was used for western blot analysis with a specific antibody against GFP (mVenus is a derivate of the GFP fluorophore) or the proteins themselves.

For the cell lysate, cells were grown as described previously in 2.4.3.5, and 10 ml of the culture was centrifuged at 3500 rpm 15 min RT. The supernatant was discarded and the pellet was resuspended in a western blot lysis buffer (table 3) freshly supplemented with 2.5 mg/ml lysozyme, 0.01 mg/ml DNase and 0.1 mg/ml RNase. The resuspended cells were incubated at 37°C until the solution was sufficiently lysed. The samples were mixed with a 4x SDS loading dye and incubated over night at RT.

The samples were run on a 10% SDS-gel at 150V until the blue dye front was run out of the gel. The SDS-gel was transferred onto a nitrocellulose membrane via a blotting chamber. The membrane was blocked for 2 h in 5% skimmed milk dissolved in PBST. After 2 h, the membrane was rinsed with PBST to remove residual skimmed milk and the first specific antibody anti GFP (1:1000) or anti mreB (1:1000) in skimmed milk was added. After incubation with the second antibody the membrane was detected and documented.

2.7.2 BOCILLIN-FL analysis of PBP activity

To confirm that the fluorophore fusions of the PBPs are still enzymatically active, the capability of them binding BOCILLIN-FL (Thermo Fisher Scientific, USA) was tested. BOCILLIN-FL is a penicillin V derivate fused to a BODIPY-FL dye and is binding to the active site of most PBPs. The protocol used was a modified version of the protocol first developed and published by Kocaoglu & Carlson (2013). The cells were only lysed with the help of lysis buffer used for the western blots after the PBPs were marked by the BOCILLIN-FL and subsequently 20 µl cell lysate were loaded on 10% SDS-PAGE gel. To visualize this gel a typhoon gel scanner was used.

2.8 Single molecule tracking (SMT)

2.8.1 Sample preparation

For the single molecule tracking approach, bacterial cells were cultured as previously described in 2.4.3. After the cultures reached an OD_{600} of 0.4 - 0.6, the cells were treated with the different osmotic stressors or the antibiotics for 30 min. Subsequently, 5 µl of the cultures were spotted on a cleaned round glass cover slide (Ø 25 mm, Paul Marienfeld GmbH & Co. KG, Germany) and covered by an agarose pad to secure the bacterial cells and keeping them from drying out.

2.8.2 SMT microscopy

All single molecule tracking experiments were performed with a customised inverted slim field Nikon Ti Eclipse microscope (100 x oil immersion objective, NA = 1.49) with a high speed EMCCD camera (ImageEM X2, Hamamatsu) and 514 nm diode beam laser as a setup. The movies were obtained with a stream acquisition every 20 ms over a period of 60 s to first bleach the fluorescence fusions to a single molecule level.

2.8.3 Data analysis of SMT data

All data obtained by the single molecule tracking was subsequently processed in the workflow shown in Figure 7 below. The movies were cropped to a total length of 1500 – 2000 frames after the protein signal was bleached to single molecule level. The cell outlines were set with the help of the summarised single molecule signal and the brightfield picture of the corresponding movie. Utrack (Jaqaman et al., 2008) was used to generate trajectories by connecting the single molecule signal between the frames of the movie. To analyse the single molecule data and to generate the figures shown in the result section, the software SMTracker (Oviedo-Bocanegra et al., 2021; Rösch et al., 2018) was used. Detailed information about the software can be found in the supplementary table S4.

Figure 7: standard workflow for analysis of SMT data

3. Results

3.1 Contributions to published articles

Super-Resolution Microscopy and Single-Molecule Tracking Reveal Distinct Adaptive Dynamics of MreB and of Cell Wall-Synthesis Enzymes

Simon Dersch, Johanna Mehl, Lisa Stuckenschneider, Benjamin Mayer, Julian Roth, Alexander Rohrbach and Peter L. Graumann

Frontiers Microbiology, 20 August 2020

I constructed the original locus mVenus-PbpH strain and performed the single-molecule tracking experiments with the mVenus-PbpH strain shown in Fig. 4, 5, S4, S5 and movie S3.

Stable inheritance of *Sinorhizobium meliloti* cell growth polarity requires an FtsN-like protein and an amidase

Elizaveta Krol, Lisa Stuckenschneider, Joana M. Kästle Silva, Peter L. Graumann and Anke Becker

Nature Communications, 22. January 2021

I performed the single-molecule tracking experiments of mVenus-RgsS with different genetic backgrounds shown in Fig. 5, S22 – S25 and table S9. I processed and analysed the data of the SMT experiments as well as wrote the part analysing the data together with Prof. Dr. Peter L. Graumann.

3.2 Unpublished manuscript

Investigation of *Bacillus subtilis* Penicillin binding proteins at the single molecule level reveals distinct dynamics indicative of changing requirements during stress adaptation

Lisa Stuckenschneider and Peter L. Graumann*

SYNMIKRO, LOEWE-Zentrum für Synthetische Mikrobiologie, Hans-Meerwein-Straße, 35043 Marburg, and Fachbereich Chemie, Hans-Meerwein-Straße 4, 35032 Marburg, Germany

*corresponding author, email: peter.graumann@synmikro.uni-marburg.de

+49(0)64212822210

Running title: Single molecule dynamics of *B. subtilis* PBPs

Contributions

I designed and carried out all of the included experiments of this unpublished manuscript, as well as the data analysis, figure and supplement preparation. The manuscript was concepted and written by me, Lisa Stuckenschneider, and Prof. Dr. Peter L. Graumann.

Abstract

The functions of proteins involved in cell wall synthesis have been investigated at a genetic and biochemical level; their dynamics in time and space are still poorly understood. We have used single molecule tracking to investigate dynamics of four penicillin-binding proteins (PBPs) in *Bacillus subtilis* to shed light on their possible modes of action. We show that Pbp2a, Pbp3, Pbp4 and Pbp4a, when expressed at very low levels, show at least two distinct states of mobility: a state of slow motion, likely representing molecules involved in cell wall synthesis, and a mode of fast motion, likely representing freely diffusing molecules. Except for Pbp4, all other PBPs showed about 50% molecules in the slow mobility state, suggesting that roughly half of all molecules are engaged in a substrate-bound mode. We observed similar coefficients for the slow-mobility state for Pbp4 and Pbp4a on the one hand, and for Pbp2a and Pbp3 on the other hand, indicating possible joint activities, respectively. Upon induction of osmotic stress, Pbp2a and Pbp4a changed from a pattern of localization mostly at the lateral cell membrane to also include localization at the septum, revealing that the site of preferred positioning for these 2 PBPs can be modified during stress conditions. While Pbp3 became more dynamic after induction of osmotic stress, Pbp4 became more static, showing that PBPs reacted markedly differently to envelope stress conditions, suggesting increased or decreased needs of the cell for specific PBPs during stress conditions. All PBPs lost their respective localization pattern after addition of vancomycin or penicillin G, showing that patterns largely depend on substrate availability, and indicating that even carboxypeptidase Pbp4a is sensitive to vancomycin and penicillin G. Our data support the idea that cell wall synthesis is driven by transient interactions of synthesis enzymes, rather than by a stable multiprotein complex, and that sites of activity and protein dynamics markedly change under stress conditions.

Introduction

Bacteria are found in different shapes (coccoid, rod shaped or higher degrees of morphologies). These shapes are maintained and determined by the cell wall, a sacculus of so-called Murein or Peptidoglycan (PG). The rigid cell wall is built up of single or multiple layers, with a thickness of ~ 3-6 nm for Gram-negative and 10 – 40 nm for Gram-positive bacteria [1], to maintain cell shape as well as to make the cell more resilient against environmental influences like osmotic changes, which can lead to a turgor change of the bacterial cell. The cell wall layers consist of Peptidoglycan chains interconnected by peptide bridges to build a mesh-like, strong sacculus. PG polymer chains may have variable lengths and are composed of N-acetylglucosamine (GlcNAc) and N-acetylmuramic acid (MurNAc) disaccharide subunits. The pentapeptide side chain, containing L- and D-amino acids, is attached to the MurNAc part of the disaccharide subunit [1, 2].

As the bacterial cell is a growing and dividing entity, the peptidoglycan layers need to grow with the cell by lateral insertion of new PG chains into the sacculus [2, 3]. Essential players in this process are Penicillin Binding Proteins (PBPs) and glycosyltransferases (GTase) RodA and FtsW [2, 3]. The *Bacillus subtilis* genome encodes 16 genes categorized as encoding PBPs, which have redundancies in their enzymatic activities. PBPs can be subdivided into four classes. Class A PBPs are high molecular weight proteins with dual functionality, having a transglycosylase (TG) and transpeptidase (TP) activity, for the elongation of PG strands or their crosslinking, respectively. Class B PBPs are monofunctional high weight proteins with TP activity, i.e., catalysing the crosslinking of the peptide side chains. Additionally, there are two low molecular weight proteins classes of PBPs with two different activities, carboxypeptidase and endopeptidase, that are required to keep the PG crosslinking at a certain level specific for the bacterial cell [1, 2, 4-7].

Class A PBPs have recently been shown to confer a role in cell wall repair, rather than cell wall extension in *Escherichia coli* [8]. In case this is true for other bacteria as well, it will be of widest interest and shed a new light on the function of some PBPs. Also, several PBPs have been shown to be involved in cell division rather than in cell elongation, because they localize to division sites rather than to the lateral sides of rod shaped (or curved) cells [4]. However, many of the functions of the multiple PBPs are still unclear. Therefore, we aimed at further understanding of the dynamic behaviour of *B. subtilis* PBPs during exponential growth, and under cell wall stress conditions, in order to gain deeper insight into three-dimensional organization of cell wall synthesis and maintenance. We used single molecule tracking (SMT) to determine and quantify molecules with different mobilities of four different PBPs, assuming that slow-moving

ones are involved in the insertion of peptidoglycan, during cell growth and under different types of stress (osmotic and antibiotic). We analysed one Class A, two Class B PBPs, and one PBP having a carboxypeptidase activity (Fig. 1A). According to *in vivo* observation, PBPs are thought to travel along paths perpendicular to the long axis of cells, together with enzymes extending the PG strands, as well as with MreB [9-11]. Mobilities of MreB and of PBPs have been determined to be in the range of 20 to 50 nm/s [12-14], which under SMT conditions is characterized by low mobility, in contrast to free diffusion, which results in much higher diffusion constants of molecules [15]. As freely diffusing molecules cannot be captured by conventional epifluorescence or TIRF microscopy, we analyzed PBP mobilities using SMT. We found similarities in movement of PBPs, indicating possible cooperation in activities, but also differences, especially during stress conditions. In such conditions, the localization and modes of motion showed considerable changes, indicating that different PBPs may play different roles during adaptation to cell wall stress, possibly by reorganizing cell wall synthesis, or by simply adapting to different conditions within the cell envelope.

Methods

Strain preparation

All strains were produced with a modified pHJDS vector [16] to generate N-terminal fusion proteins with mVenus. The pHJDS is an integration vector to insert the fusion protein into the original locus on the genome by single crossover homologous recombination. pHJDS contains two resistance cassettes (a *bla* and *cat* gene). Plasmids were constructed with the help of Gibson Assembly (Gibson-Assembly® Master Mix Hifi, New England BioLabs) to ligate the insert consisting of the first 500 base pairs of the corresponding gene with the linearized pHJDS vector. The vectors were then introduced into *E. coli* and 100 µg/ml ampicillin LB agar plates were used to select for transformants. Isolated plasmids were checked by sequencing and subsequently used for the transformation of *Bacillus subtilis* PY79 or the deletion strains. Transformants were selected by carrying the chloramphenicol resistance cassette on LB agar plates with 5 µg/ml chloramphenicol.

Cell cultivation

All strains (table S1) were cultivated on LB agar plates or in liquid LB medium with the corresponding antibiotic at 30°C under aeration for *Bacillus subtilis* PY79 or 37°C for *Escherichia coli* cultures. All fusions were induced with 0.01% xylose, such that a barely detectable level of protein was generated. For microscopy, *Bacillus subtilis* strains were grown overnight in LB medium containing 5 µg/ml chloramphenicol and were then inoculated into minimal medium ($S7_{50}$), having a low intrinsic fluorescence, at an OD_{600} of 0.1. The cultures were grown until an OD_{600} of 0.6 - 0.8 and were then used for microscopy. For the stress assays, 0.5 M NaCl, 1 M sorbitol, 4 µg/ml vancomycin or 4 µg/ml penicillin G were added to the culture that were incubated for additional 30 min.

Sample preparation for microscopy

For single molecule tracking, background fluorescence was reduced by cleaning the round slides (25 mm, Paul Marienfeld GmbH & Co. KG) with 1% Helmanex® III (Hellma GmbH & Co. KG) solution for 30 min in a sonication bath. Next, slides were washed in distilled water 3-4 times before treating them for another 30 min in the sonication bath. To immobilize cells and to keep them under continued growth, agar cover slips were prepared in 10 mm glass slides, Paul Marienfeld GmbH & Co. KG, by adding 1% extra clean agarose to $S7_{50}$ minimal medium. 5 µl of the cell culture were dropped on the slide and an agar slide was put onto the drop of cell culture.

Single molecule tracking microscopy and data processing

For single molecule tracking a customized slim field microscope (Nikon Eclipse Ti microscope; 100 x oil-immersion objective, NA= 1.49, Nikon) equipped with a 514 nm laser diode beam line (100 mW power) and an EMCCD camera (ImageEM X2 EM-CCD, Hamamatsu) was used to generate the data. The beam was extended 20-fold, and its central part was focused on the back focal plane of the objective, generating an almost parallel illumination of a circle with roughly 10 µm diameter, with relatively even energy distribution [17]. Energy values were close to 160 W cm^{-2} of power density. All movies were generated with following settings 20 ms, 20 mW laser power and 3000 frames.
For processing the data three major steps were performed. Firstly, the movies were cropped to the same length of 2001 frames to remove the initial frames not being at signal molecule level. This state can be deduced from a decay curve using SMTracker 1.5. The cropped movies were summed up to have a projection of the fluorescence signal in the cell. For this process the freely available software Fiji [18] was used. The sums and the brightfield pictures were subsequently used for the cell outlines with the help of Oufti [19]. To generate trajectories having a minimum length of 5 frames from the movies, Utrack [20] a Matlab-based program, was used. Finally, data were analysed using SMTracker software [21]. Figures generated in and taken from SMTracker 1.5 software (https://sourceforge.net/projects/singlemoleculetracker/) and were modified with the help of Matlab.

Western Blot

Cells were cultivated as for microscopy with 0.5% xylose to have a higher amount of the corresponding fusion protein. Pellets from 50 ml cultures were resuspended in 1 ml of lysis buffer containing 100 mM NaCl, 50 mM EDTA, 0.1 mg/ml RNase, 0.01 mg/ml DNase, 1.26 mg/ml Lysozyme and were subsequently mixed with 4x SDS sample buffer. 20 µl were loaded on a 10% SDS gel. The mVenus tagged proteins were detected using an anti-GFP antibody and the membrane was treated Immobilon Forte Western HRP substrate (Merck) to visualise the proteins.

Results

SMT-based determination of the spatial pattern of PBPs

We generated N-terminal mVenus-YFP fusions to Pbp2a, Pbp3, Pbp4 and Pbp4a, which were integrated at the original gene locus, and thus expressed as sole source of the protein. We found that a low level of induction using 0.01% xylose driving the xylose promoter resulted in cells that had regular rod shape, and that grew similar to wild type cells (Fig. 1B). Functionality of the constructs was tested via a western blot (Fig. S2) and by generating strains with deletions of paralogous genes and the mVenus-PBP-fusion [22-24]. Δ*pbpH* cells expressing mVenus-Pbp2a or Δ*pbpG pbpF ponA* triple mutant cells expressing mVenus-Pbp4 showed normal morphology as well as normal growth rates (Fig. S3), suggesting functionality for these two fusions. In order to avoid overexpression artefacts, all fusions were expressed at very low level; even at full induction of 0.5% xylose, they were barely detectable via Western blotting (Fig. S2). We performed growth curves of all created mVenus-PBP strains, which grew similar to wild type *Bacillus subtilis* strain PY79 lacking any fusion construct (Fig. S1). Thus, with the caveat that we could not prove functionality for the Pbp3 and Pbp4a fluorescent protein fusions, we continued to investigate the dynamics of the few molecules expressed, which is possible using single molecule imaging.

We expected that all PBPs would move within the cell membrane, which has indeed been shown for Pbp2 [8, 25, 26] in *E. coli*, as well as for GTase RodA [27, 28] in *E. coli,* and that they would be associated with the PGEM (Peptidoglycan elongation machinery) in *B. subtilis* cells. Conventional fluorescence microscopy has its limits in visualizing (membrane) proteins *in vivo*, because diffusive motion of proteins blurs out distinct signals between frames, with exposure times being in the range of several hundred milliseconds. Therefore, we turned to single molecule tracking (SMT) microscopy, to gain further insight into the behaviour and dynamics of different classes of PBPs. We used YFP-based SMT [17] to avoid inhibition of growth due to blue light inhibition, and obtain continued growth of cells [29]. We tracked molecules (signals) using 20 ms stream acquisition to visualize even freely diffusive molecules. The obtained movie data were processed to obtain molecule tracks (only 5 or more continuous steps were taken into account) using utrack [20], and all further data analyses were done using SMTracker 1.5, which is an extended version of the original program [21]. Keeping in mind the caveat of a possibly reduced functionality, we observed different localization patterns for the four PBPs, when all signals from stream acquisitions were overlaid into a single image (sum of frames from SMT): Pbp4 and Pbp4a showed a regular distribution throughout the cell membrane, while Pbp2a and Pbp3 revealed a more heterogeneous localization within

the cell membrane (Fig. 1B). Scheffers et. al [4] localized all 16 PBPs of *B. subtilis* using epifluorescence, and the patterns observed for Pbp3 and Pbp4 agree with our sums of the SMT data (Fig. 1B). Pbp2a had a more patchy/less uniform distribution in our data sets compared to those observed before, while Pbp4a was more equally distributed within the membrane compared to the more patchy localization from Scheffers et al. [4]. We believe that our analysis using high speed acquisition and high localization precision (usually below 50 nm) more accurately describes protein localization than conventional fluorescence microscopy. In any event, our data are in a qualitatively good agreement with previous studies and reveal membrane-localization for all four fusion proteins, including Pbp4a where the nature of the membrane attachment was possibly altered through the mVenus fusion.

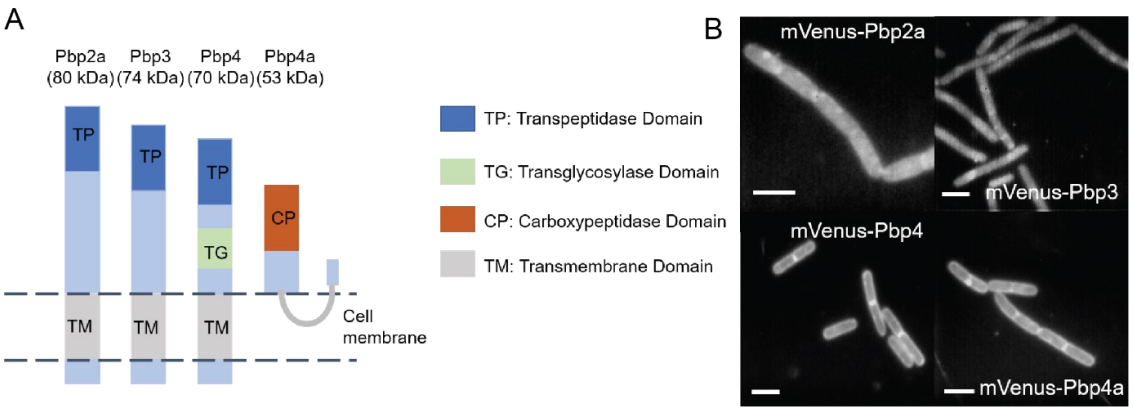

Fig. 1 membrane association and localization. A shows a schematic cartoon of the targeted four PBPs of *Bacillus subtilis* and their enzymatic domains. Note that it is still under debate whether Pbp4a has a membrane hook or α helix, which may be altered through the N-terminal fusion protein (FP) attached in this study **B** sum of single molecule tracking data of FP-PBP fusions. Scale bars 3 μm.

PBPs move as two populations with distinct mobilities

After localization was analysed via summing up of molecule tracks, we moved on to investigate the diffusive behaviour of the four PBPs. The four PBPs were chosen for their different enzymatic activities. All are predicated to interact with MreB, based on bacterial two-hybrid analyses and pull-down experiments [30]. For MreB and Pbp2a the single particle approach of Garner et al. (2011) has shown that components of the PGEM can be separated into two different population, one moving slowly and directionally, and the other one fast and non-directionally [10]. Similar results have been shown by Dersch et al. [31] for PbpH, a redundant transpeptidase of Pbp2a in *Bacillus subtilis* [22], and for RodA and MreB [15]. Interestingly, for Pbp2 in *E. coli*, SMT analysis has also shown that two distinct mobilities for molecules exist, a freely diffusive population, and a slow

mobile fraction, the latter of which has been suggested to be involved in enzymatic function, i.e., extending and /or crosslinking of newly incorporated cell wall material [12]. We wished to investigate if this is also true for different PBPs from *B. subtilis*.

To compare the different proteins, we first used jump distance (JD) analysis, which is based on squared displacement (SQD) analysis to quantify the mobility of each of the mVenus-PBP fusions. Obtained data could not be satisfactorily explained using a single Rayleigh fit, but were well explained using two fits (note that SMTracker 1.5 uses several statistical tests, R^2 values of >0.98 were obtained using two simultaneous fits), indicating the existence of two populations with significantly different diffusion constants (Fig. 2A-D). This can be seen in Fig. 2A-D, where the sum of two Rayleigh fits can explain the observed jump distances very well. Note that SMTracker uses Bayesian Information Criterion to avoid over-fitting of data. We deduce from these findings that all four PBPs alternate between a freely diffusive state, and a low mobility state in which they are engaged in cell wall synthesis, similar to what has been shown for other PBPs in *Bacillus subtilis* [10, 15] and Pbp2 in *E. coli* [12].

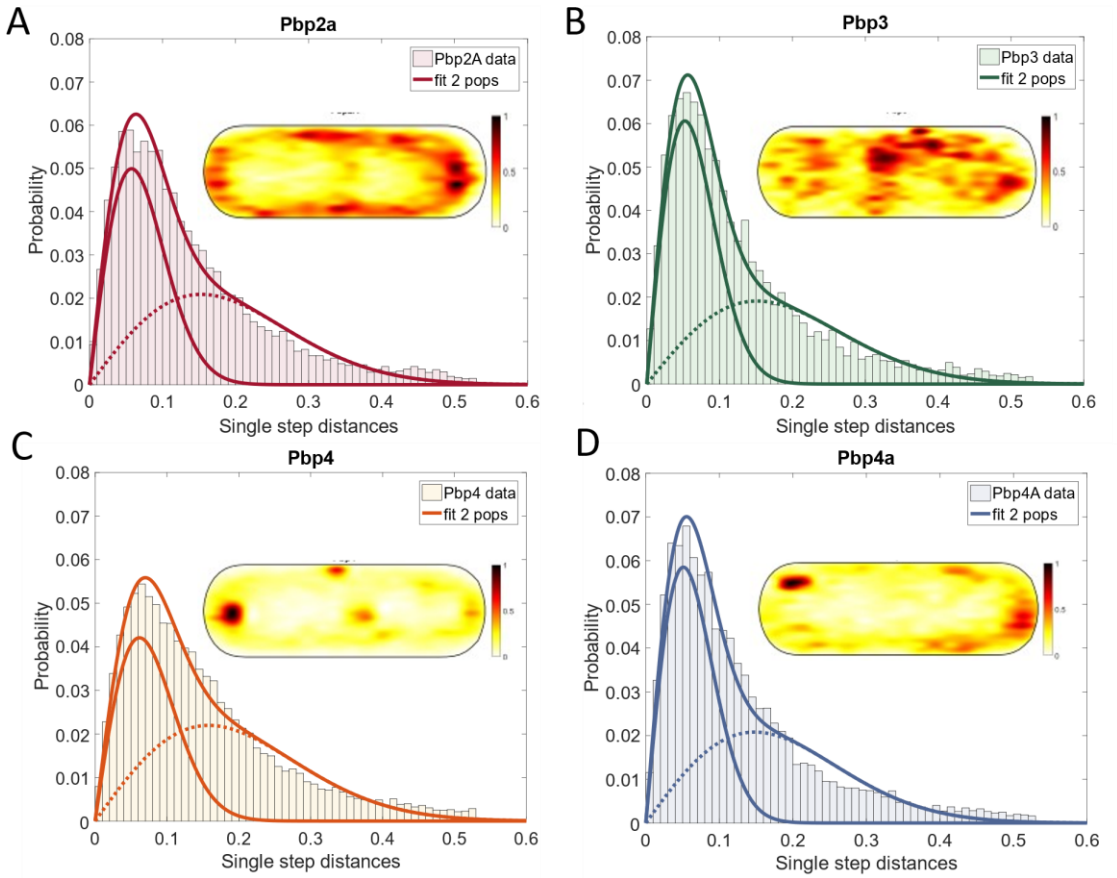

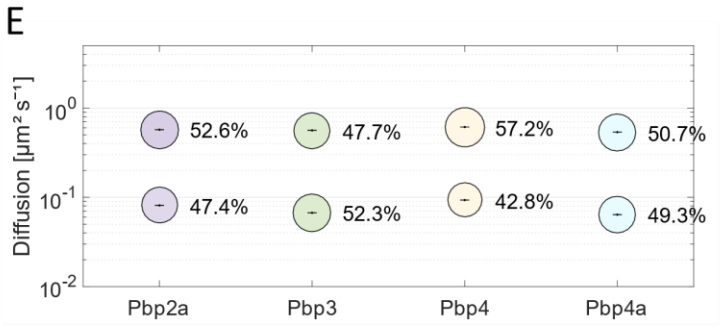

F

	Pbp2a	Pbp3	Pbp4	Pbp4a
Pop_1 [%]	47.4 ± 0.002	52.3 ± 0.002	42.8 ± 0.001	49.3 ± 0.002
Pop_2 [%]	52.6 ± 0.002	47.7 ± 0.002	57.2 ± 0.001	50.7 ± 0.002
D_1 [µm² s⁻¹]	0.0812 ± 0	0.0671 ± 0	0.0932 ± 0	0.064 ± 0
D_2 [µm² s⁻¹]	0.572 ± 0.002	0.562 ± 0.003	0.613 ± 0.002	0.537 ± 0.003

Fig. 2 Analysis of PBP dynamics and localization. **A-D** shows the jump distance fit of the SMT data of the four different PBPs in comparison. **E** visualizes the two diffusive populations of the four different PBPs in a bubble plot. **F** sums up the information of the other graphics in a table.

In SMTracker, all observed tracks can be projected into a standardized, a medium-sized cell of 3 x 1 µm. From these “heat maps”, shown as insets in Fig. 2A-D, the most probable localization for all molecules detected can be deduced. In our case, the localization was membrane-associated for all four PBPs, as expected. To most accurately follow the trajectories of molecules at the cell membrane, and thus most correctly determine diffusion coefficients, the focal plane was shifted from the middle of the cells (with regard to the short axis) to the upper part of the cells. This way, we could track molecules diffusing along the length of cells as well as those moving along the short axis (i.e., moving perpendicular to the long axis); circumferentially moving molecules move out of plane when the focus is at the cell middle. Therefore, heat maps also show enrichment of signals towards the cell centre, and away from the very edge of cells. For Pbp3 and Pbp4, a tendency to localize at the septal area was visible, in accordance to the described localization from Scheffers et al. [4] and Sassine et al. [32]. Being one of two known transpeptidases for elongation [10, 22], Pbp2a had an almost equal distribution between the size of static and mobile fractions (D_1 = 0.0812 µm^2/s (47.4%); D_2 = 0.572 µm^2/s (52,6%), Fig. 2F and table S2). These diffusion coefficients are not identical to the velocities know from the literature because we use a slightly different approach of microscopy as well as for calculations [9, 10]. A similar behaviour was observed for Pbp4a (D_1 = 0.064 µm^2/s (49.3%); D_2 = 0.537 µm^2/s (50.7%), Fig. 2F). Note that a diffusion coefficient of 0.5 to 0.6 µm^2/s is within the range of a freely diffusive membrane protein with a single transmembrane domain [33], while that of 0.06 or 0.08 is about ten-fold lower. The population sizes of Pbp3 (D_1 = 0.0671 µm^2/s (52.3%); D_2 = 0.562 µm^2/s (47.7%), Fig. 2F) were only slightly different from those of Pbp2a. These findings suggest that about half of these PBP molecules are diffusing in search of a potential binding site, while the other half is engaged in a slow mobile, likely enzymatically active state. Pbp4 diffusion coefficients (D_1 = 0.093 µm^2/s (42.8%); D_2 = 0.61 µm^2/s (57.2%), Fig. 2F) were comparable to those of Pbp2a. When comparing the diffusion coefficients of the four PBPs, there are quantitative correlations of D_1 between Pbp2a and Pbp4, and between Pbp3 and Pbp4a, indicating a possible functional interaction of those proteins in cell wall synthesis, when we assume that similar slow mobilities mean similar speeds (with regards to slow directional movement) within the enzymatically active mode. D_2 is comparable between all four PBPs, suggesting similar mobilities in the freely diffusive state. This is in agreement with the finding that diffusion constants of membrane proteins depend on the number of transmembrane domains, and not on the size of the soluble part(s) of the protein [33]. As described before [4], there seems to be an interaction between Pbp3 and Pbp4a, which is corroborated by a correlation of fraction sizes and of diffusion coefficients (Fig. 2E and F). It has also been claimed that Pbp4 might be

interacting with Pbp3 and Pbp4a, because of the localization patterns [4], but our tracking data are not supportive of this suggestion.
From our analysis, it is more likely that Pbp2a and Pbp4 are moving together, and when considering the biological functions (Pbp2a is a transpeptidase and Pbp4 is a bifunctional glycosyltransferase and transpeptidase), one might consider that a correlation of their diffusion constants may indicate a similar substrate binding - and synthesis activity.

The mobility of the PGEM (Peptidoglycan elongation machinery) transpeptidase Pbp2a is influenced by ionic stress and the antibiotic vancomycin

Based on the current level of knowledge it is assumed that all the different PBPs are responsible for parts of the peptidoglycan/cell wall synthesis, be it elongation or repair, but it is still unclear why so many PBPs are involved in this process. We wished to investigate how PBPs change their mobility under stress conditions that might have an effect on the cell wall. By analysing changes in static fractions after cell wall stress, which we assume correspond to changes in substrate binding and the enzymatically active state (or binding to the PGEM, which is less likely), we speculated we might be able to find differences in dynamics that could explain the partially overlapping functions of PBPs. We chose 0.5 M NaCl as moderate osmotic as well as ionic stress, 1 M sorbitol as moderate osmotic stress [34], 4 µg/ml vancomycin (which is similar to the commonly used concentration of 2 µg/ml (10 x MIC) [35]), as cell wall inhibitor binding to the D-alanyl- D-alanine of the peptide of nascent peptidoglycan units (inhibiting both transglycosylase and transpeptidase activity) [35-37] and 4 µg/ml penicillin G, as a β-lactam inhibiting PBPs activity via binding to the active site mimicking the terminal D-alanyl-D-alanine dipeptide as ring-opened form [36, 38, 39]. Stress conditions were applied at an OD_{600} 0.6 - 0.7 for 30 min before microscopy. All four stress factors led to a re-localization of Pbp2a compared to the non-stressed condition. The probability to find this PBP at the septal area was higher with the osmotic stress conditions (Fig. 3B and C), may be indicating a higher substrate availability at the septum during osmotic stress, since it's known that the substrate availability can alter the localization of Pbp2a [40]. Contrarily, addition of vancomycin and penicillin G led to a loss of the regular localization pattern (Fig. 3D and E). Note that diffusion coefficients remained constant because of the GMM (Gaussian mixture model) method used to analyse the data (D_1 = 0.077 µm^2/s; D_2 = 0.71 µm^2/s). GMM keeps D at one value calculated for all conditions (five in this case), to better compare changes in population sizes, which are most relevant for our analyses, and thus allow easier comparison of different conditions for one PBP. Therefore, D determined from GMM using 5 different conditions slightly differs from that estimated by JD for exponentially growing cells.

The mobility fractions of Pbp2a changed with NaCl and vancomycin stress application (30 min of treatment), however, with sorbitol the populations did not change significantly (Fig. 3F). With NaCl stress the static protein fraction became 8% smaller compared to the non-stressed condition (Fig. 3F, table S3), which was also shown for the redundant protein PbpH and the GTase RodA [15]. This effect was even more severe when the cells were stressed by vancomycin. Here, the static fraction shifted by 28% from 50% (non-stressed) to 36% (Fig. 3E). This is in agreement with reduced substrate availability for Pbp2a in the cell wall by vancomycin, which may also explain the more random localization seen in Fig. 3D. It is known that 100 µg/ml of vancomycin slow down the circumferential movement of PbpH (a transpeptidase redundant to Pbp2a [9]), which leads to the assumption that a concentration of 4 µg/ml vancomycin does not influence substrate as strongly [40]. In contrast to vancomycin, penicillin G had no considerable effect on the dynamics of Pbp2a (Fig. 3E and F). This might be explained by the phenomenon known from *E. coli*, where different ß-lactams effect different steps of the cell cycle [41]. Penicillin G or benzylpenicillin seem to just affect the division site-associated PBPs, while Pbp2a is known to be part of the elongasome, and it also known for the *E. coli* homologue to be less affected by penicillin G treatment [41]. However, our data suggest that PBPs relocates to the septum during mild stress conditions (Fig. 3B and C), hinting towards a possible secondary function of Pbp2a at the septum beside the important one in the PGEM machinery.

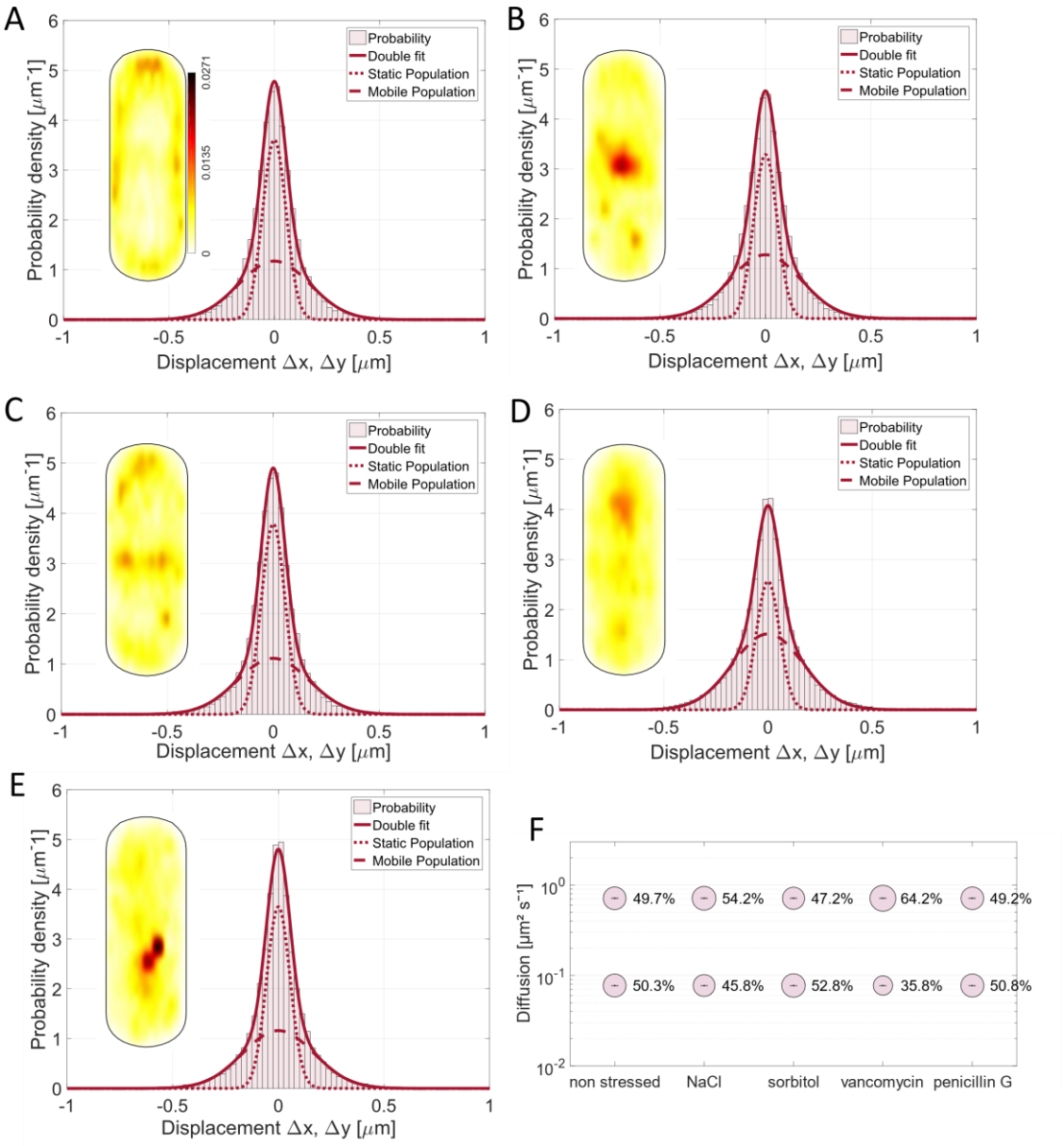

Fig. 3 Analyses of Pbp2a dynamics. A-E the Gaussian Mixture model fit of Pbp2a is shown for the non-stressed, 0.5 M NaCl, 1 M sorbitol, 4 µg/ml vancomycin and 4 µg/ml penicillin G conditions (30 min of treatment) indicating that the two-population fit sufficiently well explains the measured data. For each conditions the probability heat map of the localization is included as an inset, showing the different localization patterns of mV-Pbp2a. **A** contains the scale for all the heat maps. **F** bubble plot is showing the size of the population in % and the diffusion coefficients for Pbp2a mobility fractions.

Pbp3 mobility changes markedly under osmotic stress and antibiotic treatment

Pbp3 is a class B PBP with transpeptidase activity [4, 5, 32]. It most likely interacts with the divisome, but it has also been described to localize along the cell periphery as distinct foci and bands [4, 32]. This is in agreement with our SMT data, showing that Pbp3 is also enriched away from the division septum (Fig. 2B), and also shows a large concentration at mid cell (Fig. 2B, 4A). As observed for Pbp2a, we found a shift in the preferred localization of Pbp3 from the lateral sides to the septal area taking place under the applied osmotic stress conditions (Fig. 4A- C), indicating that the substrate for PG synthesis might be sensitive to high osmotic pressure conditions and might be available at different site. A stronger impact was observed upon the addition of vancomycin and penicillin G. This led to a completely altered pattern, where Pbp3 was entirely delocalized within the cell membrane (Fig. 4D and E). This suggests that availability of substrate plays a major role in the localization for Pbp3 as it is already known for Pbp2a/H, as well as for two other TPases of *B. subtilis* [40].

While 0.5 M NaCl had a minor effect on the diffusive behaviour of the protein (static fraction in non-stressed cells 55.4% or 59.2% after NaCl stress, Fig. 4F), the effects of 1 M sorbitol, 4 µg/ml vancomycin or 4 µg/ml penicillin G were more pronounced. The number of slow-moving molecules decreased by 15.9% (sorbitol stress) or 24.7% (vancomycin stress) or 21.8% (penicillin G stress) compared to the data from non-stressed cells (Fig. 4F). For vancomycin, we had expected that many Pbp3 molecules would shift from a substrate-bound to a mobile mode due to loss of binding sites as well as for penicillin G, which is in accordance to *E. coli* data stating that penicillin G is influencing the division site [41]. For sorbitol, we were surprised to see a large change, because on the other hand, the ionic stress caused by NaCl did not lead to such a marked difference in mobility. (Fig. 4F). Although we have no explanation for this phenomenon, it is apparent that the two stress conditions result in a considerably different mode of mobility for Pbp3, which we propose reflects changed conditions for cell wall synthesis during different environmental conditions.

As vancomycin forms a complex with the terminal D-Ala-D-Ala of the peptide side chain of the PG and binds to PG precursors [36, 37], it makes sense that addition of vancomycin lead to a higher proportion of unbound mVenus-Pbp3 proteins (as reflected by the increase in longer steps seen in Fig. 4D, compared with 4A) searching for an interaction site with the peptide side chains of PG strands, similar to Pbp2a. This indicates that substrate availability is an important determinant for PBP mobility, rather than an interaction with other proteins or a protein complex to extend or crosslink PG strands.

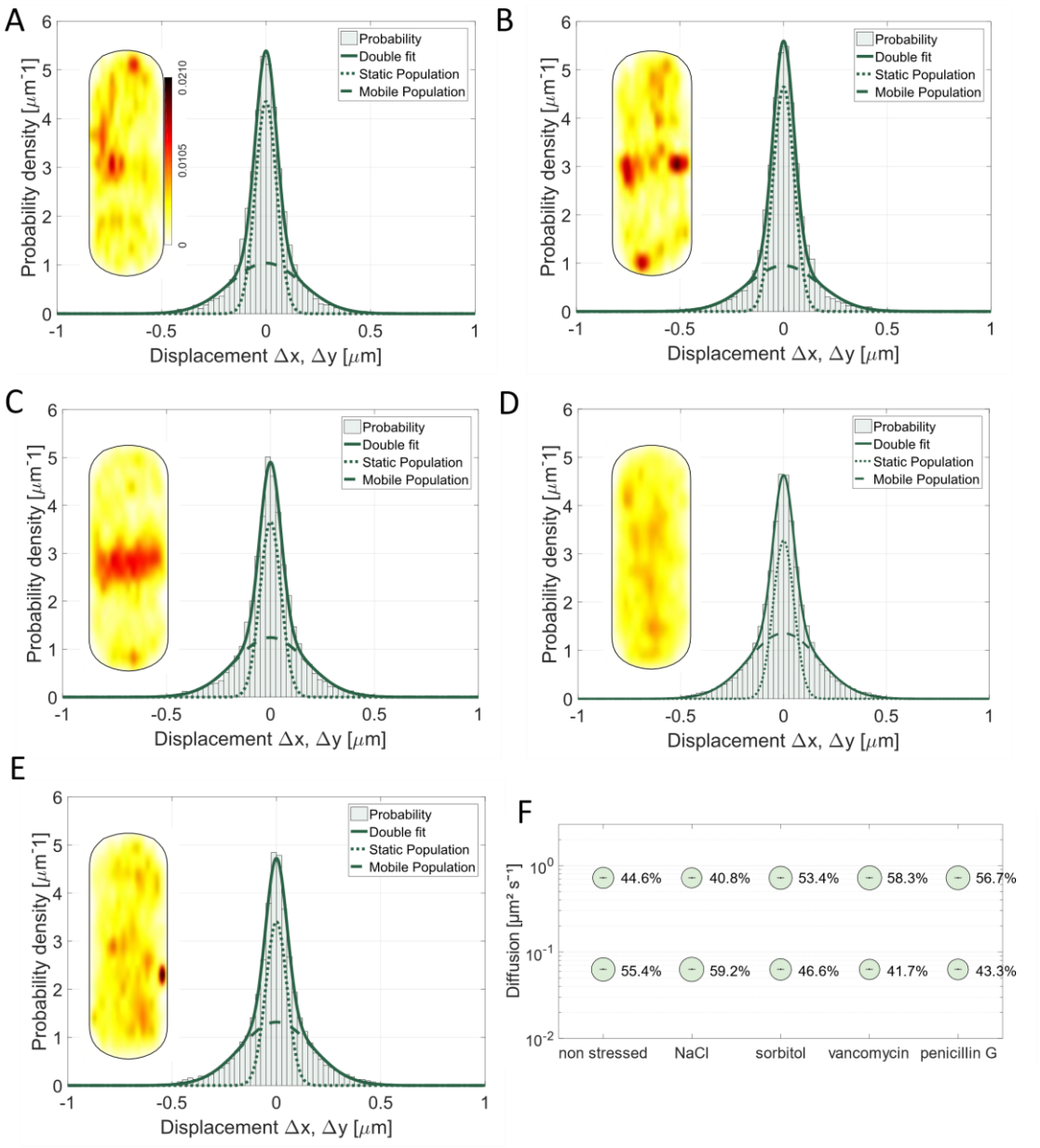

Fig. 4 Gaussian Mixture model fit of Pbp3 is shown for cells growing **A** non-stressed, **B** 30 min after addition of 0.5 M NaCl, **C** of 1 M sorbitol, **D** of 4 µg/ml vancomycin or **E** of 4 µg/ml penicillin G. A two-population fit was sufficient to explain the data sets. For each conditions the probability heat map of the localization is included, showing the different localization pattern of mV-Pbp3. **A** contains the scale for all the heat maps. **F** bubble plot showing the size of populations in %, and the corresponding diffusion coefficients for Pbp3.

Osmotic stress leads to an altered localization of Pbp4 but not the substrate availability altered by vancomycin

Pbp4 is a class A PBP with bifunctional activity (TG and TP) [4, 5, 23, 24]. The heat maps of the unstressed conditions correlate with the published localization of Pbp4 (septal localization and some peripheral orientations, Fig. 5A) [4]. When cells were stressed with 0.5 M NaCl for 30 minutes, no severe effect involving the Pbp4 fusion was noticeable. Despite of this, addition of 1 M sorbitol led to a profound increase of the static fraction, by 50.1% (Fig. 5C and F, table S5). This is in stark contrast to Pbp3, which became more mobile during sorbitol stress (Fig. 4C and F). Our findings suggest that during osmotic stress, Pbp3 can find fewer substrate binding sites, and Pbp4 more, while osmotic plus ionic stress (NaCl) leaves binding and diffusion patterns relatively unaltered. Sorbitol stress also led to a change in localization of Pbp4 (Fig. 5C), and addition of vancomycin led to a slight delocalization (Fig. 5D). However, vancomycin did not influence the fraction size of slow and fast-diffusing molecules (Fig. 5F).

Penicillin G led to an increase of the static fraction by 17.6% (from 39.7% to 46.7%) (Fig. 5F), and was thus almost as affected by penicillin G like Pbp3. Pbp4 changed its localization pattern to a more even distribution around the cell. Thus, penicillin G treatment influenced class A and class B PBPs from the division site in a similar manner. These findings show that slow mobility, in our interpretation indicating binding to a substrate, continues during inhibition/reduction of peptide crosslinking as well as of elongation, while the preferred positioning of the enzyme is less noticeably altered compared to that of the other PBPs. Lages et al. (2015) showed for Pbp1, another class A PBP and for Pbp2b, a class B PBP, both are division associated PBPs like the investigated Pbp4, that the substrate availability is not leading to an altered localization of these PBPs and that the substrate availability is more influencing the PBPs with peripheral localizations. Since we applied a different spatiotemporal resolution (normal fluorescence microscopy vs SMTracking), we might see a slight alteration of the localization pattern caused by the vancomycin treatment or maybe the not purely septal localization has an influence on the behavior of Pbp4. Thus, the underlying mechanism why the substrate availability is more important for PBPs with a peripheral localization compared to the division associated ones still remains unclear [40].

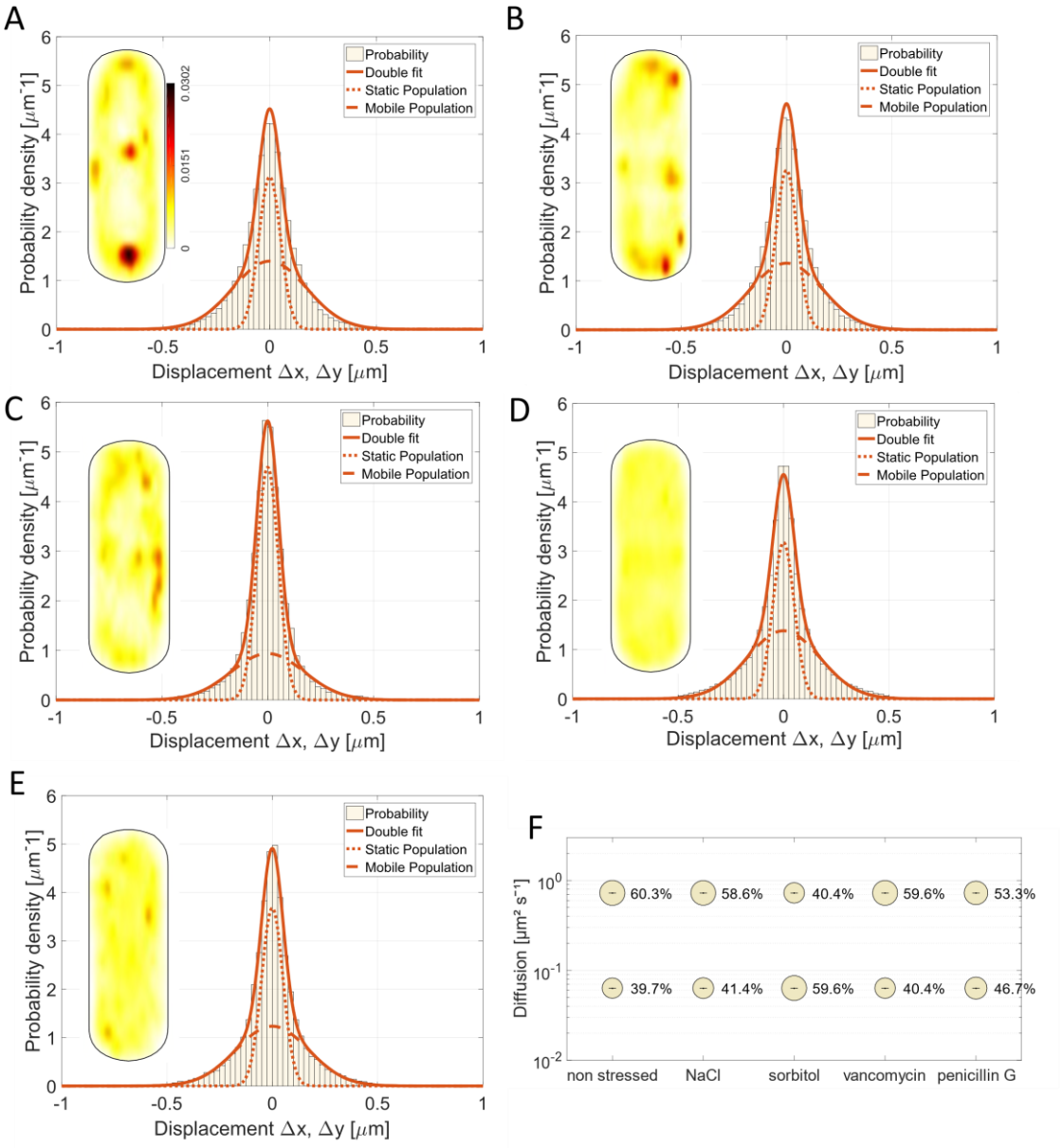

Fig. 5 Gaussian Mixture model fit of Pbp4 is shown for **A** the non-stressed, **B** 0.5 M NaCl, **C** 1 M sorbitol, **D** 4 µg/ml vancomycin or **E** 4 µg/ml penicillin G conditions, using a two-population fit. For each conditions the probability heat map of the localization is included as an inset, showing the different localization pattern of mV-Pbp4. Panel **A** contains the scale for all the heat maps. **F** bubble plot shows the size of the populations in % and the corresponding diffusion coefficients of Pbp4.

Pbp4a motion is mainly affected by vancomycin, and undergoes a relocalization under stress conditions

Pbp4a (encoded by *dacC* gene) is a D,D - carboxypeptidase, one of two D,D-carboxypeptidases that are involved in vegetative growth [1, 4, 6, 7]. Because of its function as a carboxypeptidase, it contributes to the regulation of cell wall cross linking [5, 7]. Its localization in the cell was characterized by a patchy pattern along the cell periphery [4]. In the heat map of exponentially growing cells (Fig. 6A), a preference to locating at subpolar regions is apparent, as well to sites at the lateral cell wall, but not at the septal region. When cells were stressed with NaCl or sorbitol, a relocalization of Pbp4a took place, towards the septum (Fig. 6B and C), similar to what was observed for Pbp2a and for Pbp3. However, the sizes of the mobile and static fractions did not alter considerably (Fig. 6B-C). Interestingly, in response to vancomycin and penicillin G treatment, the localization pattern became more diffuse (Fig. 6D, E and F), and 22.1% (vancomycin) or 35.3% (penicillin G) of the molecules lost the static/slow mobile mobility (Fig. 6D, E and F, table S6). These data suggest that vancomycin masks Pbp4a binding sites, or that Pbp4a activity is coupled to that of other PBPs, especially of Pbp2a and Pbp3 who also became more mobile during vancomycin treatment (Fig. 3D and 4D). Compared to the other PBPs, Pbp4a had an overall larger static fraction, suggesting that two thirds of all Pbp4a molecules are engaged in substrate binding, and its diffusion coefficients (D_1 = 0.091 $\mu m^2/s$) in the low-mobility mode differed somewhat from that of the other three proteins, while being most similar to that of Pbp2a. These findings suggest that Pbp4a may operate in a mixture of independent movement and PBP-dependent substrate association. Please note that values between SQD and GMM analyses differ, because they are independently calculated in SQD, but are based on a comparison between different conditions used in GMM; however, obtained values were in a comparable range.

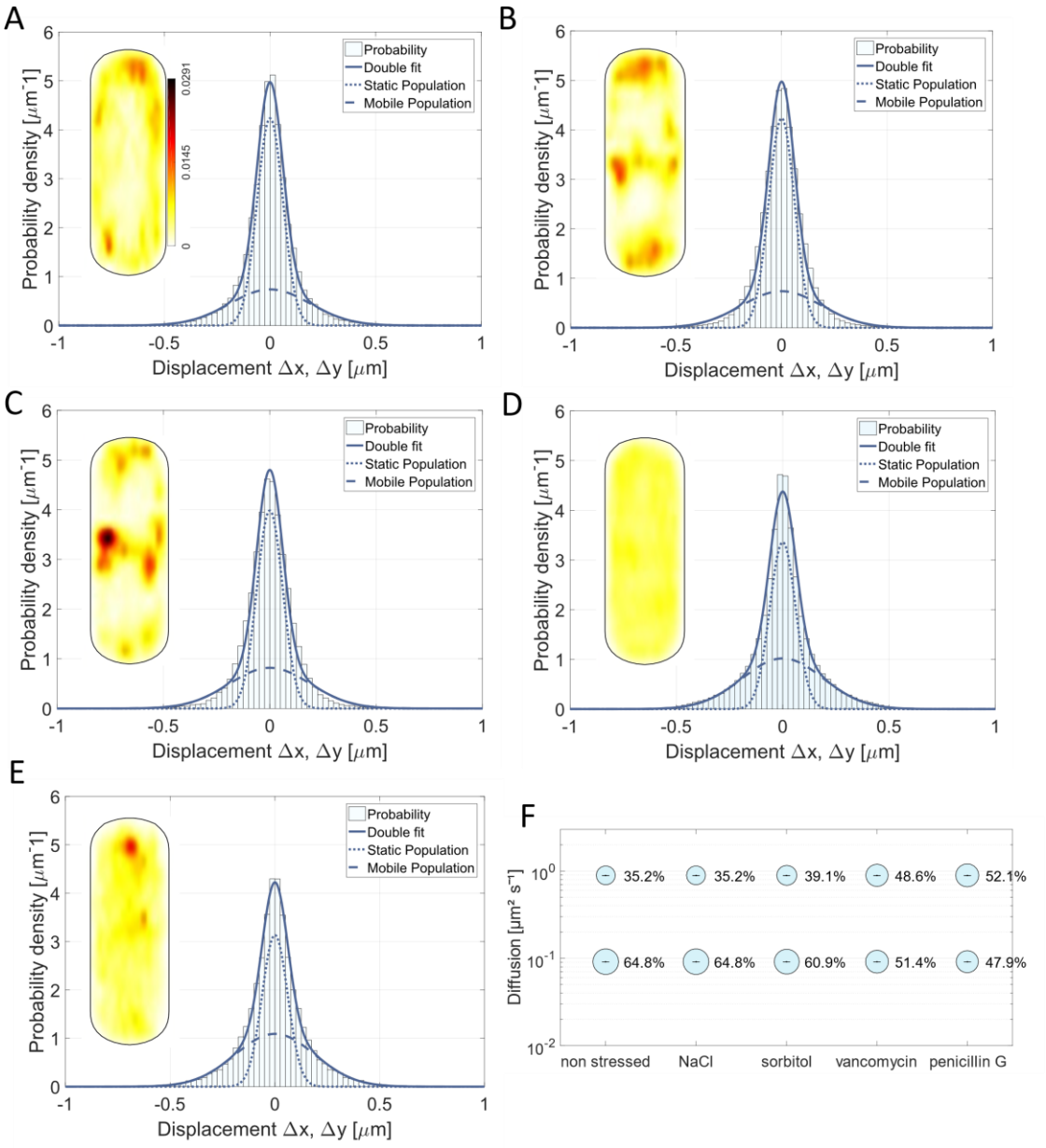

Fig. 6 dynamics of Pbp4a with stress conditions A-E the Gaussian Mixture model fit of Pbp4a is shown for the non-stressed, 0.5 M NaCl, 1 M sorbitol, 4 µg/ml vancomycin and 4 µg/ml penicillin G conditions indicating that the two-population fit is sufficient for the data set. For each conditions the probability heat map of the localization is included, showing the different localization pattern of mV-Pbp4a. **A** contains the scale for all the heat maps. **F** bubble plot shows the size of the population in % and the diffusion coefficients of Pbp4a.

PBPs have different average residence times

By analysing the average residence time of all molecules, we wanted to understand how long molecules stay in a set radius of 120 nm (about three times our localization error) for 9 intervals or longer, and whether this behaviour changes with different stress conditions. Of note, our determined values are an underestimation of true dwell times *in vivo*, due to molecule bleaching during acquisitions (average half-life of YFP is about 1200 ms under comparable experimental conditions [21]. Keeping this in mind, we can still use dwell times to compare behaviour between proteins that carry the same chromophore, and between different conditions. Additionally, while being related, changes in dwell times do not directly reflect alterations seen in static and dynamic populations, because slowly moving molecules captured for 5 to 9 steps were not included in dwell time analyses.

For Pbp2a and Pbp3, no noticeable changes between exponential growth and osmotic stress conditions were visible (Fig. 7), but the residence times were increased with vancomycin treatment, and likewise significantly longer with penicillin G treatment. Note that the statistically significant difference between exponential growth and vancomycin stress for Pbp3 is likely due to narrow SD values and high numbers of determined events, but does not hold true in terms of its actual significance. The residence time for Pbp3 was marginally lowered under osmotic stress. As population size for the slow-mobile mode changed for Pbp3 during sorbitol stress (Fig. 4C), but (long) dwell times did not alter markedly, it is evident that once a molecule is in a slow-mobile (static) mode, it remains there for roughly the same time, no matter if cells grow exponentially or if they are stressed. This is different for Pbp4a: this PBP showed noticeable changes in its residence time in response to all stress conditions. With 0.5 M NaCl and 1 M sorbitol, average residence time became somewhat shorter from 0.30 s ± 0.011 s to 0.28 s ± 0.0042 s (0.5 M NaCl) and 0.28 s ± 0.0035 s (sorbitol). Vancomycin or penicillin G led to a decrease of the residence time from 0.30 s ± 0.011 s to 0.27 s ± 0.0033 s (vancomycin) or 0.27 ± 0.0029 s (penicillin G). Note that these changes were statistically significant (Fig. 7). This supports the idea that Pbp4a binding is directly affected by vancomycin, rather than indirectly via inhibition of Pbp2 or Pbp3, because their dwell times did not change much in response to inhibition of peptide crosslinking. For Pbp4, residence times decreased during most of the stress conditions, except for the sorbitol stress where the residence time increased (Fig. 7). For all four PBPs, residence time changed the most after penicillin G treatment, especially for Pbp2a, which is remarkable because its mobility did not change after penicillin G treatment.

Interestingly, Pbp4 and Pbp4a showed significantly longer dwell times than Pbp2a and Pbp3, indicating that enzymatic activity of Pbp2a and Pbp3 may not be directly coordinated with that of the other two PBPs, which we proposed above based on similar diffusion coefficients for Pbp2a and Pbp4, and Pbp3 and Pbp4a, respectively. Coordination would be based on joint circumferential movement of PBPs together with TG enzymes [13, 27]. Thus, Pbp2a, Pbp3 and Pbp4 showed relatively robust residence times, and therefore apparently robust enzymatic activities during stress conditions, while those of Pbp4a were affected by stress. Different dwell times of PBPs support the idea of dynamic associations/dissociations rather than coordinated formation and dissociation of stable protein complexes.

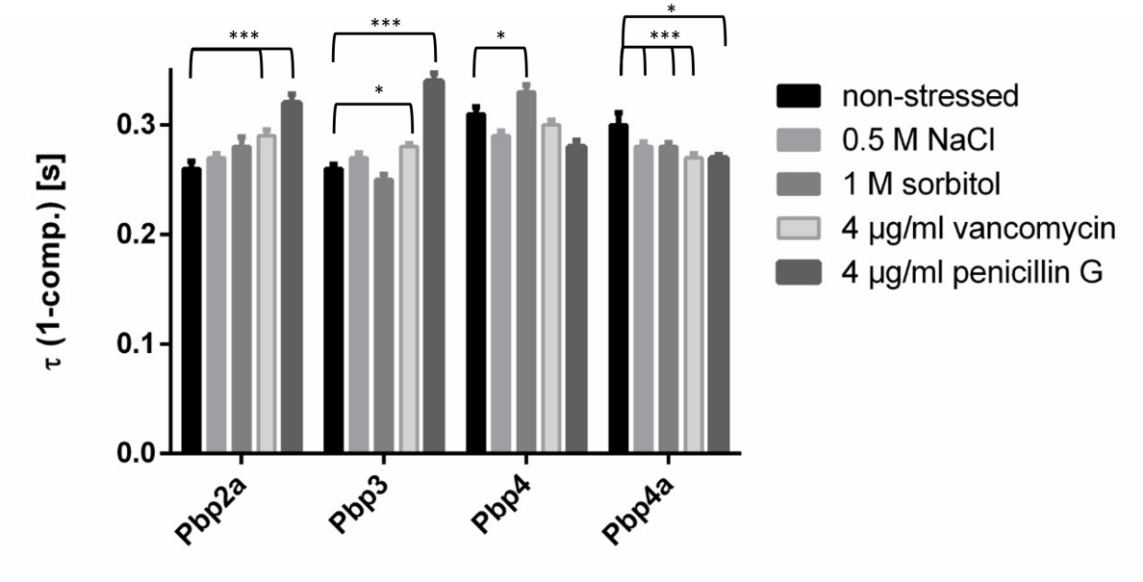

Fig. 7 Dwell times of all four PBPs under applied conditions, as judged by events where molecules stay for 9 or more consecutive steps within a limited radius. Pbp4 and Pbp4a are staying within a radius of 120 nm slightly longer than Pbp2a and Pbp3. * and *** indicate a p-value lower than 0.1 and 0.01 by this the significance level of conditions to each other, calculated by a Levene test (Variances of the ƈ (1-comp.)).

Discussion

Peptidoglycan synthesis is performed by a large array of proteins in bacteria. The *Bacillus subtilis* PBPs have different but possibly redundant enzymatic capabilities, asking the questions if PBPs may be performing specific functions, possibly related to environmental conditions. We have investigated the dynamic behaviour of four *B. subtilis* PBPs having different domains/activities, at a single molecule level. This allowed us to determine speeds of slow-moving molecules, analyse how many molecules are in a low-mobility (likely active synthesis) mode and how many are in a diffusive mode. Our findings that the diffusion coefficients, population sizes and preferred localization patterns correlate between Pbp3 and Pbp4a suggests that PG transpeptidases and carboxypeptidases maybe have coordinated activities. We further found that Pbp2a and Pbp4 show a quantitatively similar dynamic behaviour. This correlation could indicate a similar coordinated binding to their substrate, meaning that the transpeptidase domain could influence the dynamics of both PBPs. Since Pbp4 has a structure homologous to that of Pbp1b of *E. coli,* which was recently shown to have a PG repair function [8], it would be interesting to test if Pbp4 of *Bacillus subtilis* has a similar function.

Our data showing two distinct mobility fractions for PBPs are in complete agreement with findings on PbpH and RodA in *Bacillus subtilis,* and Pbp2 in *E. coli,* which changes between a freely diffusive and a substrate-bound manner, thus dynamically exchanging with the PGEM complex [15, 26], rather than being predominantly bound to a slow-moving PG synthesis complex. For *E. coli* Pbp2, it has recently been shown that an entirely static as well as a slow-mobile fraction exist, besides a freely diffusive one, suggesting two different “active” states, one that is based on substrate binding, and one arising from slow extension of the PG strands [12]. We have not investigated if PBPs might have two distinct slow-mobile speeds in *B. subtilis*, our fast acquisition speed does not allow for this distinction. Our goal was to use a simpler two state model in order to better compare dynamics of four different PBPs. However, it will be interesting to determine if distinct “substrate binding” (entirely static) and “actively synthesizing” (slow mobile) fractions exist in Gram positive cell walls in future work.

Importantly, we found that inhibition of binding to PG precursors or of peptide crosslinking by the addition of vancomycin or penicillin G leads to a loss of preferred localization patterns for all four PBPs. This finding suggests that substrate availability is an important determinant for preferred PBP locations (keeping in mind that several PBPs are recruited to the septal region through direct protein interactions). During masking of D-Ala-D-Ala sites and loss of precursors, PBPs become more mobile in case of Pbp2a and Pbp3, as well as for CPase Pbp4a. For penicillin G, Pbp2a was the only PBP not showing any changes between slow and high mobility fractions of molecules, which might be caused

by the fact that it is not stably interacting with penicillin G, since it has been shown that division-related PBPs are more affected by penicillin G [41] than elongation related PBPs. Our experiments also suggest that toxicity of penicillin G is not caused by strong inhibition of PBPs, but is likely based on moderate but additive inhibition of many PBPs. In earlier studies, PBP dynamics (looking at PbpH) were shown to be strongly reduced after vancomycin treatment (100 µg/ml for 8 min), with regard to ensemble movement of many molecules in TIRF mode, using acquisition intervals in the seconds range [9]. Using SMT and 20 ms intervals, we can show that this effect is based in part on fewer PBPs being in a slow-movement mode, with a diffusion constant of close to 0.1 $\mu m^2/s$, roughly corresponding to the speed of directed movement found for PbpH, RodA and MreB [9, 10, 15].

Osmotic stress is one of the most common challenges in the natural environment, so especially soil bacteria need to be well prepared to deal with osmotic fluctuations. For turgor adaptation, the cell wall plays a key role, besides membrane-integral ion and amino acid transporters [42]. Our data support the idea that PBPs might have functions that become more or less important under certain stress conditions, indicated by the changes in their diffusive behaviour. In terms of its single molecule dynamics, Pbp2a strongly reacted towards sodium chloride stress, which triggers osmotic as well as ionic stress in the cell, whereas Pbp3 and Pbp4 showed considerable, but opposing changes when just an osmotic stress inducer like sorbitol was added. Pbp4a underwent relocalization under osmotic stress, but no significant changes were observed in the diffusive coefficient of the slow mobile population. The changes we have observed agree with experiments from Peters et al. (2016), who showed that Pbp6b is a specialized D,D-CPase in *E. coli* that contributes to cell shape maintenance at low pH, showing that redundancy of D,D-CPases plays an important role in stress response [43]. Additionally, it is known that Pbp4* (encoded by gene *pbpE*) a D,D-Endopeptidase of *Bacillus subtilis* is also involved in high salt adaption of *Bacillus subtilis* [37]. Interestingly, following osmotic stress, Pbp2a and Pbp3 showed relocalization to the septum, suggesting that under changing conditions the sites of activity for PBPs can be different, and that the mode of synthesis of peptidoglycan may be altered under stress conditions.

Interestingly, dwell times remained relatively similar between exponential growth and stress conditions, for molecules staying in a confined radius for 9 steps or longer. Only Pbp4a showed moderately but significantly reduced dwell times following envelope stress, especially after penicillin G treatment. These findings suggest that when PBP molecules change to a confined motion/bound state, they remain there relatively robustly during stress conditions, but with regards to increased or decreased slow-moving

molecules, their transition to the bound state is reduced. These ideas still need to be corroborated by the quantification of transition kinetics *in vivo*.

Recently the Dion et al. (2019) showed that a balance between two systems, the Rod system and the A-PBP system, is needed to maintain rod shape in *Bacillus subtilis* and that under hyperosmotic conditions the Rod system (including Pbp2a) is important for reinforcing the cell wall [13]. The next steps would be to gain more inside into the mechanisms that influence cell wall synthesis under osmotic and ionic stress conditions for example via the protein levels of PBPs or to investigate altered interaction of PBPs and cell synthesis-related proteins.

Inhibition of cell wall synthesis is still one of the most prominent targets for constraining bacterial cell growth and infections. The mechanisms how the antibiotics work in the cell are well understood, but the influence on the inhibited proteins in terms of localization and diffusion are less clear. For the purpose of this study, we analysed the influence of vancomycin and penicillin on four PBPs, which all showed a disturbed localization pattern and an increased mobile fraction (except for Pbp4). It will be interesting to study the effect of inhibiting other aspects of cell wall synthesis on the dynamics of synthetic enzymes and further dissect special requirements for enzymes during stress conditions.

Acknowledgments

This work has been funded by the Deutsche Forschungsgemeinschaft, GR1670/23-1 and TRR 174. We thank the laboratory of Anke Becker for providing deletion strains, and Katharina Höfer, Max Planck Institute Marburg, for gel visualizing assays. Help with cloning of some constructs and with Western blotting by Rebecca Hinrichs and Svenja Fiedler is much appreciated. We thank Vitan Blagotinsek for critical reading of the manuscript.

References

1. Egan, A.J.F., et al., *Regulation of bacterial cell wall growth.* The FEBS Journal, 2016. **284**(6): p. 851-867.

2. Höltje, J.V., *Growth of the stress-bearing and shape-maintaining murein sacculus of Escherichia coli.* Microbiology and molecular biology reviews : MMBR, 1998. **62**(1): p. 181-203.

3. Typas, A., et al., *From the regulation of peptidoglycan synthesis to bacterial growth and morphology.* Nat Rev Microbiol, 2011. **10**(2): p. 123-36.

4. Scheffers, D.J., L.J. Jones, and J. Errington, *Several distinct localization patterns for penicillin-binding proteins in Bacillus subtilis.* Mol Microbiol, 2004. **51**(3): p. 749-64.

5. Sauvage, E., et al., *The penicillin-binding proteins: structure and role in peptidoglycan biosynthesis.* FEMS Microbiol Rev, 2008. **32**(2): p. 234-58.

6. Duez, C., et al., *Purification and characterization of PBP4a, a new low-molecular-weight penicillin-binding protein from Bacillus subtilis.* J Bacteriol, 2001. **183**(5): p. 1595-9.

7. Sauvage, E., et al., *Crystal structure of the Bacillus subtilis penicillin-binding protein 4a, and its complex with a peptidoglycan mimetic peptide.* J Mol Biol, 2007. **371**(2): p. 528-39.

8. Vigouroux, A., et al., *Class-A penicillin binding proteins do not contribute to cell shape but repair cell-wall defects.* Elife, 2020. **9**.

9. Dominguez-Escobar, J., et al., *Processive Movement of MreB-Associated Cell Wall Biosynthetic Complexes in Bacteria.* Science, 2011. **333**(225-228): p. 225-228.

10. Garner, E.C., et al., *Coupled, Circumferential Motions of the Cell Wall Synthesis Machinery and MreB Filaments in B. subtilis.* Science, 2011. **333**: p. 222-225.

11. van Teeffelen, S., et al., *The bacterial actin MreB rotates, and rotation depends on cell-wall assembly.* Proc. Natl. Acad. Sci. U S A, 2011. **108**(38): p. 15822-15827.

12. Ozbaykal, G., et al., *The transpeptidase PBP2 governs initial localization and activity of the major cell-wall synthesis machinery in E. coli.* Elife, 2020. **9**.

13. Dion, M.F., et al., *Bacillus subtilis cell diameter is determined by the opposing actions of two distinct cell wall synthetic systems.* Nat Microbiol, 2019. **4**(8): p. 1294-1305.

14. Olshausen, P.V., et al., *Superresolution imaging of dynamic MreB filaments in B. subtilis--a multiple-motor-driven transport?* Biophys. J., 2013. **105**(5): p. 1171-1181.

15. Dersch, S., et al., *Super-Resolution Microscopy and Single-Molecule Tracking Reveal Distinct Adaptive Dynamics of MreB and of Cell Wall-Synthesis Enzymes.* Front Microbiol, 2020. **11**: p. 1946.

16. Defeu Soufo, H.J. and P.L. Graumann, *Dynamic movement of actin-like proteins within bacterial cells.* EMBO Rep., 2004. **5**(8): p. 789-794.

17. Schibany, S., et al., *Single molecule tracking reveals that the bacterial SMC complex moves slowly relative to the diffusion of the chromosome.* Nucleic Acids Res., 2018. **46**(15): p. 7805-7819.

18. Schindelin, J., et al., *Fiji: an open-source platform for biological-image analysis.* Nat Methods, 2012. **9**(7): p. 676-82.

19. Paintdakhi, A., et al., *Oufti: an integrated software package for high-accuracy, high-throughput quantitative microscopy analysis.* Mol Microbiol, 2016. **99**(4): p. 767-77.

20. Jaqaman, K., et al., *Robust single-particle tracking in live-cell time-lapse sequences.* Nat Methods, 2008. **5**(8): p. 695-702.

21. Rosch, T.C., et al., *SMTracker: a tool for quantitative analysis, exploration and visualization of single-molecule tracking data reveals highly dynamic binding of B. subtilis global repressor AbrB throughout the genome.* Sci Rep, 2018. **8**(1): p. 15747.

22. Wei, Y., et al., *Rod shape determination by the Bacillus subtilis class B penicillin-binding proteins encoded by pbpA and pbpH.* J Bacteriol, 2003. **185**(16): p. 4717-26.

23. McPherson, D.C. and D.L. Popham, *Peptidoglycan synthesis in the absence of class A penicillin-binding proteins in Bacillus subtilis.* J Bacteriol, 2003. **185**(4): p. 1423-31.

24. Popham, D.L. and P. Setlow, *Phenotypes of Bacillus subtilis mutants lacking multiple class A high-molecular-weight penicillin-binding proteins.* J Bacteriol, 1996. **178**(7): p. 2079-85.

25. Lee, T.K., et al., *Single-molecule imaging reveals modulation of cell wall synthesis dynamics in live bacterial cells.* Nat Commun, 2016. **7**: p. 13170.

26. Lee, T.K., et al., *A dynamically assembled cell wall synthesis machinery buffers cell growth.* Proc Natl Acad Sci U S A, 2014. **111**(12): p. 4554-9.

27. Cho, H., et al., *Bacterial cell wall biogenesis is mediated by SEDS and PBP polymerase families functioning semi-autonomously.* Nat Microbiol, 2016. **1**: p. 16172.

28. Morgenstein, R.M., et al., *RodZ links MreB to cell wall synthesis to mediate MreB rotation and robust morphogenesis.* Proc Natl Acad Sci U S A, 2015. **112**(40): p. 12510-5.

29. El Najjar, N., et al., *Bacterial cell growth is arrested by violet and blue, but not yellow light excitation during fluorescence microscopy.* BMC Mol Cell Biol, 2020. **21**(1): p. 35.

30. Kawai, Y., R.A. Daniel, and J. Errington, *Regulation of cell wall morphogenesis in Bacillus subtilis by recruitment of PBP1 to the MreB helix.* Mol Microbiol, 2009. **71**(5): p. 1131-44.

31. Dersch, S., et al., *Super-Resolution Microscopy and Single-Molecule Tracking Reveal Distinct Adaptive Dynamics of MreB and of Cell Wall-Synthesis Enzymes.* Front. Microbiol., 2020. **11**: p. 1946.

32. Sassine, J., et al., *Functional redundancy of division specific penicillin-binding proteins in Bacillus subtilis.* Mol Microbiol, 2017. **106**(2): p. 304-318.

33. Lucena, D., et al., *Microdomain formation is a general property of bacterial membrane proteins and induces heterogeneity of diffusion patterns.* BMC Biol, 2018. **16**(1): p. 97.

34. Hoffmann, T., et al., *Osmotic control of opuA expression in Bacillus subtilis and its modulation in response to intracellular glycine betaine and proline pools.* J Bacteriol, 2013. **195**(3): p. 510-22.

35. Cao, M.W., Tao; Ye, Rick; Helmann, John D., *Antibiotics that inhibit cell wall biosynthesis induce expression of the Bacillus subtilisσW and σM regulons.* Molecular microbiology, 2002. **45**(5): p. 1267-1276.

36. Kohanski, M.A., D.J. Dwyer, and J.J. Collins, *How antibiotics kill bacteria: from targets to networks.* Nat Rev Microbiol, 2010. **8**(6): p. 423-35.

37. Palomino, M.M., C. Sanchez-Rivas, and S.M. Ruzal, *High salt stress in Bacillus subtilis: involvement of PBP4* as a peptidoglycan hydrolase.* Res Microbiol, 2009. **160**(2): p. 117-24.

38. Hutter, B., et al., *Prediction of mechanisms of action of antibacterial compounds by gene expression profiling.* Antimicrob Agents Chemother, 2004. **48**(8): p. 2838-44.

39. Salzberg, L.I., et al., *The Bacillus subtilis GntR family repressor YtrA responds to cell wall antibiotics.* J Bacteriol, 2011. **193**(20): p. 5793-801.

40. Lages, M.C., et al., *The localization of key Bacillus subtilis penicillin binding proteins during cell growth is determined by substrate availability.* Environ Microbiol, 2013. **15**(12): p. 3272-81.

41. Spratt, B.G., *Distinct penicillin binding proteins involved in the division, elongation, and shape of Escherichia coli K12.* Proc Natl Acad Sci U S A, 1975. **72**(8): p. 2999-3003.

42. Csonka, L.N., *Physiological and Genetic Responses of Bacteria to Osmotic Stress.* Microbiological reviews, 1989. **53**(1): p. 121-147.

43. Peters, K., et al., *The Redundancy of Peptidoglycan Carboxypeptidases Ensures Robust Cell Shape Maintenance in Escherichia coli.* mBio, 2016. **7**(3).

Supplement Investigation of *Bacillus subtilis* Penicillin binding proteins at the single molecule level reveals distinct dynamics indicative of changing requirements during stress adaptation

Lisa Stuckenschneider and Peter L. Graumann

SYNMIKRO, LOEWE-Zentrum für Synthetische Mikrobiologie, Hans-Meerwein-Straße, 35043 Marburg, and Fachbereich Chemie, Hans-Meerwein-Straße 4, 35032 Marburg, Germany

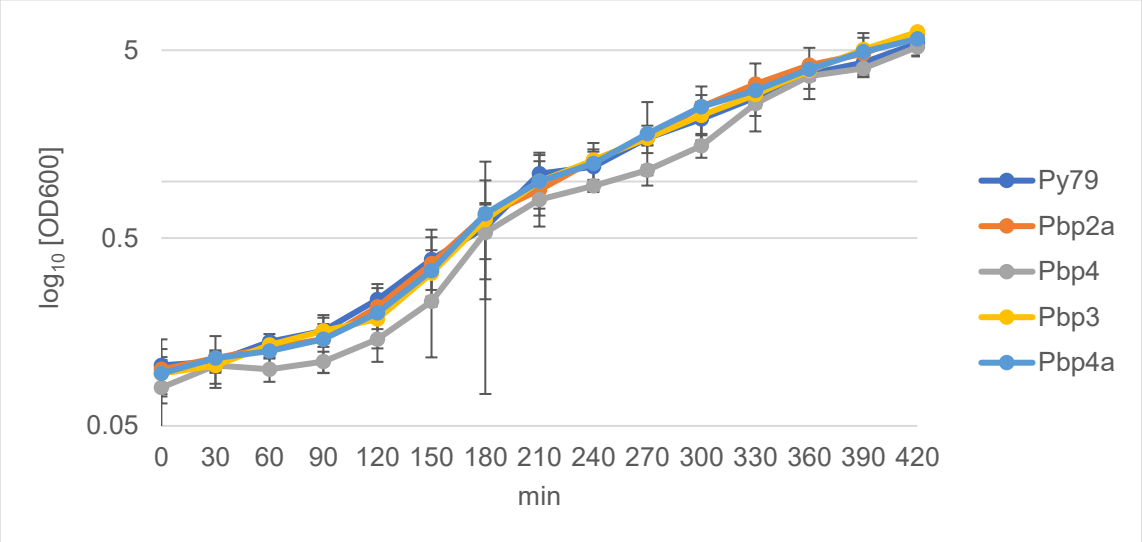

Fig. S1 growth curves of mVenus -PBP fusion strains compared to *Bacillus subtilis* PY79 wild type cells. The growth experiment was performed in 50 ml LB medium with 0.01% xylose for the mVenus-PBP fusion strains as a duplicate starting with an initial optical density (OD_{600}) of 0.1 (t_0). Measuring the OD_{600} every 30 minutes for 7 hours.

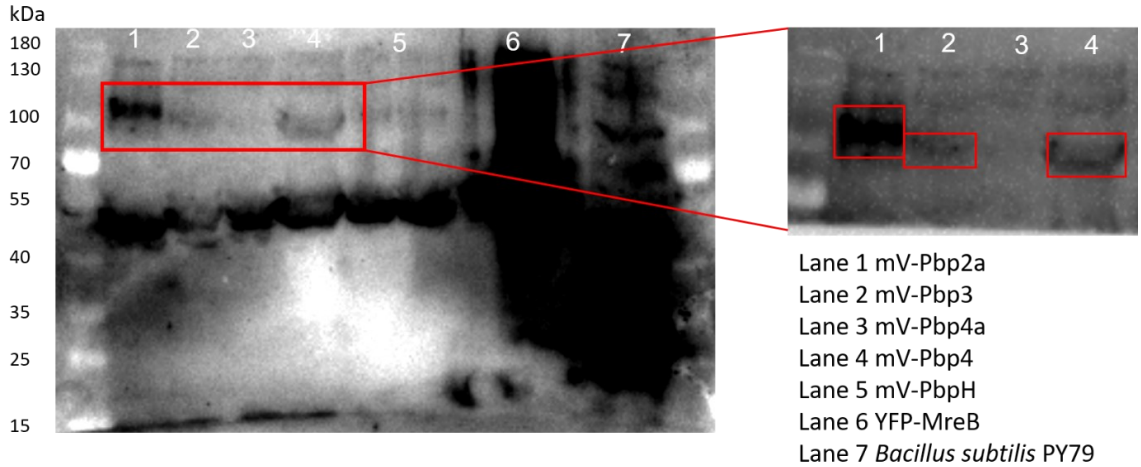

Fig. S2 western blot analysis of the mVenus- PBP fusion strains with an anti GFP antibody, legend is indicating the lanes of the gel with the corresponding fusion loaded, YFP-mreB was used as a positive control for antibody binding and *Bacillus subtilis* PY79 was used to indicate unspecific binding of the antibody. Marked with red boxes are the expected bands.

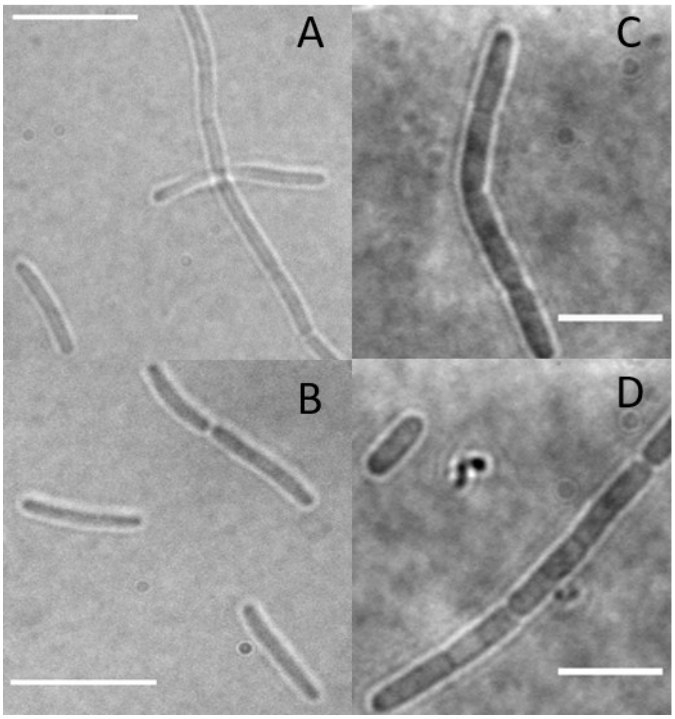

Fig. S3 brightfield pictures of mVenus-fusions with a deletional background to provide evidence for functionality by no phenotypical change or known phenotypes. A and B is showing Δ*pbpGFponA* mVenus-Pbp4 and C and D is Δ*pbpH* mVesnus-Pbp2a. Note that there were no additional substances added and the cell were cultured in LB until an OD_{600} 0.6 was reached. Scale bar is 5 µm in all pictures.

Table S1: List of strains

Strain	Genotyp	Resistance	Source
***E. coli* DH5α**	Wild type	-	
***Bacillus subtilis* PY79**	Wild type	-	
***E. coli* pHJDS-mVenus**	Plasmid pHJDS-P_{xyl}- mVenus	amp	This study
PY79 mV-Pbp2A	P_{xyl}- *mV-pbpA* (original locus)	Cm	This study
PY79 mV-Pbp3	P_{xyl}- *mV-pbpC* (original locus)	Cm	This study
PY79 mV-Pbp4	P_{xyl}- *mV-pbpD* (original locus)	Cm	This study
PY79 mV-Pbp4a	P_{xyl}- *mV-dacC* (original locus)	Cm	This study
PY79 ΔpbpH mV-Pbp2A	P_{xyl}- *mV-pbpA* (original locus), pbpH::kan^R	Cm, kan	This study
168 ΔpbpGFponA mV-Pbp4	P_{xyl}- *mV-pbpD* (original locus), pbpG and pbpF markerless deletion, ponA::kan^R	Cm, kan	This study

Table S2: Table of detailed information generated by the SMTracker data analysis. Data complementary to Fig. 2.

Comparison of Pbps	**Pbp2a**	**Pbp3**	**Pbp4**	**Pbp4a**
# movies	33	29	24	32
# cells	208	230	165	271
av. cell length [µm]	2.8700	3.1600	3.1200	2.6700
# tracks	2030	943	2969	1844
#tracks/cell	9.7596	4.1000	17.9939	6.8044
Dwell time radius [nm]	120	120	120	120
static tracks [%]	1.9000	4.1000	2	3.3000
mobile tracks [%]	98.1000	95.9000	98	96.7000
free [%]	94.9000	91.5000	94.2000	93.4000
mixed behaviour [%]	3.2000	4.3000	3.8000	3.3000
Diffusion constants from SQD and JD				
pop_1 [%]	47.4 ± 0.002	52.3 ± 0.002	42.6 ± 0.001	48.8 ± 0.002
pop_2 [%]	52.6 ± 0.002	47.7 ± 0.002	57.4 ± 0.001	51.2 ± 0.002
D_1 [µm² s^{-1}]	0.0812 ± 0	0.0671 ± 0	0.0934 ± 0	0.0666 ± 0
D_2 [µm² s^{-1}]	0.572 ± 0.002	0.562 ± 0.003	0.616 ± 0.002	0.545 ± 0.003
Dwell times				
ƈ (1-comp.) ± sd [ms]	0.27 ± 0.007 s	0.26 ± 0.004 s	0.31 ± 0.006 s	0.3 ± 0.01 s
stars / p-value	**Pbp2a**	**Pbp3**	**Pbp4**	**Pbp4a**
Pbp2a	-	(lv)* / 0.057814	(lv)* / 0.074121	(lv) *** / 0.00047204
Pbp3	-	-	(lv) *** / 0.00038642	(lv) *** / 1.3537e-05
Pbp4	-	-	-	(lv) *** / 0.0020699
Pbp4a	-	-	-	-

Table S3: Table of detailed information generated by the SMTracker data analysis. Data complementary to Fig. 3.

Condition of strain mV-Pbp2a	**Non stressed**	**500 mM NaCl**	**1 M sorbitol**	**4 µg/ml vancomycin**	**4 µg/ml penicillin G**
# movies	33	30	30	27	28
# cells	232	188	192	222	217
av. cell length [µm]	2.8200	3.1400	2.9800	3.2600	3.0900
# tracks	2030	3619	1673	8116	2976
#tracks/cell	10.1400	21.1548	9.1803	38.5856	15.5370
dwell time radius [nm]	120	120	120	120	120
static tracks [%]	1.9000	2.2000	2.7000	2.5000	3.5000
mobile tracks [%]	98.1000	97.8000	97.3000	97.5000	96.5000
free [%]	94.9000	93.8000	93.7000	94.4000	91.4000
mixed behaviour [%]	3.2000	4	3.6000	3.1000	5.2000
Diffusion constants from GMM					
Static D ± sd [µm² s⁻¹]	0.077 ± 0.00027	0.077 ± 0.00027	0.077 ± 0.00027	0.077 ± 0.00027	0.077 ± 0.00027
Mobile D ± sd [µm² s⁻¹]	0.71 ± 0.0021	0.71 ± 0.0021	0.71 ± 0.0021	0.71 ± 0.0021	0.71 ± 0.0021
Static fraction ± sd [%]	50.3 ± 0.14	45.8 ± 0.13	52.8 ± 0.14	35.8 ± 0.12	50.8 ± 0.13
Mobile fraction ± sd [%]	49.7 ± 0.14	54.2 ± 0.13	47.2 ± 0.14	64.2 ± 0.12	49.2 ± 0.13
Dwell times					
ƈ (1-comp.) ± sd [ms]	0.26 ± 0.0066 s	0.27 ± 0.0035 s	0.28 ± 0.0088 s	0.29 ± 0.0054 s	0.32 ± 0.008 s
stars / p-value	**Non stressed**	**500 mM NaCl**	**1 M sorbitol**	**4 µg/ml vancomycin**	**4 µg/ml penicillin G**
Non-stressed	-	(tt) ns / 0.96507	(lv) *** / 0.008692	(tt) ns / 0.2015	(lv) *** / 0.00058067
500 mM NaCl	-	-	(lv) *** / 1.4291e-05	(lv) *** / 0.0011055	(lv) *** / 5.3127e-09
1 M sorbitol	-	-	-	(lv) ** / 0.022889	(tt) ns / 0.23315
4 µg/ml vancomycin	-	-	-	-	(lv) *** / 5.6086e-05
4 µg/ml penicillin G	-	-	-	-	-

Table S4: Table of detailed information generated by the SMTracker data analysis. Data complementary to Fig. 4.

Condition of strain mV-Pbp3	**Non stressed**	**500 mM NaCl**	**1 M sorbitol**	**4 µg/ml vancomycin**	**4 µg/ml penicillin G**
# movies	29	29	28	24	26
# cells	277	216	179	202	180
av. cell length [µm]	3.1400	3.1700	3.5400	3.4500	3.1400
# tracks	943	884	1610	6860	1511
#tracks/cell	4.2130	4.8309	9.9787	39.3305	8.7685
dwell time radius [nm]	120	120	120	120	120
static tracks [%]	4.1000	6.4000	1.7000	3.3000	3.3000
mobile tracks [%]	95.9000	93.6000	98.3000	96.7000	96.7000
free [%]	91.5000	88.6000	94.3000	93.2000	93.6000
mixed behaviour [%]	4.3000	5	3.9000	3.5000	3
Diffusion constants from GMM					
Static D ± sd [µm² s⁻¹]	0.063 ± 0.0002	0.063 ± 0.0002	0.063 ± 0.0002	0.063 ± 0.0002	0.063 ± 0.0002
Mobile D ± sd [µm² s⁻¹]	0.72 ± 0.002	0.72 ± 0.002	0.72 ± 0.002	0.72 ± 0.002	0.72 ± 0.002
Static fraction ± sd [%]	55.4 ± 0.12	59.2 ± 0.12	46.6 ± 0.11	41.7 ± 0.1	43.3 ± 0.11
Mobile fraction ± sd [%]	44.6 ± 0.12	40.8 ± 0.12	53.4 ± 0.11	58.3 ± 0.1	56.7 ± 0.11
Dwell times					
ƈ (1-comp.) ± sd [ms]	0.26 ± 0.0038 s	0.27 ± 0.0042 s	0.25 ± 0.0047 s	0.28 ± 0.0028 s	0.34 ± 0.0071 s
stars / p-value	**Non stressed**	**500 mM NaCl**	**1 M sorbitol**	**4 µg/ml vancomycin**	**4 µg/ml penicillin G**
Non-stressed	-	(tt) ns / 0.55131	(tt) ns / 0.69622	(lv)* / 0.055643	(lv) *** / 0.00013165
500 mM NaCl	-	-	(tt) ns / 0.97333	(tt) ns / 0.41856	(lv) *** / 0.00084379
1 M sorbitol	-	-	-	(tt) ns / 0.43051	(lv) ** / 0.034142
4 µg/ml vancomycin	-	-	-	-	(lv) *** / 0.0048857
4 µg/ml penicillin G	-	-	-	-	-

Table S5: Table of detailed information generated by the SMTracker data analysis. Data complementary to Fig. 5.

Condition of strain mV-Pbp4	**Non stressed**	**500 mM NaCl**	**1 M sorbitol**	**4 µg/ml vancomycin**	**4 µg/ml penicillin G**
# movies	24	30	24	25	26
# cells	256	292	265	275	221
av. cell length [µm]	3.0600	3.1000	3.1100	3.4700	3.3100
# tracks	2969	7377	1463	15515	2902
#tracks/cell	17.7866	41.3938	6.5387	58.3139	14.2948
dwell time radius[nm]	120	120	120	120	120
static tracks [%]	2	1.9000	4	3	4.4000
mobile tracks [%]	98	98.1000	96	97	95.6000
free [%]	94.2000	93.4000	90.8000	93.9000	91.7000
mixed behaviour [%]	3.8000	4.6000	5.3000	3.2000	3.9000
Diffusion constants from GMM					
Static D ± sd [µm² s⁻¹]	0.063 ± 0.00027	0.063 ± 0.00027	0.063 ± 0.00027	0.063 ± 0.00027	0.063 ± 0.00027
Mobile D ± sd [µm² s⁻¹]	0.73 ± 0.0024	0.73 ± 0.0024	0.73 ± 0.0024	0.73 ± 0.0024	0.73 ± 0.0024
Static fraction ± sd [%]	39.7 ± 0.14	41.4 ± 0.13	59.6 ± 0.17	40.4 ± 0.13	46.7 ± 0.15
Mobile fraction ± sd [%]	60.3 ± 0.14	58.6 ± 0.13	40.4 ± 0.17	59.6 ± 0.13	53.3 ± 0.15
Dwell times					
ƈ (1-comp.) ± sd [s]	0.31 ± 0.0063 s	0.29 ± 0.004 s	0.33 ± 0.0064 s	0.3 ± 0.0042 s	0.28 ± 0.0057 s
stars / p-value	**Non stressed**	**500 mM NaCl**	**1 M sorbitol**	**4 µg/ml vancomycin**	**4 µg/ml penicillin G**
Non-stressed	-	(tt) ns / 0.40334	(lv)* / 0.052432	(tt) ns / 0.6974	(tt) ns / 0.65515
500 mM NaCl	-	-	(lv) *** / 0.0072279	(lv) ** / 0.023322	(tt) ns / 0.80676
1 M sorbitol	-	-	-	(tt) ns / 0.37461	(tt) ns / 0.15913
4 µg/ml vancomycin	-	-	-	-	(tt) ns / 0.35744
4 µg/ml penicillin G	-	-	-	-	-

Table S6: Table of detailed information generated by the SMTracker data analysis. Data complementary to Fig. 6.

Condition of strain mV-Pbp4a	**Non stressed**	**500 mM NaCl**	**1 M sorbitol**	**4 µg/ml vancomycin**	**4 µg/ml penicillin G**
# movies	32	38	37	36	25
# cells	322	307	350	218	179
av. cell length [µm]	2.6500	2.8500	2.7600	3.4100	3.0700
# tracks	1844	6246	4270	15923	1856
#tracks/cell	7.1800	24.1588	20.2282	69.9525	10.8275
dwell time radius [nm]	120	120	120	120	120
static tracks [%]	3.3000	3.6000	3.9000	2.8000	2.1000
mobile tracks [%]	96.7000	96.4000	96.1000	97.2000	97.9000
free [%]	93.4000	88.9000	89.4000	93.5000	94.2000
mixed behaviour [%]	3.3000	7.4000	6.7000	3.7000	3.7000
Diffusion constants from GMM					
Static D ± sd [µm² s⁻¹]	0.091 ± 0.00033	0.091 ± 0.00033	0.091 ± 0.00033	0.091 ± 0.00033	0.091 ± 0.00033
Mobile D ± sd [µm² s⁻¹]	0.89 ± 0.0048	0.89 ± 0.0048	0.89 ± 0.0048	0.89 ± 0.0048	0.89 ± 0.0048
Static fraction ± sd [%]	64.8 ± 0.19	64.8 ± 0.17	60.9 ± 0.17	51.4 ± 0.17	47.9 ± 0.2
Mobile fraction ± sd [%]	35.2 ± 0.19	35.2 ± 0.17	39.1 ± 0.17	48.6 ± 0.17	52.1 ± 0.2
Significantly different dwell times					
ƈ (1-comp.) ± sd [s]	0.3 ± 0.011 s	0.28 ± 0.0042 s	0.28 ± 0.0035 s	0.27 ± 0.0033 s	0.27 ± 0.0029 s
stars / p-value	**Non stressed**	**500 mM NaCl**	**1 M sorbitol**	**4 µg/ml vancomycin**	**4 µg/ml penicillin G**
Non-stressed	-	(lv) *** / 2.7843e-05	(lv) *** / 1.2465e-09	(lv) *** / 0.00023352	(lv) ** / 0.015592
500 mM NaCl	-	-	(lv) ** / 0.022042	(tt) ns / 0.82601	(tt) ns / 0.8092
1 M sorbitol	-	-	-	(lv) ** / 0.037105	(tt) ns / 0.7364
4 µg/ml vancomycin	-	-	-	-	(tt) ns / 0.90286
4 µg/ml penicillin G	-	-	-	-	-

3.3 Additional and unpublished results

3.3.1 Influence of antibiotic treatment on elongasome-associated proteins MreB, PbpH and Pbp2a

The experiments in this section were performed to gain further insights into the dynamics of the components of the elongasome, (also named Rod complex or PGEM) and are following up on the single molecule tracking results published in Dersch et al., 2020 (including PbpH tracking data performed by the author of this thesis) and those presented in the doctoral thesis of Dr. Simon Dersch. The results presented here are also building on previous work by the author of this thesis, in particular the Pbp2a experiments from the unpublished manuscript (3.2). In this upcoming section, single molecule experiments with antibiotic treatments for MreB, PbpH and Pbp2a were performed.

3.3.1.1 Antibiotic treatment-induced changes of MreB dynamics

MreB is one of the key components of the rod complex and is still thought to lead the peptidoglycan synthesis in a perpendicular manner around the cell (Reimold et al., 2013). Since the PG synthesis is known to be one of the main targets for antibiotics and MreB is involved in it, the aim was to understand the influence of cell wall synthesis inhibitors on the dynamics of MreB expressed at a low level from an ectopic site.
Some effects of antibiotics are already known for MreB on the cellular level. Especially antibiotics that lead to depletion of the PG precursors are showing an impact on the MreB patches (Dominguez-Escobar et al., 2011; Garner et al., 2011; Schirner et al., 2015), but the influence on the motion of MreB at a high spatiotemporal resolution was not described yet. The aim was to investigate the dynamics of MreB after treatment with cell wall synthesis-influencing antibiotics. These include vancomycin (inhibiting transglycosylation and transpeptidation by masking the nascent PG precursors (Breukink & de Kruijff, 2006)), penicillin G (as a ß-lactam inhibiting PBPs transpeptidation activity (Strominger et al., 1971)), nisin (with dual function, making holes into the membrane and delocalizing lipid II (Breukink & de Kruijff, 2006)), fosfomycin (interacts with the MurA and by that inhibits the synthesis of the PG precursor lipid II (Kahan et al., 1974a)) and bacitracin (inhibits the recycling of UndPP (Economou et al., 2013)). The raw data for cells treated with vancomycin (Fig. 8 panel B) and bacitracin (Fig. 8 panel F) were kindly provided by Dr. Simon Dersch and are included in this thesis.

It was determined that the motion of MreB can best be described as assuming at least two populations, a slow-moving bound molecule population (D_{static} 0.043±4.1x10^{-9}, 49.6%) and a fast, freely diffusing one (D_{mobile} 0.44±4.1x10^{-8}, 50.4%). To be able to easily compare the data of the different conditions and the fraction size of the population, a simultaneous Gaussian Mixture Model (GMM) fit was used to calculate the diffusion coefficient. Similar to the osmotic stress data published in Dersch et al., 2020, MreB reacts with an increased slow-moving population to the antibiotic treatment with nisin and fosfomycin. To penicillin G, vancomycin and bacitracin, MreB reacts with a minimal change (under 10%, from 49,6% to 47.1% for vancomycin, 47.3% for penicillin G or 46% for bacitracin) decreased slow- moving population (Fig. 8G).

Fosfomycin and bacitracin were observed to have the biggest influence on the diffusion of MreB. Additionally, it is already described in the literature that the PG precursor availability might have an impact on MreB (Schirner et al., 2015). Surprisingly, vancomycin and the ß-lactam penicillin G just have a minimal effect on the static fraction of MreB, especially since it is known that vancomycin, ampicillin and mecillinam can stop the paralog Mbl from moving (Garner et al., 2011). Since a different time resolution was applied in this case compared to most of the other studies (Dominguez-Escobar et al., 2011; Garner et al., 2011; Schirner et al., 2015), a slightly controversial and opposite observation can be made to the ones known from the literature.

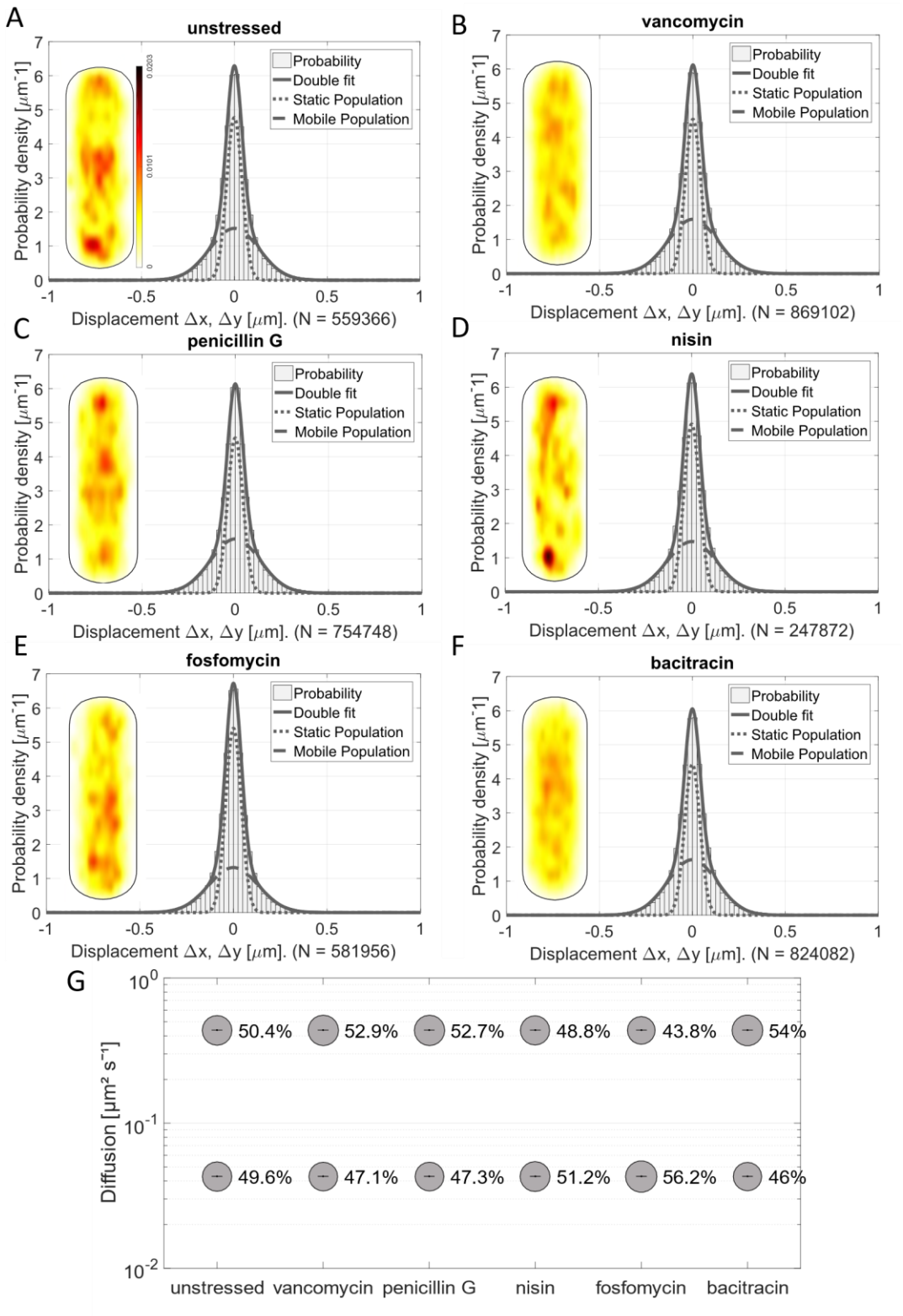

Figure 8 MreB single-molecule dynamics. A-F Two-population fit of YFP-MreB single-molecule dynamics using simultaneous Gaussian-mixture-model (GMM) under normal growth conditions (unstressed) and treated with vancomycin, penicillin G, nisin, fosfomycin and bacitracin. Included in the GMM fit is the corresponding heat map of the probability distribution of all trajectories **G** Bubble-plot of the diffusive populations (relative fraction sizes, D [$\mu m^2 / s^2$]) as identified by simultaneous two-population GMM curve fit for YFP-MreB. The raw data for the vancomycin (panel B) and bacitracin (panel F) treatment were kindly provided by Simon Dersch. The analysis of this raw data was subsequently performed by the author of this thesis, as well as the other antibiotic treatments experiments.

3.3.1.2 PbpH

For further investigation of the connection of the Rod complex and PbpH, mVenus-PbpH was treated with the same antibiotics as MreB in 3.3.2.1, as a follow up experiment to Dersch et al., 2020. A two-population fit was sufficiently describing the diffusive behaviour of PbpH, showing diffusion coefficients D_{static} 0.063 ± $1.3x10^{-7}$ and D_{mobile} 0.61 ± $5.7x10^{-7}$, which are in a similar range to the previously observed diffusion coefficients of PbpH shown in Dersch et al., 2020.

Penicillin G and nisin do not influence the diffusive behaviour of PbpH, but nisin does have a strong impact on the localization of PbpH to a more septal orientation (Fig. 9 D). Since nisin is delocalizing the lipid II in the cell, this also leads to a redistribution of PbpH. Penicillin G is not causing a change in the behaviour for PbpH (Fig. 9 C and G), or the redundant transpeptidase Pbp2a (see the unpublished manuscript). The explanation for PbpH could be the same as for Pbp2a, in that penicillin G is not interacting with the transpeptidase, since PbpH is involved in the elongation, but not in the division of the bacterial cell. For *E. coli* it was shown that different β lactams are interacting with different PBPs at different stages of the cell cycle (Spratt, 1975). Additionally, penicillin G is blocking the active site of PbpH and is not leading to a delocalization of lipid II, and therefore also no delocalization of PbpH, since this seems to be related to the substrate availability (Lages et al., 2013). On the other hand, the biggest changes are triggered by vancomycin and bacitracin, leading to a change of 44,3% (vancomycin from 57% to 82.1%) and 42,2% (bacitracin from 57% to 80.9%) of the mobile population (Fig. 9 G). Furthermore, fosfomycin is also decreasing the fast-moving population by 16.3% (from 57% to 47.6%), leading to the assumption that the substrate availability is influencing the mode of motion of PbpH. This likely occurs because fosfomycin and bacitracin are both directly lowering the lipid II amount in the bacterial cells. In the case of vancomycin, the lipid II amount is lowered indirectly, however, through the binding of the D-Ala-D-Ala residues of lipid II, which results in a freer diffusion since PbpH is searching for an insertion site and substrate (lipid II) to be enzymatically active again. Thus, the increase in the slower population observed in the case of bacitracin could be interpreted as a possible deregulation of the lipid II cycle, leading to a lower production of lipid II because the recycling of the UndPP is inhibited and the carrier lipid for building lipid II is missing.

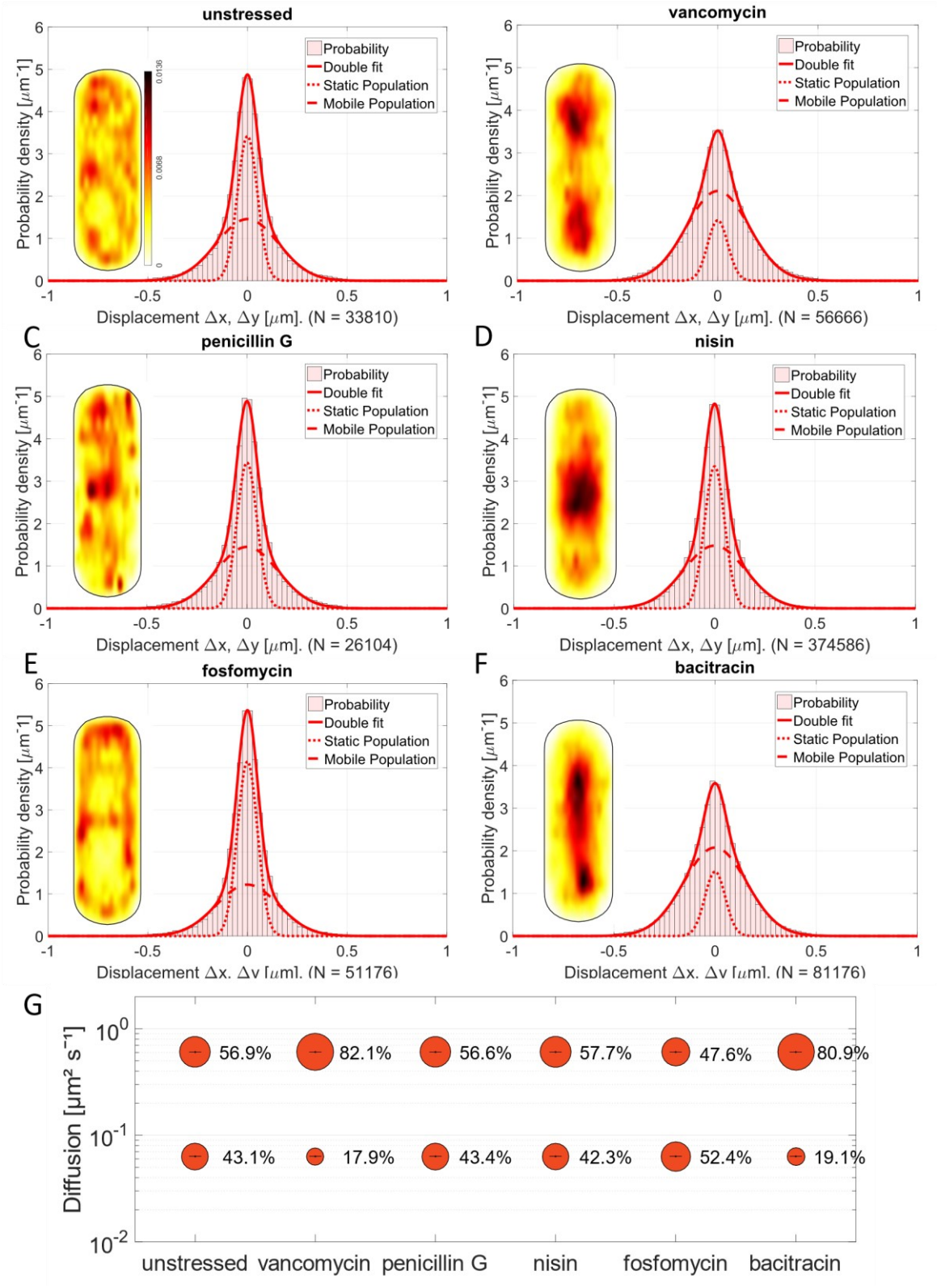

Figure 9: PbpH single-molecule dynamics after antibiotic treatment. A-F Two-population fit of mVenus-PbpH single-molecule dynamics using simultaneous Gaussian-mixture-model (GMM) under normal growth conditions (unstressed) and treated with vancomycin, penicillin G, nisin, fosfomycin and bacitracin. Included in the GMM fit is the corresponding heat map of the probability distribution of all trajectories **G** Bubble-plot of the diffusive populations (relative fraction sizes, D [µm^2 /s^2]) analysed as a simultaneous two-population GMM curve fit for mVenus-PbpH.

To further investigate the connection between the different components of the elongasome, mV-PbpH was analysed in different genetically modified backgrounds (deletion of *pbpA* and depletion of MreB). The strain mV-PbpH with the deletion of the redundant transpeptidase Pbp2a (encoded by *pbpA*) and mV-PbpH with the option to deplete MreB by higher addition of xylose were constructed and subsequently all the strains were verified via a western blot using antibodies anti-GFP (Fig. S2) to check for the presence of the full length protein and the absence of any degradation, and anti-mreB (Fig. S3) to validate the induced depletion of MreB. The depletion MreB strain was provided by the BGSC and the expression can be down regulated by a Cas9 sytems under the control of a xylose promotor (J. M. Peters et al., 2016).

In comparison between the original mV-PbpH and the two deletion/depletion strains, for all three the two-population fit was still the best fitting to describe the dynamics of mVenus-PbpH in the different strain backgrounds and the diffusion coefficient was calculated by simultaneous Gaussian Mixture Model fit (D_{static} 0.058±3.9x10^{-7}, D_{mobile} 0.6±4.4x10^{-6}) (Fig. 10 A-C). In this context, the deletion of *pbpA* led to a small change of 8% in the diffusive behaviour of PbpH. The depletion of MreB, on the other hand, increased the slow-moving fraction by 11% (from 41.7% to 53.7%) (Fig. 10 D). This hints towards the assumption that MreB is regulating the mobility of the transpeptidase PbpH. The localisation of PbpH is only marginally influenced by the different genetic backgrounds. A slightly more septal localisation of PbpH can be observed in the Δ*pbpA,* as indicated in the probability heat map of a standardized cell inset in the GMM fits. When MreB was depleted, PbpH seemed to be more diffuse localized in the cell compared to the two other strains. In conclusion, PbpH diffusion is mainly influenced by the substrate availability of lipid II in the cell, as was already observed for Pbp2a and other PBPs from the unpublished manuscript (see 3.2.1).

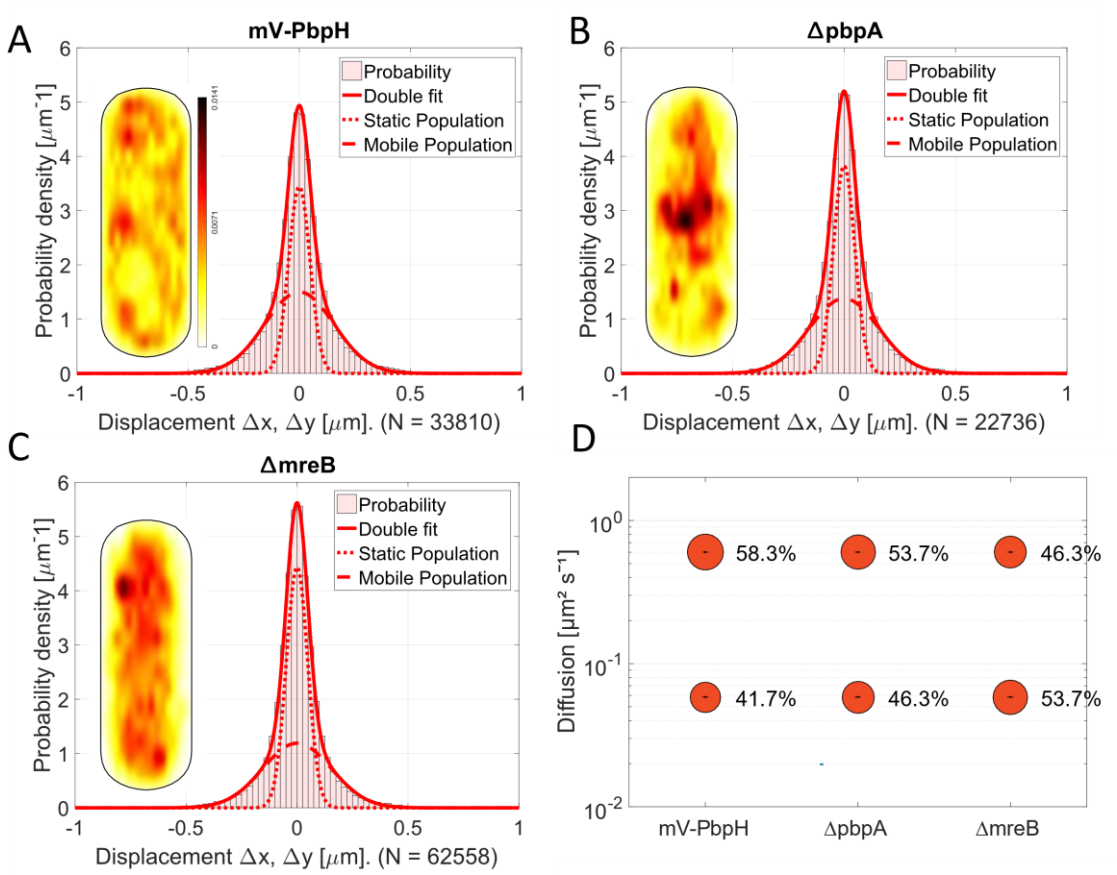

Figure 10: Analysis of PbpH dynamics and localization. **A-C** shows the GMM fit of the SMT data of three strains expressing mVenus-PbpH in different genetic background (deletion of *pbpA* and depletion of MreB) in comparison. Included in the GMM fits are the corresponding heat maps showing the probable localization pattern of the single molecules. **E** visualizes the two diffusive populations of the three different strains in a bubble plot.

3.3.1.2.1 PbpH dynamics in the Δ*pbpA* background

To investigate further, the deletion of *pbpA* mV-PbpH strain was stressed with osmotic stress-inducing reagents (1 M sorbitol and 500 mM NaCl). The diffusion of PbpH is minimally influenced by the osmotic stress, as was already shown for the mV-PbpH strain with a genetically non-modified background (Dersch et al., 2020). The mobile fraction of PbpH increases by 6.2% for 500 mM NaCl and 9.3% for 1 M sorbitol (Fig. 11 D), but a relocalization and higher probability of the molecules at the septal region, as well as at the polar regions, are visible in the probability heat map. As already observed in the previous data as well as in the two manuscripts, osmotic stress doesn't seem to influence the dynamics of PbpH and the deletion of *pbpA* is also not changing PbpH behaviour.

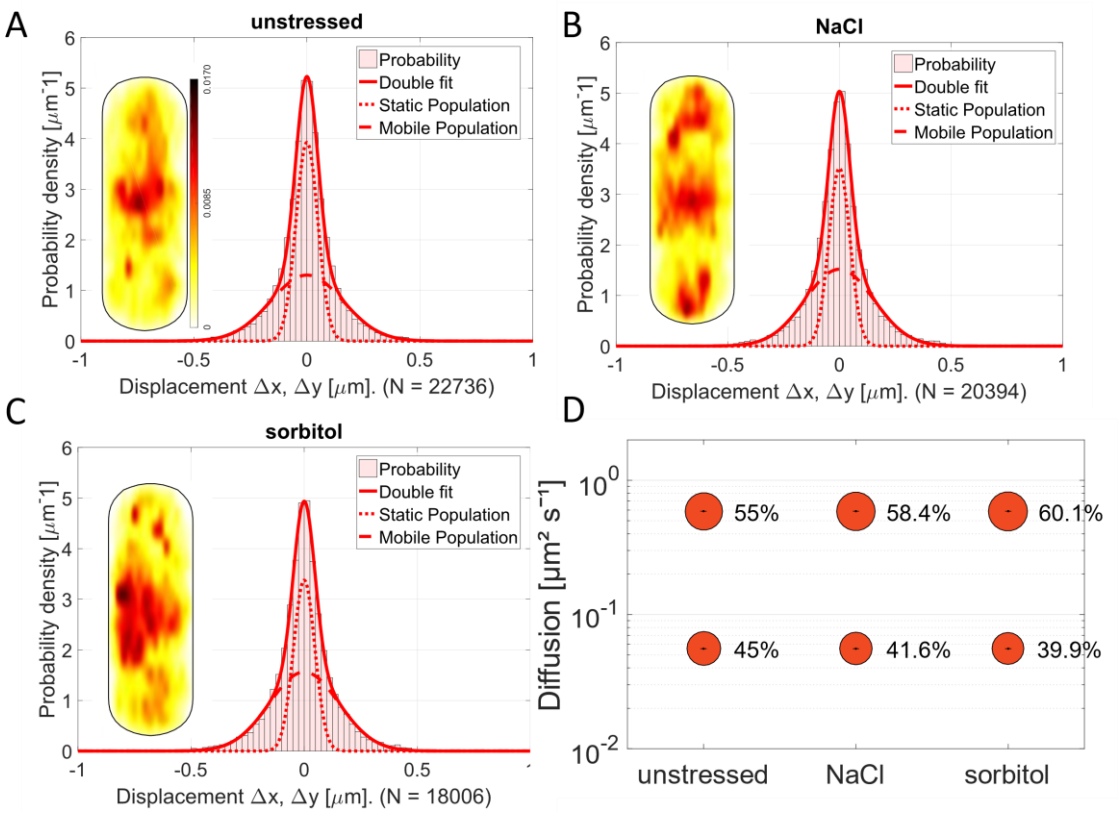

Figure 11: Analysis of PbpH dynamics in a Δ*pbpA* strain. A-C the Gaussian Mixture model fit of PbpH is shown for the non-stressed, 0.5 M NaCl and 1 M sorbitol conditions (30 min of stress) indicating that the two-population fit sufficiently well explains the measured data. For each conditions the probability heat map of the localization is included as an inset, showing the different localization patterns of mV-PbpH. **A** contains the scale for all the heat maps. **D** bubble plot is showing the size of the population in % and the diffusion coefficients for PbpH mobility fractions.

Since the osmotic stress wasn't influencing the diffusive behaviour of PbpH in a Δ*pbpA* background (as seen from Fig. 11), the different antibiotics were tested as well. Especially vancomycin and nisin led to a relocalization of PbpH to a high probability of a septal localisation (Fig. 12 B and D). The other three antibiotics were not changing the localization pattern of PbpH to a large extent. Furthermore, vancomycin and nisin also lead to an increased population of the fast-moving fraction, to 59% (vancomycin) and 32,1% (nisin) of PbpH (Fig. 12 G). Compared to the non-deletion background (mV-PbpH strain), the effect of the deletion of PbpA in combination with the addition of nisin on the motility of PbpH is remarkable; in the non-deletion background, there is almost no observable effect. It seemed that in the absence of Pbp2a, the substrate availability is even more important for the localization of PbpH, and is leading to an increased need to search for an active site to crosslink the PG strands, correlating with the localisation of the lipid II as a PG precursor. On the other hand, vancomycin has the same influence on PbpH, regardless of the genetic background of the strain.

Penicillin G leads to an increased mobile fraction of PbpH, by 15% (from 52.3% to 60.2%). Interestingly, when compared to the non-genetically modified PbpH strain, which is not showing any response to the penicillin G treatment, it led to the hypothesis that PbpH is getting more sensitive to the binding of penicillin G, or that the amount of crosslinking of the PG sacculus might lead to a bigger mobile fraction searching for an active site to catalyse the transpeptidase reaction.

Fosfomycin is increasing the mobile population by 12,5%, which is in a similar range as the influence it has on the mV-PbpH strain without a genetically modified background. Therefore, fosfomycin seems to have a general effect on the dynamics of PbpH, because it is known to inhibit the function of MurA, therefore reducing the lipid II amount in the cell (Kahan et al., 1974a). Since bacitracin is also leading to a reduction of lipid II, a precursor of PG synthesis, by inhibiting the recycling of UndPP (Economou et al., 2013), an increased mobile population of PbpH is following the change in substrate availability. Generally, all of the antibiotics led to an increased fast-moving fraction of PbpH, likely by reduction of the substrate availability or its binding capabilities.

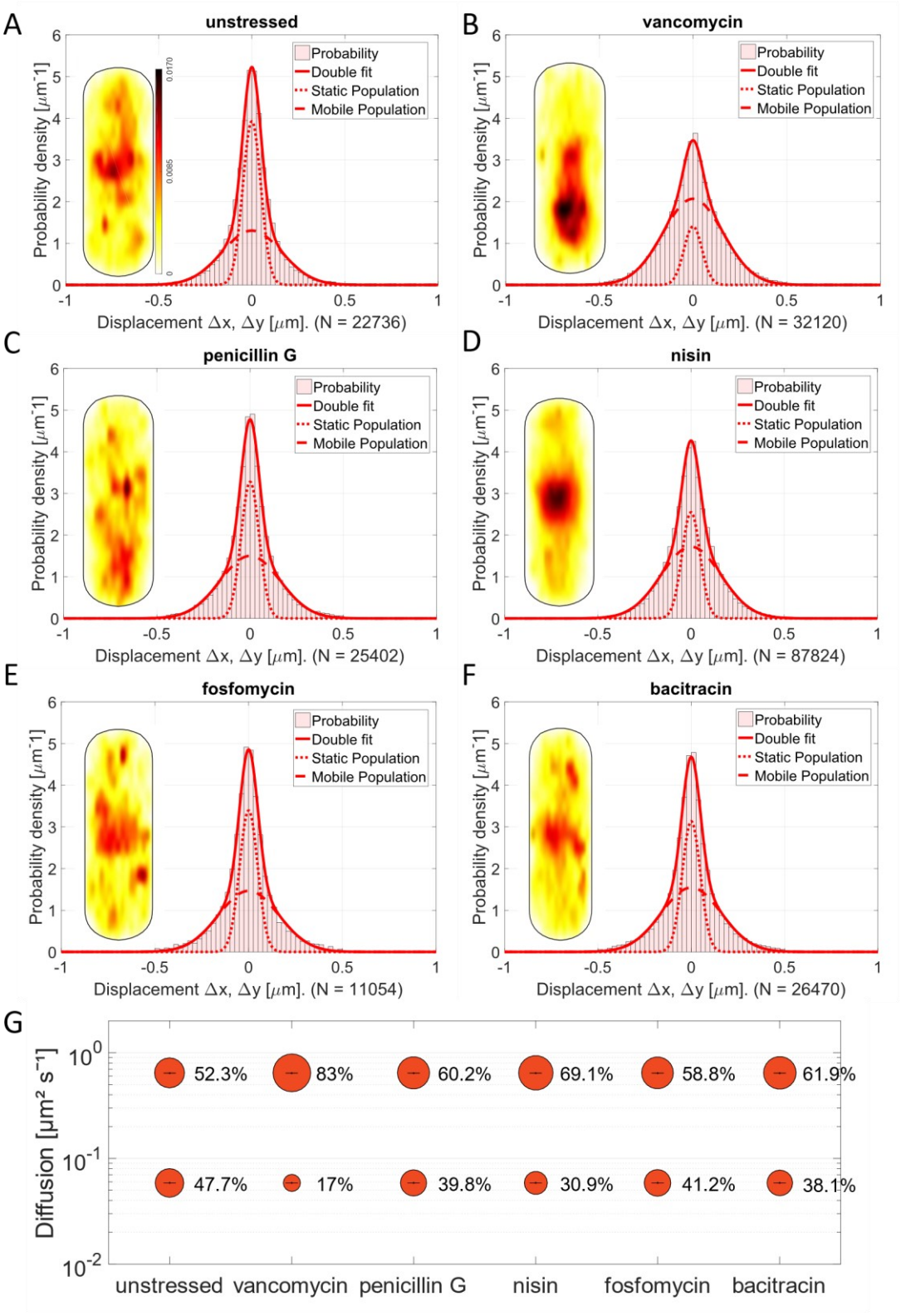

Figure 12: PbpH single-molecule dynamics in a Δ*pbpA* strain before and after antibiotic treatment (or with and without treatment). A-F Two-population fit of mVenus-PbpH single-molecule dynamics using simultaneous Gaussian-mixture-model (GMM) under normal growth conditions (unstressed) and treated with vancomycin, penicillin G, nisin, fosfomycin and bacitracin. Included in the GMM fit is the corresponding heat map of the probability distribution of all trajectories **G** Bubble-plot of the diffusive populations (relative fraction sizes, D [μm² /s²]) analysed as a simultaneous two-population GMM curve fit for mVenus-PbpH.

3.3.1.2.2 The *mreB* depletion is altering the diffusive behaviour of PbpH

Additional research was performed using an mV-PbpH strain depleted of MreB and treated with cell wall stress reagents. As already discussed in 3.3.1.2.2, the diffusive behaviour of PbpH is altered by the depletion of MreB. In contrast to the other experiments with PbpH, the results of these experiments -where the cell was treated with sorbitol and NaCl - are showing that the cells are now more susceptible to osmotic stress in the absence of MreB. This is indicated by the changes in the diffusive behaviour, although the localization pattern is unaffected. The mobile fraction of PbpH is increased by 31,6% (NaCl) or 46,7% (sorbitol) (Fig. 13 D) with a diffusion coefficient of D_{static} 0.061±1.4x10^{-7} and D_{mobile} 0.7±9.9x10^{-7} after incubation of the cell for 30 min with either 500mM NaCl or 1M sorbitol.

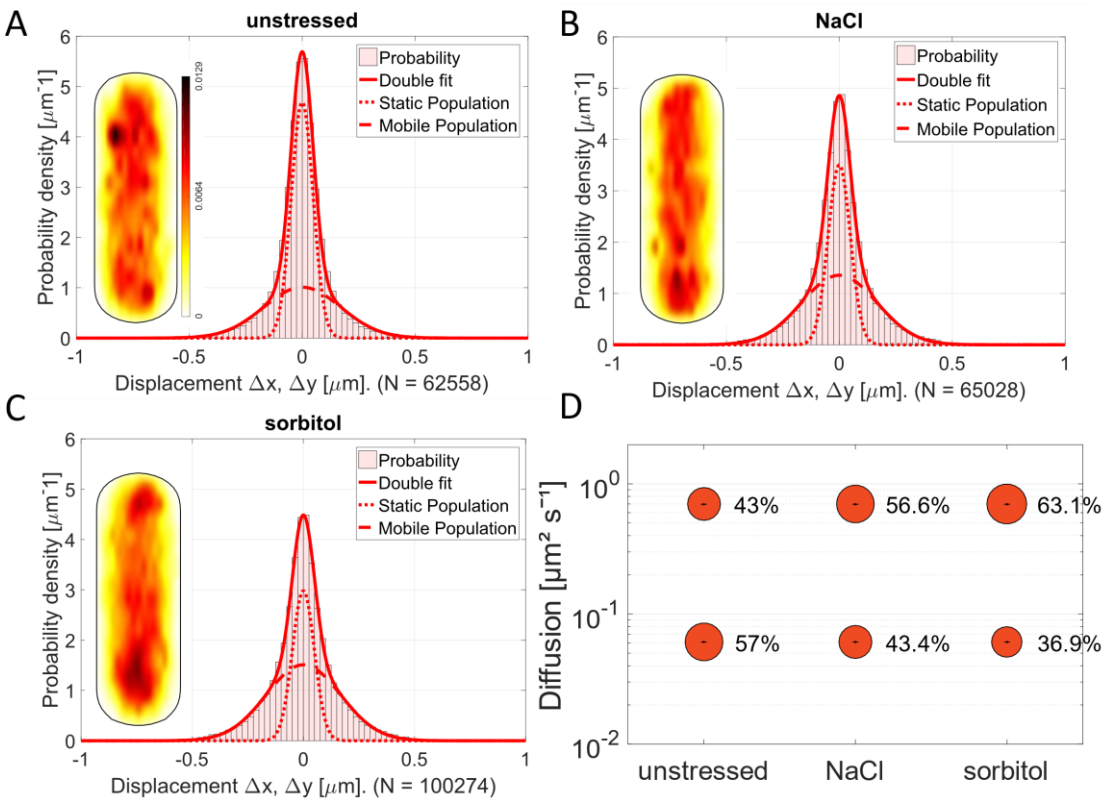

Figure 13: Analysis of PbpH dynamics in a MreB depletion strain. A-C the Gaussian Mixture model fit of PbpH is shown for the unstressed, 0.5 M NaCl and 1 M sorbitol conditions (30 min of treatment) indicating that the two-population fit sufficiently well explains the measured data. For each conditions the probability heat map of the localization is included as an inset, showing the different localization patterns of mV-PbpH. **A** contains the scale for all the heat maps. **D** bubble plot is showing the size of the population in % and the diffusion coefficients for PbpH mobility fractions.

As observed previously, all used antibiotics have a bigger influence on the diffusive behaviour of PbpH in a background without modification compared to the Δ*pbpA* background. Afterwards, it was additionally investigated whether the antibiotic influence on PbpH in a depletion MreB background is decreased, as was the case in the Δ*pbpA* background. First of all, it's visible that the antibiotics are not influencing the localization pattern of PbpH in the absence of MreB, but the influence of the antibiotics is even more obvious in the changes in the diffusive behaviour (Fig. 14).

PbpH showed a static population with D_{static} of 0.059 ±9x10^{-8} and a fast-moving population with D_{mobile} of 0.73 ± 5.2x10^{-7}, which is slightly different to the diffusion coefficients observed for PbpH single-molecule dynamics in an unmodified genetic background. Vancomycin is increasing the mobile fraction of PbpH by 57% (from 43.2% unstressed to 67.9% with vancomycin) (Fig. 14 G), which is even stronger than the influence it has on the non-genetically modified PbpH strain. The effect of penicillin G is also more pronounced than in the other two genetic backgrounds. The mobile fraction is increased by 33% when the cells get treated with penicillin G. In a similar range nisin also has an effect on the mobile population (increased by 38%) of PbpH. In contrast to the effect of fosfomycin in the non-genetically modified background which led to a decrease in the mobile fraction, fosfomycin is leading to a strong increase (by 59%) in the absence of MreB. Bacitracin is also having a strong influence on the fast-moving population of PbpH and is increasing it by 42%.

These results have inspired the conclusion that MreB - in combination with the alteration of the substrate availability by antibiotic treatment - is strongly influencing the mobility of PbpH and that not only the substrate availability effects the diffusion.

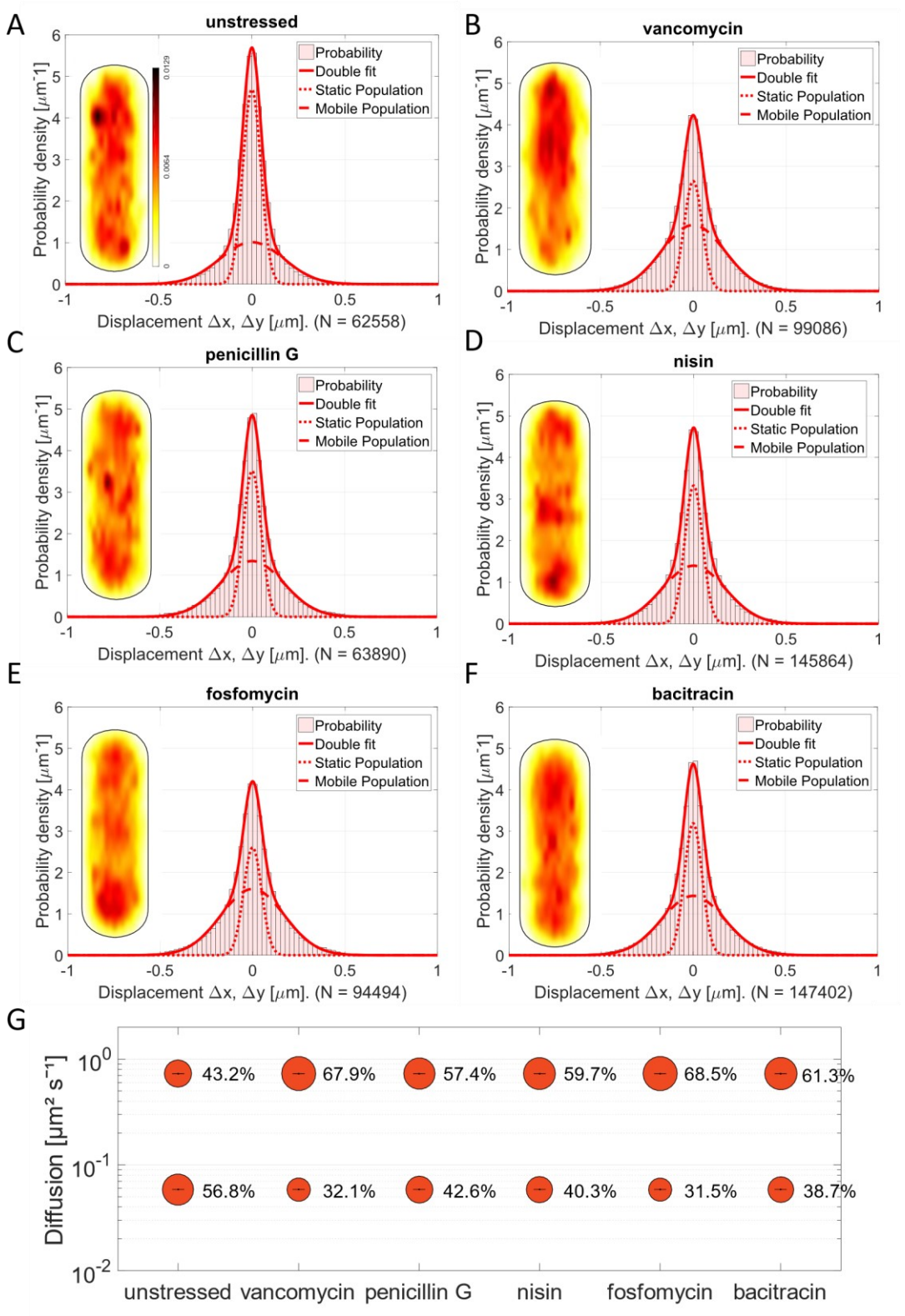

Figure 14: PbpH single-molecule dynamics in a MreB depletion strain. **A-F** Two-population fit of mVenus-PbpH single-molecule dynamics using simultaneous Gaussian-mixture-model (GMM) under normal growth conditions (unstressed) and treated with vancomycin, penicillin G, nisin, fosfomycin and bacitracin. Included in the GMM fit is the corresponding heat map of the probability distribution of all trajectories **G** Bubble-plot of the diffusive populations (relative fraction sizes, D [μm^2 /s^2]) analysed as a simultaneous two-population GMM curve fit for mVenus-PbpH.

3.3.1.3 Pbp2a

In addition to MreB and PbpH, another component of the rod complex is Pbp2a. Pbp2a is a transpeptidase and has functionally redundant enzymatic activity, like PbpH. For further experiments, Pbp2a was fused to an N-terminal mVenus to see if it has a different diffusive behaviour compared to PbpH. A part of this data was already included in the unpublished manuscript under 3.2. Additional antibiotics were now tested to provide comparable data for all of the antibiotics used to treat PbpH before (see chapter 3.3.1.2). As shown in Fig. 15, all three antibiotics (nisin, fosfomycin and bacitracin) led to a small increase of the mobile population of Pbp2a, with bacitracin having the biggest influence of these antibiotics. In contrast to the diffusive fraction, the localization pattern of Pbp2a did change to resemble a more septal localization, indicating that Pbp2a is responding to the altered lipid II distribution in the cell as already shown by Lages et al., 2013.

Next, the question was how the deletion of the redundant transpeptidase PbpH (or depleted MreB) is affecting the distribution and diffusion of mV-Pbp2a (Fig. 16), since PbpH diffusion changed strongly in the absence of either *pbpA* or MreB. Similar to the mVenus-PbpH experiments, mVenus-Pbp2a Δ*pbpH* or mVenus-Pbp2a depletion MreB were constructed. As in (chapter 3.3.1.2), all strains were checked by a western blot for correct and full-length expression of the mVenus-Pbp2a (Fig. S4) or depletion of MreB (Fig. S5).

For both genetically modified backgrounds, the probable distribution of the Pbp2a molecules is more diffuse and less localized at the septum or cell periphery (Fig. 16 B and C). Not only is the localization altered, also the fast-moving population decreases by 24% if Pbp2a is analysed in an MreB depletion background. In contrast, the diffusion of Pbp2a is only minimally changed in a Δ*pbpH* strain.

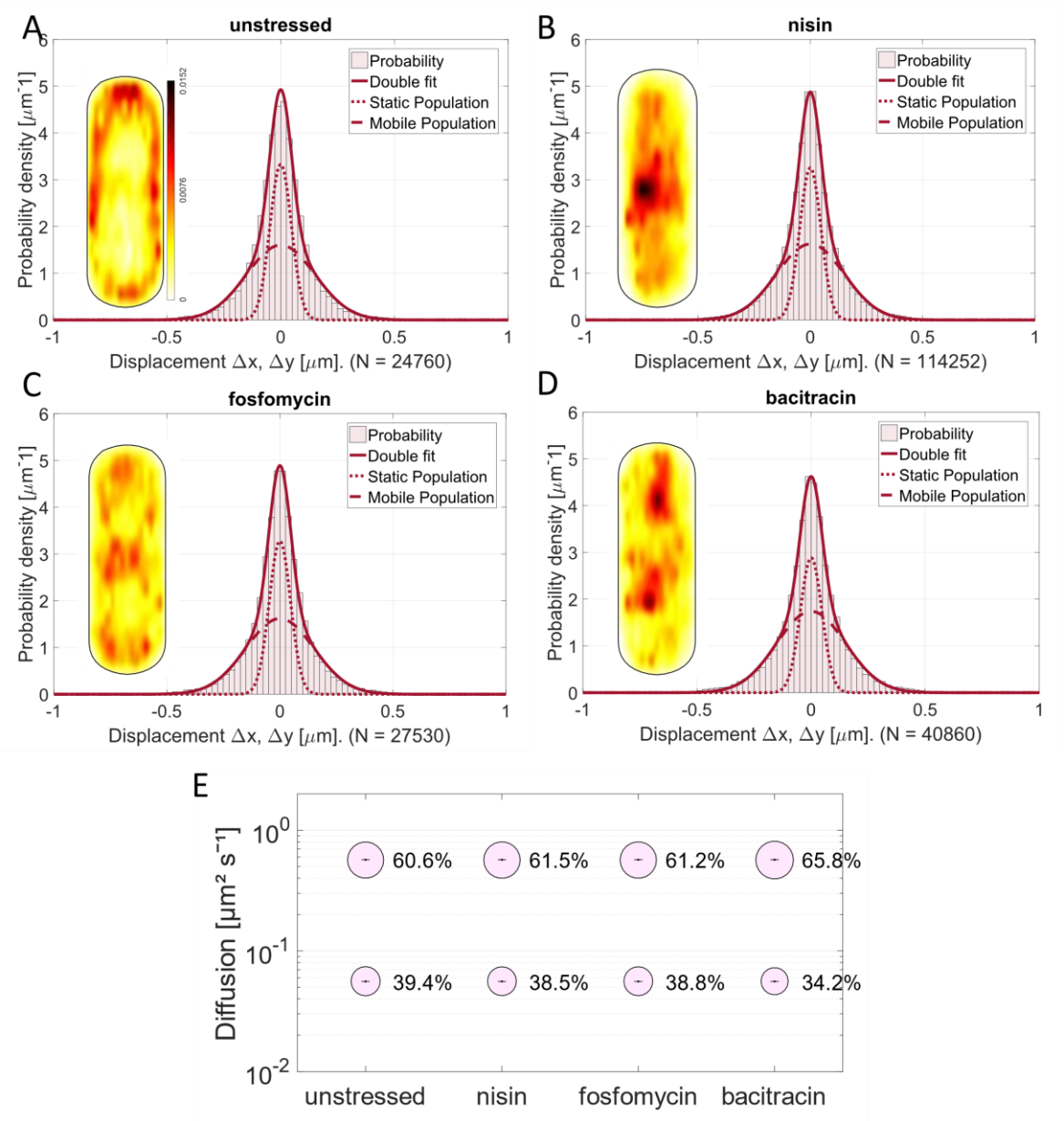

Figure 15: Analysis of Pbp2a dynamics after antibiotic treatment A-E the Gaussian Mixture model fit of Pbp2a is shown for the unstressed, 30 µg/ml nisin, 300 µg/ml fosfomycin and 200 µg/ml bacitracin conditions (30 min of treatment) indicating that the two-population fit sufficiently well explains the measured data. For each conditions the probability heat map of the localization is included as an inset, showing the different localization patterns of mV-Pbp2a. **A** contains the scale for all the heat maps. **F** bubble plot is showing the size of the population in % and the diffusion coefficients for Pbp2a mobility fractions.

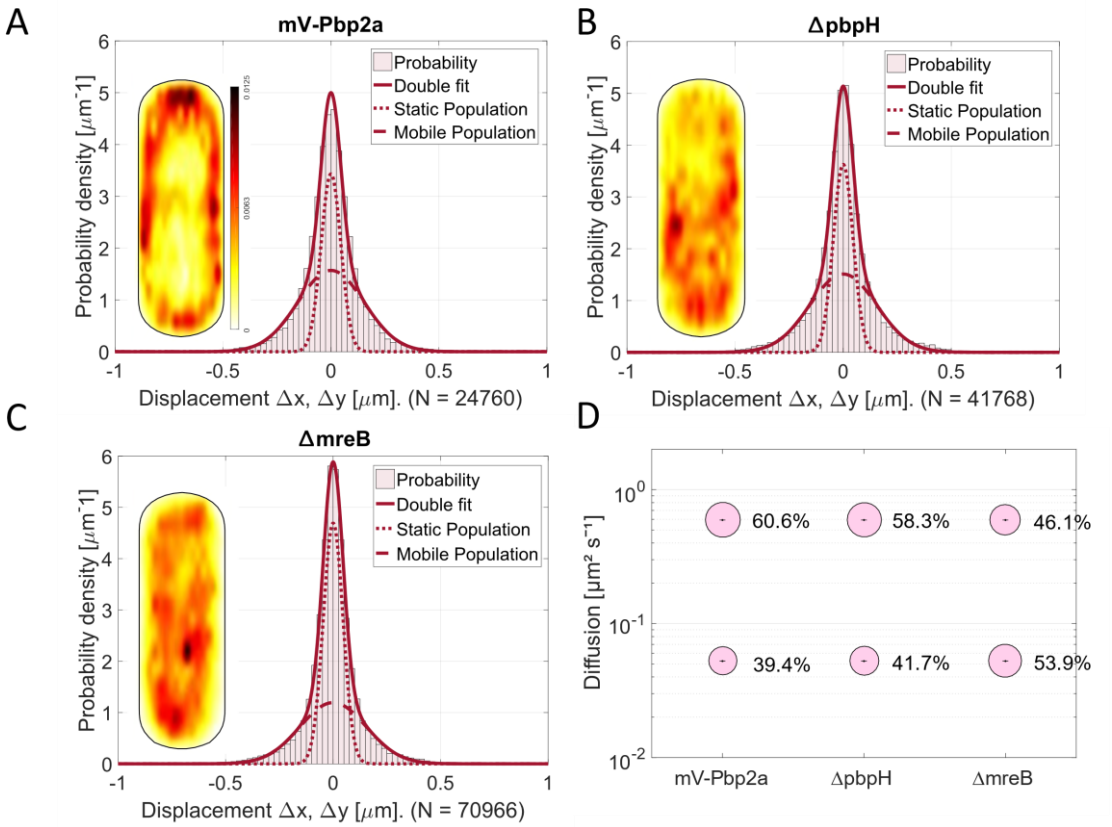

Figure 16: Analysis of Pbp2a dynamics and localization. A-C shows the GMM fit of the SMT data of three strains expressing mVenus-Pbp2a in different genetic background (deletion of *pbpH* and depletion of MreB) in comparison. **E** visualizes the two diffusive populations of the three different strains in a bubble plot.

3.3.1.3.1 Pbp2a diffusion in a Δ*pbpH* background

As with the previously discussed strains, the reaction to osmotic reagents was investigated. The stronger effect was triggered by 0.5M NaCl, which led to a high probability of Pbp2a localising at the septum and an increase in the mobile population by 26% (Fig 17 B and D). Sorbitol is leading to a small change in the fast-moving fraction of 10% (Fig. 17 D) and a slightly higher probability of a septal localization (Fig. 17 C). Overall, the diffusion coefficient was slightly different from the diffusion coefficient of Pbp2a without genetic modifications (see unpublished manuscript chapter 3.2), with a slow-moving population of D_{static} 0.055 ±1.6x10^{-7} and a fast diffusive population of D_{mobile} 0.7 ±1.6x10^{-6}. It can be assumed that having both transpeptidases makes the cell more resilient to osmotic stress and that a deletion of one can be partially replaced by the still functional redundant one, but might also make the strains more sensitive to osmotic stress and turgor changes.

If the influence of the antibiotics to the unmodified mVenus-Pbp2a strain from Fig. 15 and Fig. 3 (unpublished manuscript, 3.2.1) is compared with the one of Δ*pbpH* (Fig. 18), it is visible that a loss of *pbpH* led to a greater susceptibility to the effects of antibiotics. Particularly the influence of penicillin G is greater when treating the cells with a deletion *pbpH* background, which leads to an increase of the mobile population by 25,3% (Fig. 18 C and G). Whereas nisin is the antibiotic with the smallest effect on the diffusive behaviour of Pbp2a, meaning that holes in the membrane and a delocalization of lipid II aren't changing the diffusion of Pbp2a. The three other antibiotics have a minor effect on the diffusion of Pbp2a by increasing it by 14% (vancomycin) and 19% (bacitracin) or decreasing it by 15% (fosfomycin), but why only fosfomycin is leading to a lower fast-moving population size is unclear, since it's altering the lipid II concentration, as are most of the other antibiotics (Fig. 18 G).

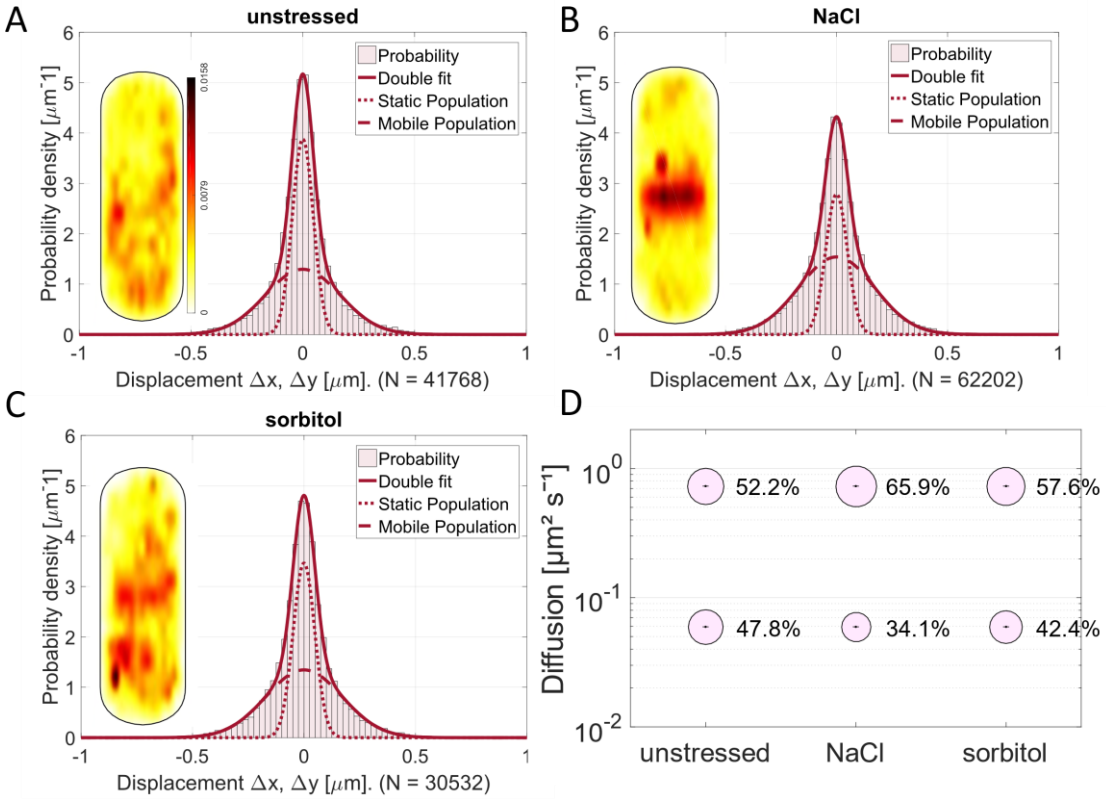

Figure 17: Analysis of Pbp2a dynamics in a Δ*pbpH* strain. **A-C** the Gaussian Mixture model fit of Pbp2a is shown for the non-stressed, 0.5 M NaCl and 1 M sorbitol conditions (30 min of treatment) indicating that the two-population fit sufficiently well explains the measured data. For each conditions the probability heat map of the localization is included as an inset, showing the different localization patterns of mV-Pbp2a. **A** contains the scale for all the heat maps. **D** bubble plot is showing the size of the population in % and the diffusion coefficients for Pbp2a mobility fractions.

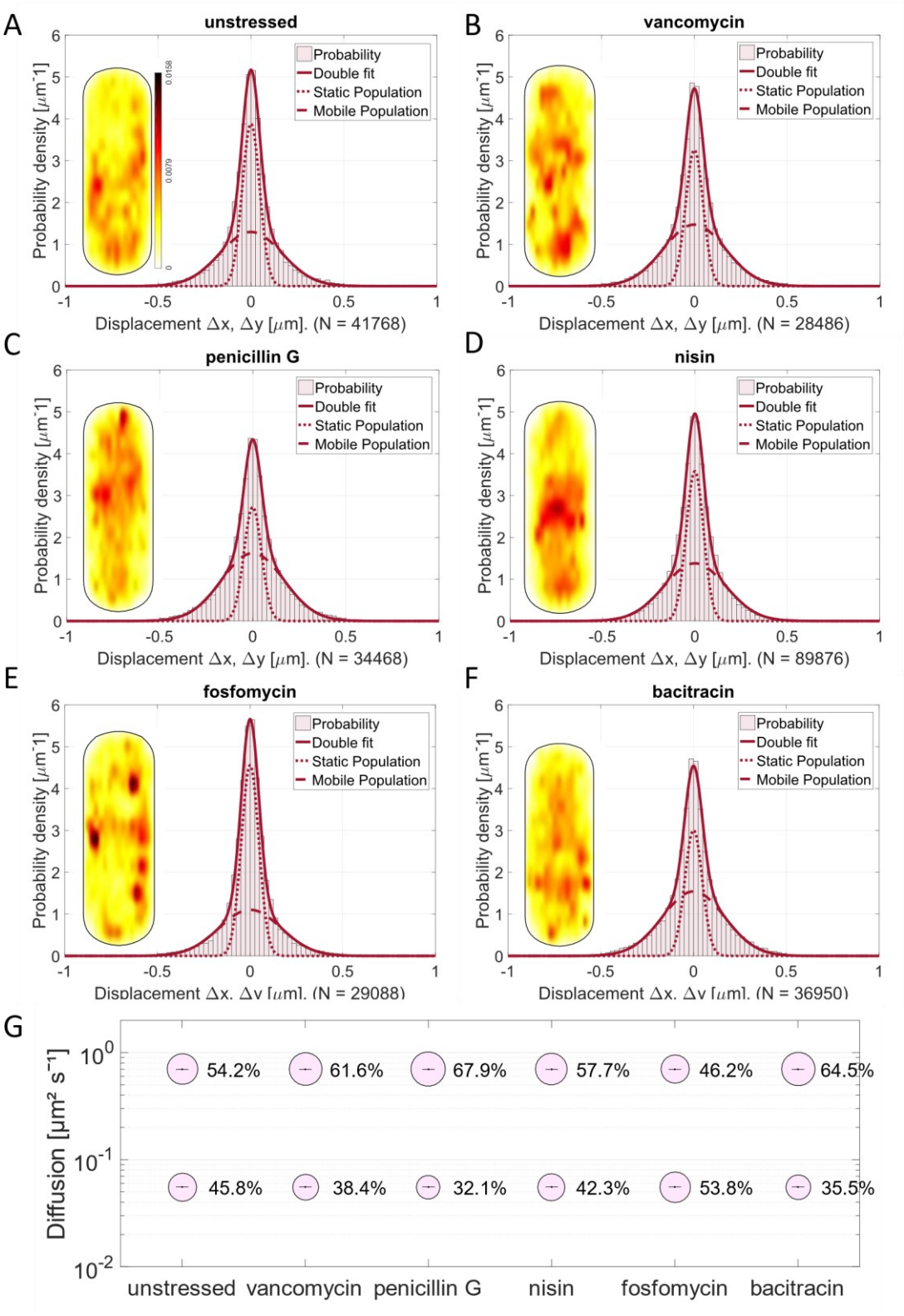

Figure 18: Pbp2a single-molecule dynamics in a Δ*pbpH* strain. A-F Two-population fit of mVenus-Pbp2a single-molecule dynamics using simultaneous Gaussian-mixture-model (GMM) under normal growth conditions (unstressed) and treated with vancomycin, penicillin G, nisin, fosfomycin and bacitracin. Included in the GMM fit is the corresponding heat map of the probability distribution of all trajectories **G** Bubble-plot of the diffusive populations (relative fraction sizes, D [$\mu m^2 / s^2$]) analysed as a simultaneous two-population GMM curve fit for mVenus-Pbp2a.

3.3.1.3.2 Pbp2a dynamics in a depletion MreB background

As the depletion of MreB had quite a remarkable effect on the diffusion of PbpH, a strong effect on the diffusive behaviour of Pbp2a was expected as well. Surprisingly, the osmotic stress only led to a minimal change of under 10% of the fraction size of Pbp2a for both conditions, in contrast to the more severe change of PbpH in the absence to MreB (Fig. 19 D). But the diffusion coefficients of Pbp2a changed to a slightly more mobile (D_{mobile} 0.65±2.9x10^{-6}) and a relatively large change could be observed in the localization pattern of Pbp2a (Fig. 19).

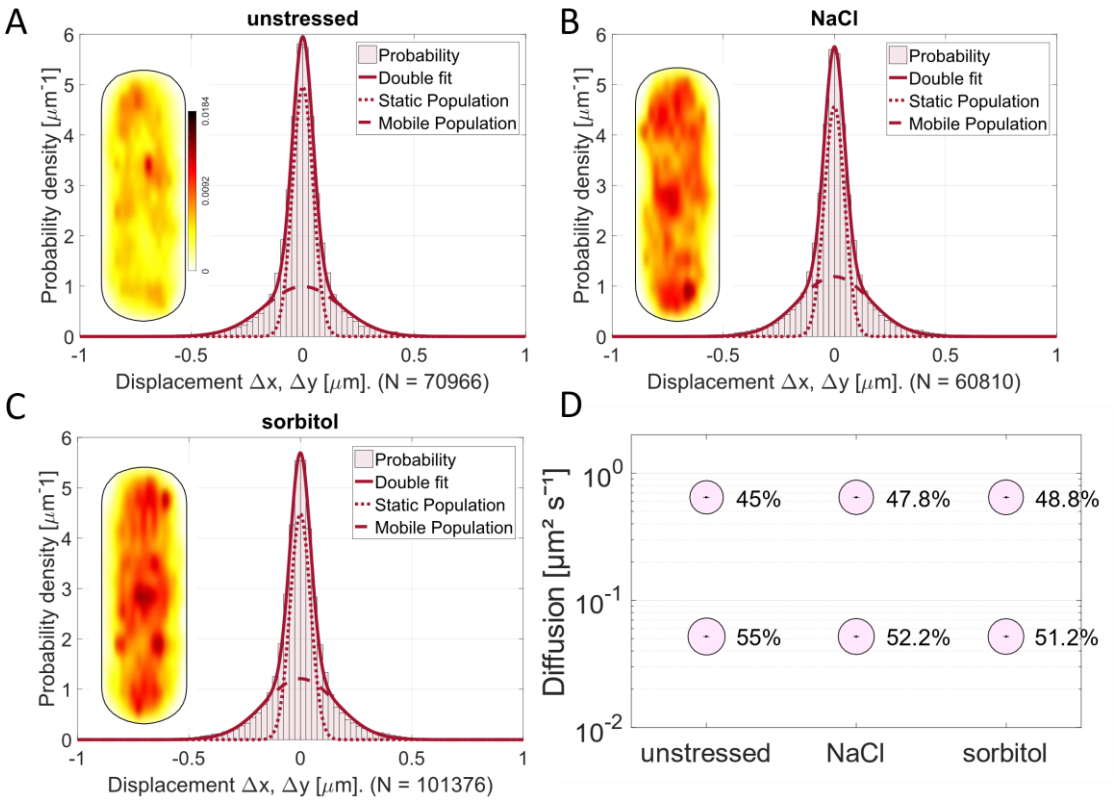

Figure 19: Analysis of Pbp2a dynamics in a MreB depletion strain. **A-C** the Gaussian Mixture model fit of Pbp2a is shown for the non-stressed, 0.5 M NaCl and 1 M sorbitol conditions (30 min of treatment) indicating that the two-population fit sufficiently well explains the measured data. For each conditions the probability heat map of the localization is included as an inset, showing the different localization patterns of mV-Pbp2a. **A** contains the scale for all the heat maps. **D** bubble plot is showing the size of the population in % and the diffusion coefficients for Pbp2a mobility fractions.

After these quite surprising results of the effects of osmotic stress on the depletion of MreB mVenus-Pbp2a strains, the following experiments were meant to elucidate whether antibiotics might lead to an even more severe effect on the dynamics of Pbp2a. Osmotic stress, but also antibiotics didn't lead to a change in the localization pattern of Pbp2a. Thus, nisin and bacitracin had a stronger effect on the fast-moving population of Pbp2a in the depletion MreB genetical background then compared to the Δ*pbpH* background. Nisin changes the mobile fraction from 42.6% to 49.4% by 16% and bacitracin was strongly increasing the fast-moving molecule population from 42.6% to 59% by 38.5% (Fig. 20 G). The absence of MreB compared to deletion of *pbpH* is not changing the diffusive behaviour of Pbp2a with the treatment with vancomycin or fosfomycin. Even more interesting is that penicillin G is not as effective in the depletion MreB background compared to the Δ*pbpH* one and is only increasing the mobile fraction by 8.9% (Fig. 20 G) in contrast to the 25.3% when *pbpH* is deleted (Fig. 18 G). The results of the dynamic behaviour of Pbp2a are supporting the idee that Pbp2a is quite robust in its behaviour and PbpH is the more sensitive one of the two redundant transpeptidases involved in the elongation process during the *Bacillus subtilis* cell cycle.

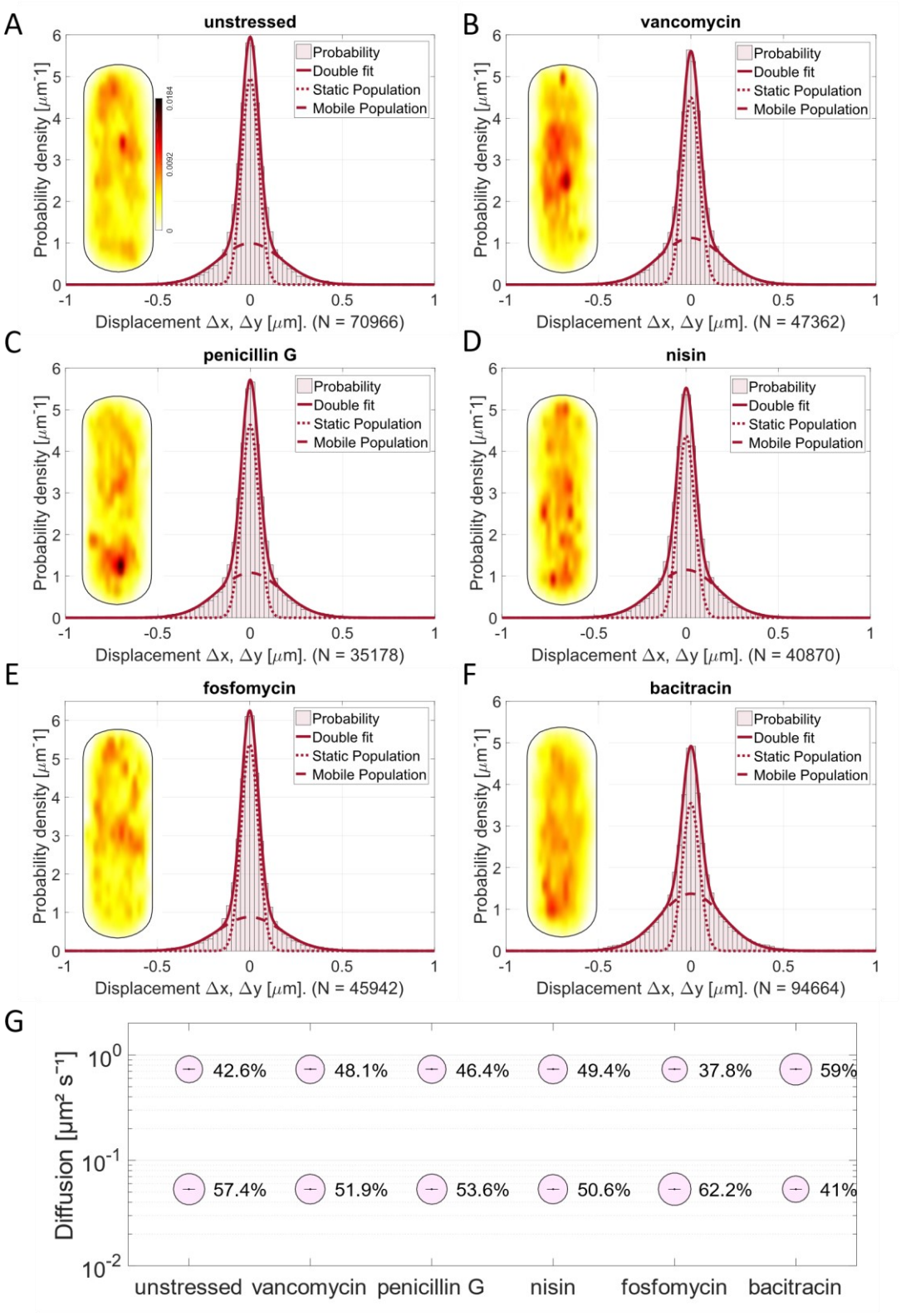

Figure 20: Pbp2a single-molecule dynamics in an MreB depletion strain. **A-F** Two-population fit of mVenus-Pbp2a single-molecule dynamics using simultaneous Gaussian-mixture-model (GMM) under normal growth conditions (unstressed) and treated with vancomycin, penicillin G, nisin, fosfomycin and bacitracin. Included in the GMM fit is the corresponding heat map of the probability distribution of all trajectories **G** Bubble-plot of the diffusive populations (relative fraction sizes, D [$\mu m^2 / s^2$]) analysed as a simultaneous two-population GMM curve fit for mVenus-Pbp2a.

3.3.2 Antibiotic treatment influence on PBP representatives of different classes of PBPs

To follow up with the experiments from the unpublished manuscript (3.2), all three strains mVenus-Pbp3, mVenus-Pbp4 and mVenus-Pbp4a were treated with the additional antibiotics nisin, fosfomycin and bacitracin to obtain a full data set comparable to the ones of Pbp2a or PbpH.

3.3.2.1 Pbp3 diffusive behaviour treated with additional antibiotics

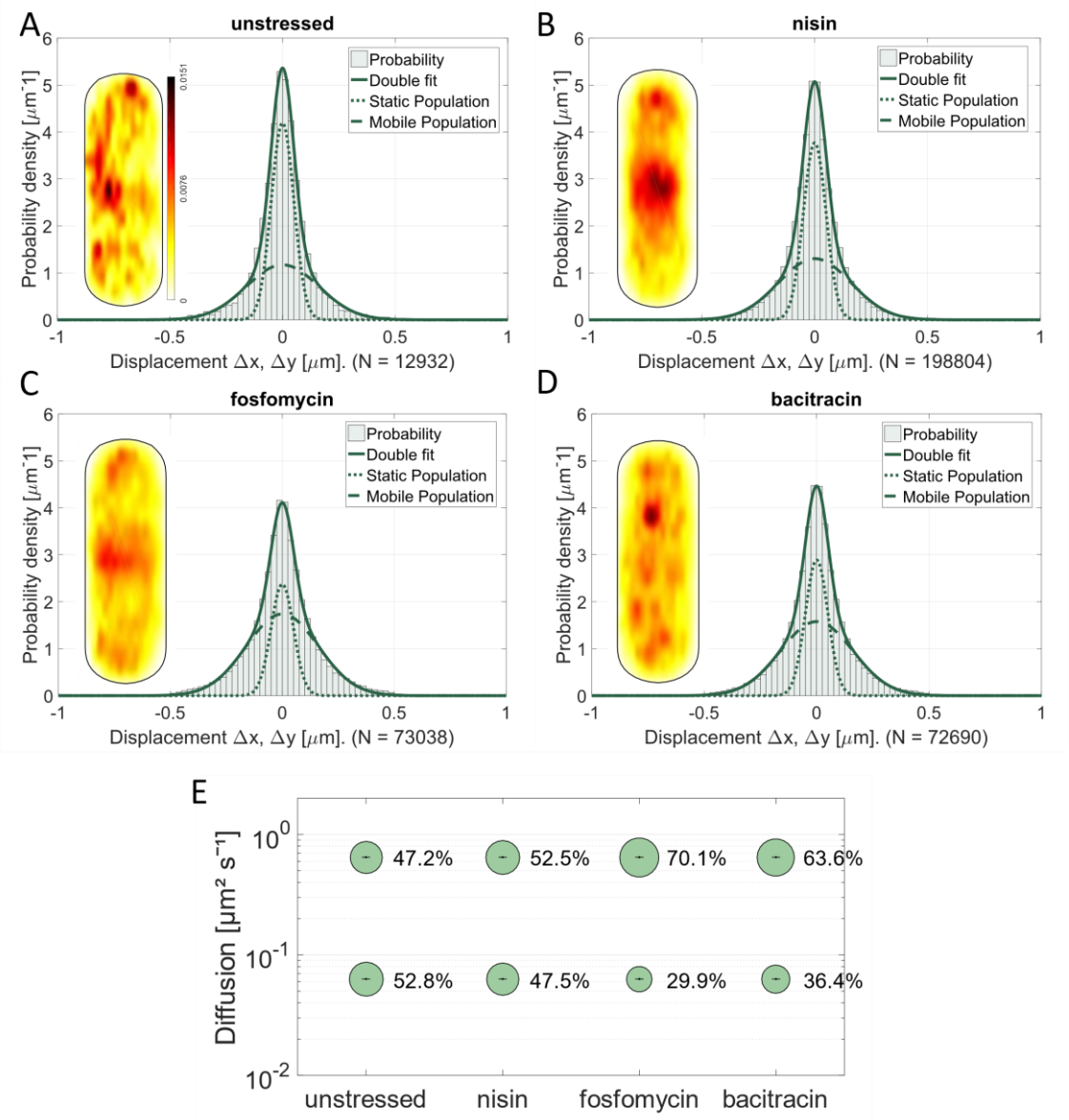

Figure 21: Analysis of Pbp3 dynamics with antibiotic treatments. **A-E** the Gaussian Mixture model fit of Pbp3 is shown for the unstressed, 30 µg/ml nisin, 300 µg/ml fosfomycin and 200 µg/ml bacitracin conditions (30 min of treatment) indicating that the two-population fit sufficiently well explains the measured data. For each conditions the probability heat map of the localization is included as an inset, showing the different localization patterns of mV-Pbp3. **A** contains the scale for all the heat maps. **F** bubble plot is showing the size of the population in % and the diffusion coefficients for Pbp3 mobility fractions.

To follow up the experiments done with mVenus-Pbp3 from the unpublished manuscript (see 3.2.1), the single molecule tracking data after treatment with three additional antibiotics nisin, fosfomycin and bacitracin was investigated. Pbp3 is another transpeptidase of *B. subtilis* and has a partly redundant function to Pbp2b, thus having a septal localisation also independent of Pbp2b (Daniel et al., 1996; Sassine et al., 2017; Sharifzadeh et al., 2020). All three antibiotics affected the diffusive behaviour of Pbp3. Especially fosfoymcin and bacitracin had a quite pronounced effect, they led to a change of the fast-moving population from 47.2% (unstressed) to 70.1% (fosfomycin) or 63.6% (bacitracin), while nisin is just increasing the mobile fraction by 11.2% (Fig. 21 E). As already explained in the manuscript, the substrate availability is a crucial factor for PBP dynamics, and this data is underpinning the extent of this, since all three are influencing either the location or the amount of the PG precursor lipid II and have a marked impact on the dynamic behaviour of Pbp3. Not only the diffusive mode of motion is altered by those three antibiotics, though - also the localization pattern of Pbp3 is changed to have a somewhat higher probability to localise at the septal area or, in the case of bacitracin, to have a more diffusive distribution.

3.3.2.2 Pbp4 dynamics is altered by antibiotics

Pbp4 is a bifunctional PBP with a transpeptidase and transglycosylase activity. The experiments also include PBPs with a different enzymatic activity, which were still known to have a connection to MreB (Kawai, Daniel, et al., 2009). After the treatment with nisin and fosfomycin, mVenus-Pbp4 cells showed a decrease in the fast-moving population of 13.8% (from 67.2% to 57.9%) for nisin or 24.1% (from 67.2% to 51%) for fosfomycin (Fig. 22 E). In contrast, bacitracin wasn't really changing the diffusive behaviour or the localization pattern at all. Nisin, on the other hand, was shown to be changing the localization pattern of Pbp4 to be more septal, whereas fosfomycin didn't alter the distribution of Pbp4 molecules in the cells (Fig. 22 B).

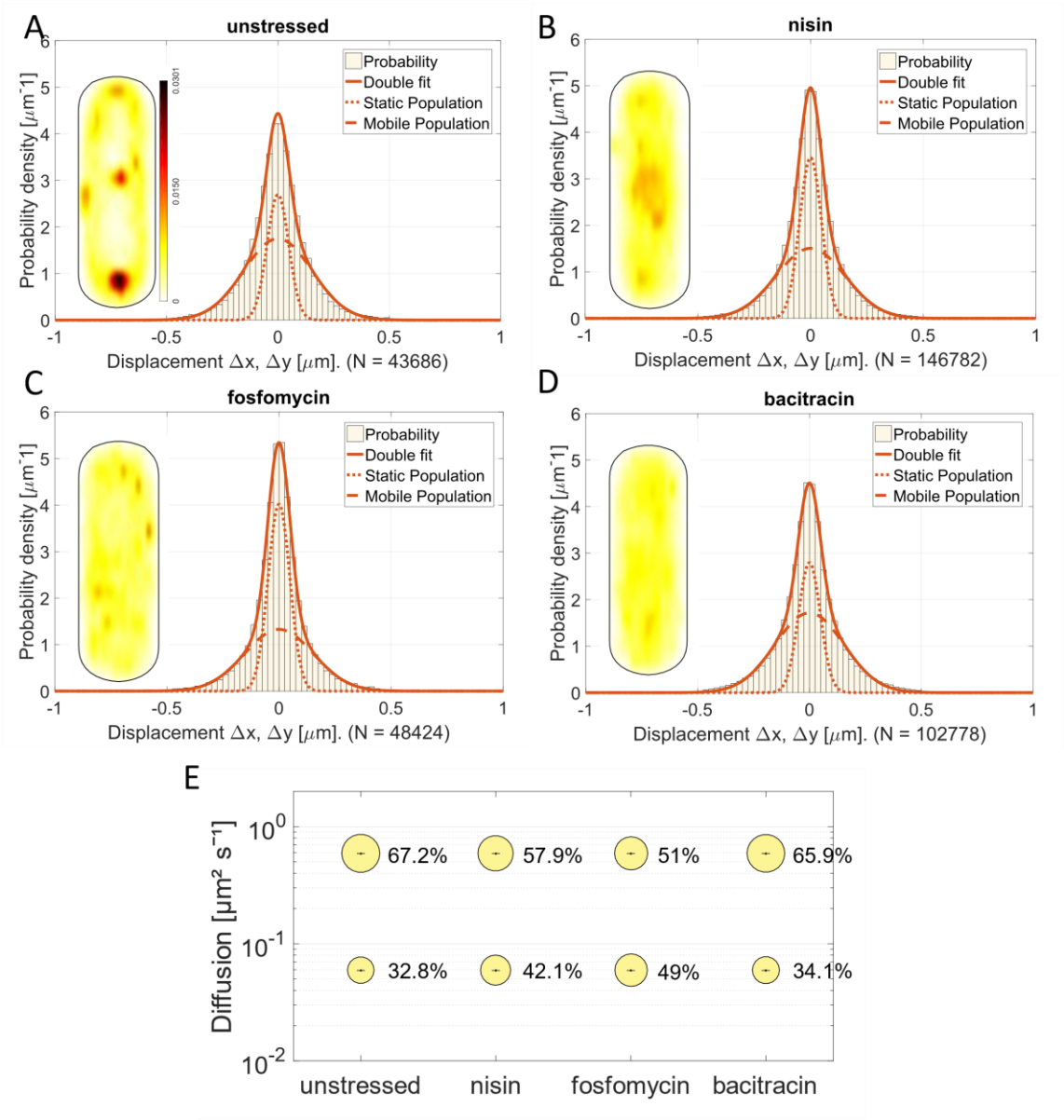

Figure 22: Analysis of Pbp4 dynamics with antibiotic treatments. **A-E** the Gaussian Mixture model fit of Pbp4 is shown for the unstressed, 30 µg/ml nisin, 300 µg/ml fosfomycin and 200 µg/ml bacitracin conditions (30 min of treatment) indicating that the two-population fit sufficiently well explains the measured data. For each conditions the probability heat map of the localization is included as an inset, showing the different localization patterns of mV-Pbp4. **A** contains the scale for all the heat maps. **F** bubble plot is showing the size of the population in % and the diffusion coefficients for Pbp4 mobility fractions.

3.3.2.3 The dynamic behaviour of Pbp4a

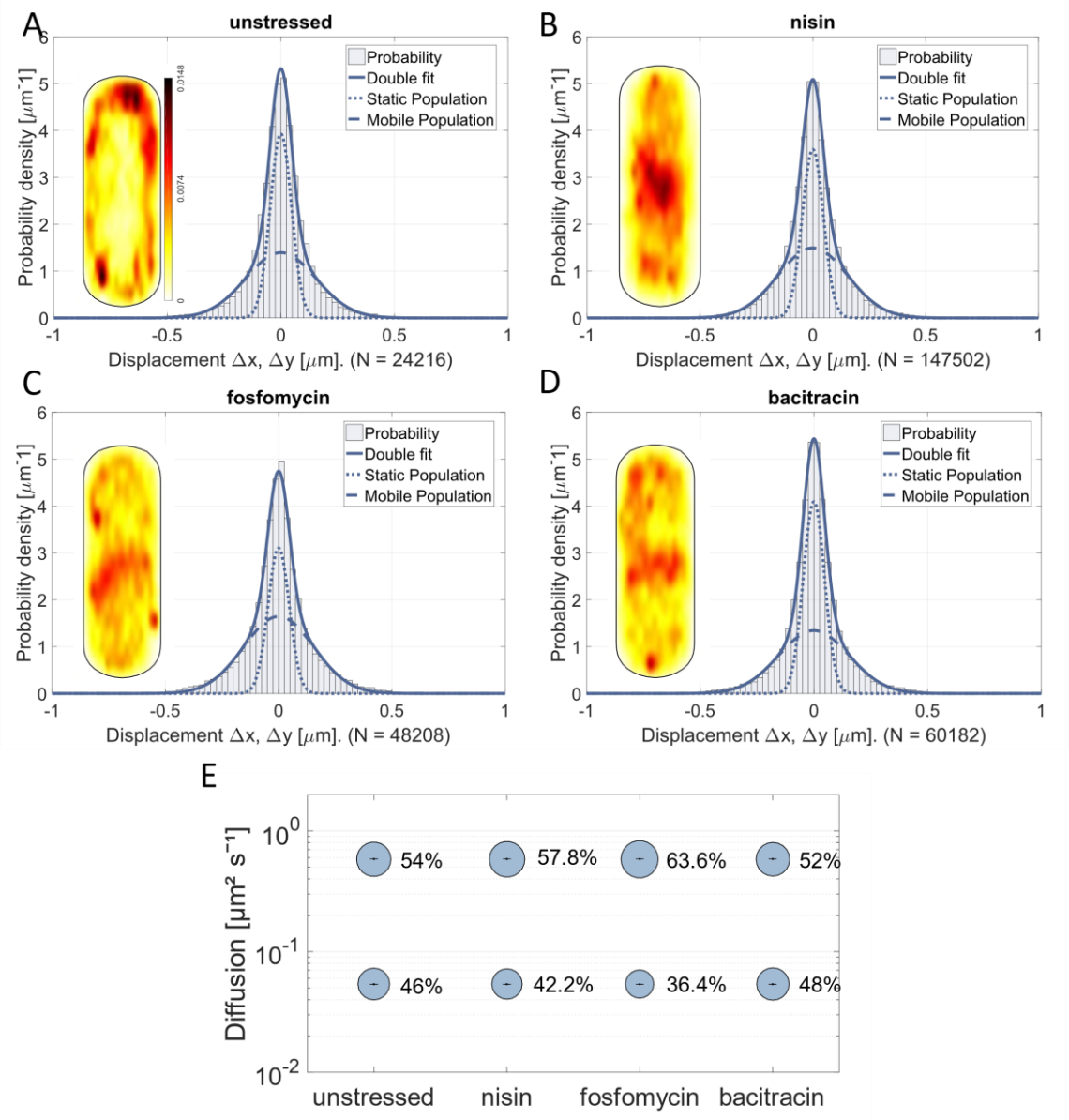

Figure 23: Analysis of Pbp4a dynamics with antibiotic treatments. A-E the Gaussian Mixture model fit of Pbp4a is shown for the unstressed, 30 µg/ml nisin, 300 µg/ml fosfomycin and 200 µg/ml bacitracin conditions (30 min of treatment) indicating that the two-population fit sufficiently well explains the measured data. For each conditions the probability heat map of the localization is included as an inset, showing the different localization patterns of mV-Pbp4a. **A** contains the scale for all the heat maps. **F** bubble plot is showing the size of the population in % and the diffusion coefficients for Pbp4a mobility fractions.

Pbp4a is exhibiting another enzymatic activity of the penicillin-binding proteins, functioning as a D,D-carboxypeptidase, cleaving the terminal D-Ala of the stem peptide to inhibit transpeptidation (Sauvage et al., 2007, 2008). Pbp4a is changing its molecule distribution strongly, when treated with all the three tested antibiotics nisin, fosfomycin and bacitracin. It appears to possess a more septal and diffuse localization shown in the normalized cell inset (heat map) of the GMM fit graphic in Fig. 23 B-D. In contrast, the diffusive behaviour only changed noticeably if the cells were treated with fosfomycin, where it led to an increase of the fast-moving mobile population by 17.2% (from 54% to 63.6%) (Fig. 23 E) and the assumption that the diffusion of Pbp4a is somehow not so much related on the substrate availability, since the other antibiotics altering the precursor amount don’t seem to influence the diffusive behaviour of Pbp4a.

4 Discussion

This work was performed to further investigate the attributes of the peptidoglycan synthesis machinery from *Bacillus subtilis*, especially the spatiotemporal dynamics of the two participating transpeptidases, Pbp2a and PbpH, as well as three additional PBPs, which were shown to interact with MreB via a bacteria two hybrid experiment (Kawai, Daniel, et al., 2009). In the discussion, the most important points from my unpublished manuscript (see section 3.2.1) and the additional results will be brought into a context after a short summary of the relevant results.

In the last decades a lot of new insights into peptidoglycan synthesis and its related proteins were gathered. Despite this, the spatiotemporal organization, and thus dynamics with different genetic backgrounds or cell wall-inhibiting conditions, are still poorly understood. MreB is important for the coordinated peptidoglycan synthesis during the elongation of bacterial cells and several highly debated hypotheses exist about how it is involved in the localization of the rod complex. The most recently proposed one is that MreB is moving in a perpendicular fashion around the cell, underneath the cell membrane, and the PGEM proteins can “hop” on and off the MreB filaments. This means that PBPs can move alongside the MreB filaments in the short term (Dersch et al., 2020), which is indicated in the left half of the model in Fig. 24. Since MreB is still quite often seen as a marker for peptidoglycan synthesis, not many studies look at the PBPs directly to study their spatiotemporal behaviour. Recently, it was published that PBPs have two main populations as their mode of motion (Özbaykal et al., 2020; Vigouroux et al., 2020). Additionally, it was shown that some PBPs have specific functions under certain conditions (Palomino et al., 2009; Peters et al., 2016; Vigouroux et al., 2020), likely revealing why *Bacillus subtilis* codes for 16 PBP genes with functional similarities.

4.1 Single molecule motion of the rod complex components MreB and different PBPs

In this section I wanted to compare the movement of Pbp2a (the redundant transpeptidase of PbpH) with the other two components of the PGEM, MreB and PbpH. as well as with three additional PBPs (Pbp3, Pbp4 and Pbp4a) known to interact with MreB (Kawai, Daniel, et al., 2009). To analyse the differences between these proteins, a single-molecule tracking approach employing high spatiotemporal resolution microscopy was used. An SMT setup was used, which is based on bleaching of yellow fluorophores and avoids the inhibition of cell growth otherwise induced by blue light, as in the case of the more commonly used blue light photoactivated localization microscopy (PALM) (El Najjar et al., 2020). To distinguish the diffusive population of the examined

proteins, the Gaussian mixture model (GMM) was normally used (Oviedo-Bocanegra et al., 2021; Rösch et al., 2018). The exception was the case of direct comparison of the proteins Pbp2a, Pbp3, Pbp4 and Pbp4a (shown in the data of the unpublished manuscript – see section 3.2.1), where the square displacement and jump distance analysis was used to obtain the diffusion coefficient and the number of the populations. All data could be sufficiently explained by at least two populations, which is also in agreement with the proposed biological function of PBPs, meaning that the molecules can have a low-mobility enzymatically active mode and a fast-mobility mode of freely diffusing molecules (Özbaykal et al., 2020). In general, the diffusion coefficients are in a similar range as known previously for other membrane proteins of *B. subtilis* mainly influenced by the membrane anchoring domains and not the MW (Lucena et al., 2018). MreB was already published to have two populations by my colleague Simon Dersch, who also performed SMT experiments, which this thesis work follows up on. This publication also included SMT data of the transpeptidase PbpH and of RodA, both showing two populations with a similar range of diffusion coefficients that Pbp2a, Pbp3, Pbp4 and Pbp4a of this thesis have (Dersch et al., 2020).

Since this thesis work is based on the same experimental setup as Dersch et al., 2020, the more comparable assumptions were made by Özbaykal et al., 2020, who show that the diffusive behaviour of the PG transpeptidase Pbp2 from *E. coli* (the corresponding transpeptidase in *B. subtilis* is Pbp2a) can also be described by two main fractions, one that is free diffusing and one that is slower and assumed to be in an active state. They are also suggesting that the slow mobile population can be divided into two additional slow sub-fractions: a substrate-bound state and a slow moving one associated with the slow movement of the PGEM with three different time intervals used (1s, 3.6s and 12s). This thesis is only distinguishing between free and slow diffusion, since the fast acquisition (20 ms between frames) of the setup doesn't allow for the differentiation between the two slow fractions corresponding to diffusive behaviour. But of course, it would be interesting to follow up on the idea that the slow-moving population of PBPs of *B. subtilis* can also be subdivided into two distinct fractions. Perhaps this can also indicate whether some of the PBPs with still unclear functions can be associated by their diffusion coefficients to one of the possible interaction partners, or this can help reveal their potential, previously unknown function in the stress response of the cell.

It has been shown previously that the bifunctional class A PBPs Pbp1 of *Bacillus subtilis* and Pbp1a and Pbp1b of *E. coli* exhibit a two-population behaviour (Cho et al., 2016; Lee et al., 2016). These two populations correspond to the two slow fractions shown by Özbaykal et al., 2020. Thus, this thesis' results can show that there is also a free diffusing

fraction for class A PBPs in Bacillus subtilis. Again; the slow-moving fraction are most likely comparable to the slow-moving fraction, but not the static fraction related to the publication by Özbaykal et al., 2020.

4.2 Dynamic adaptation of MreB to antibiotic treatment

Certain aspects of the population structure and the dynamics of MreB under normal and osmotic stress conditions (but not under antibiotic stress) were previously explored by Dr. Simon Dersch (doctoral thesis and Dersch et al., 2020). In the preparation of my thesis, I wanted to understand the reaction of MreB to antibiotic treatments (which have an inhibitory effect on the peptidoglycan synthesis) to figure out if antibiotic stress also has an effect on the dynamics of MreB. As already described before, MreB was expressed from an ectopic *amyE* site at a low level for 30 min before acquisition. At this time point the cultures (30 min before acquisition) were supplemented with the antibiotics. Here, as with the other conditions published in Dersch et al., 2020, two population were fitting the best to describe the data for all antibiotic stress conditions. MreB shows only a minor change in the mobile population for most of the antibiotics. This change is always under 10%, only fosfomycin leads to a decrease of the mobile population by 13,1 % (from 50.4% to 43.8%). In general, this data indicates that MreB movement is not strongly dependent on the PG synthesis or is affected by its inhibition.

Only fosfomycin, which inhibits the first cytosolic step of PG synthesis catalysed by MurA and by this is lowering the lipid II amount in the cell, leads to a change in the diffusive behaviour of MreB. On a different note, compared to the data presented in this thesis, it is already known that certain antibiotics can trigger a movement stop of MreB (Dominguez-Escobar et al., 2011; Garner et al., 2011). On the other hand, it is known that antibiotic treatments can also lead to dissolving filaments of MreB (Schirner et al., 2015). Since those studies are based on either epifluorescence microscopy (Schirner et al., 2015) or are applying a different time scale (Dominguez-Escobar et al., 2011; Garner et al., 2011), it is difficult to compare the results presented in this thesis to the literature. Since the dissolved filaments are visible in epifluorescence microscopy and the cells are shown to have a diffuse fluorescence signal all over the cell, it could be that the different applied time scale is not showing any changes even though in the overall signal in the cell it does. As already discussed before in section 4.1, the SMT approach used is covering the fast and slow population of the diffuse molecules, which means that the more static population is not detected by the shown data set. This more static population could correspond to the arrested MreB signal from the studies of Dominguez-Escobar et al., 2011 and Garner et al., 2011. Also, a shorter incubation time with the antibiotics was

already suggested by Schirner et al., 2015 to be potentially not sufficient to lead to a disassembly of the MreB filaments. It might, however only stop them from moving, which is why Schirner et al., 2015 applied a longer antibiotic treatment corresponding to 1-2 generation times. Therefore, the diffusive behaviour of MreB would likely also be influenced more strongly in the type of experiments presented in this thesis, if the antibiotic treatments had lasted 1 h instead of 30 min.

4.3 PbpH dynamics and the different factors influencing them

The transpeptidase PbpH is part of the PGEM and is the functionally redundant protein of Pbp2a. It is known that neither PbpH nor Pbp2a are necessary for normal bacterial growth, but deletion of both is lethal for *B. subtilis* cells (Wei et al., 2003). The results shown in this thesis are following up on the results published in Dersch et al., 2020 and the experiments involving PbpH in this publication were performed by this thesis author. In this thesis, additional results on the diffusive behaviour of PbpH with antibiotic treatments and in relation to some interaction partners (Δ*pbpA* and the depletion of MreB) were also presented (see section 3.3.1.2).

PbpH dynamics were analysed together with a varied set of antibiotics, which inhibit different steps of the peptidoglycan synthesis pathway. The diffusion of PbpH is mainly altered by the two antibiotics vancomycin, which is shielding the D-Ala-D-Ala residues of the lipid II, and bacitracin. The antibiotic bacitracin, which inhibits the recycling of UndPP and flipping it back to the cytoplasm, also leads to an increase in the mobility and mainly free diffusion of PbpH molecules in the cell, which could be explained by the search of PbpH for a substrate to then perform it enzymatic activity. The same explanation can be applied for the reaction to the vancomycin treatment. On the other hand, the bacitracin treatment led to an overall lower recycling rate of the carrier lipid UndPP, meaning that the new lipid II synthesis is impaired and leading to a lower level of lipid II in the cell (see section 1.4 about antibiotics).

Even though another antibiotic, nisin, is not changing the diffusive behaviour of PbpH, it still leads to a relocalisation of the probability distribution of the PbpH molecules. Nisin is a unique antibiotic with two diverse functions. First, it forms pores in the cell membrane, and second, it binds lipid II molecules. As Lages et al., 2013 have shown, a derivative of nisin, PP-nisin, can lead to a delocalization of PbpH, Pbp2a and Pbp1, which are localized at the peripheral cell membrane, similar to lipid II. Since nisin is also changing the membrane potential, relocalisation of the PBPs could be dependent on this factor as well. So, in the end, the localization of the peripheral proteins in studied by Lages et al.,

2013 could be achieved by the changed localization of lipid II, the membrane potential changes or a combination of both effects. In contrast to this study, the generated heat maps for PbpH with nisin treatment show a higher probability of PbpH molecules to localize in the mid cell region. In this case the localization would be more influenced by the membrane fluidity and additional proteins involved in PG synthesis such as various cytoskeletal elements and the Min inhibitory system (Strahl & Hamoen, 2010), which also preferentially localize in regions with high fluidity. Thus, one hypothesis would be that PbpH is aiming to reach the lipid II directly after getting flipped out and before nisin can interact with lipid II. This is also a hypothesis that can generally be applied to all PBPs of this study and their different genetic backgrounds, since most of the enzymatic functions of the PBPs are dependent on the interaction with lipid II, when it is flipped to the outside of the cell. As nisin can only act outside of the cell, nisin and PBPs are competing for lipid II binding.

Similar effects of the antibiotics on PbpH were noticeable in the Δ*pbpA* background, showing a less pronounced effect of bacitracin, which is striking since the mechanism of action of bacitracin is the same. Therefore, the recycling of the lipid carrier and lowered lipid II amounts in the cell might lead to a slightly increased diffusion of PbpH, meaning that just additional PbpH molecules are looking for an interaction site, since the level of their substrate has dropped. This small effect could perhaps be explained more generally by an inadequate incubation time with the antibiotic. This could have a more severe effect, while alternatively, another explanation would be that the high temporal resolution of the microscopy is not capturing the fraction of molecules that are most affected by the antibiotic treatment. As evidence for this, Pbp2 in *E. coli* was also discovered as a static fraction within the slow-moving molecule population (Özbaykal et al., 2020).

The depletion of MreB has a greater influence on the diffusive behaviour of PbpH than Δ*pbpA,* and it was discovered to increase the static population by 11% (from 41.7% to 53.7%), leading to the assumption that not only the substrate availability of lipid II is important for the dynamics of PbpH (Lages et al., 2013), but that MreB movement also influences PbpH. Perhaps the protein becomes more static because of the missing directionality of the PG synthesis that MreB normally provides to a certain extent (Dersch et al., 2020; Dominguez-Escobar et al., 2011; Garner et al., 2011; Özbaykal et al., 2020).

As already mentioned, lipid II might be one of the main factors (in addition to MreB) to position PbpH in the cell, and might be influencing its diffusion. Therefore, it is not surprising that treatment with antibiotics decreases the availability of the substrate lipid II, and has a very strong effect by increasing the free diffusive population of PbpH by up

to almost 60%. This led to the assumption that in the absence of MreB the diffusion of PbpH is more sensitive towards the effects of antibiotics, showing the underlying mechanisms of a synergistic effect of MreB and antibiotics on keeping the rate of cell elongation regulated in *Bacillus subtilis*. The next step would be to find out if the PGEM can still normally form after the synergistic effect of absence of MreB and antibiotic treatment and to see if the static fraction might show a different adjustment to the antibiotic treatment in the absence of MreB.

4.4 Dynamic behaviour of Pbp2a in adaptation to different influences

As the diffusive behaviour of PbpH was already examined in this thesis as well as in Dersch et al., 2020 and it is known that *Bacillus subtilis* has two functional redundant transpeptidases within the PGEM (Wei et al., 2003), the other transpeptidase Pbp2a was analysed to gain a better understanding, at which point which transpeptidase is more involved in PG synthesis and what effect stress conditions have on the dynamics of Pbp2a if PbpH or MreB are missing. The dynamics of Pbp2a appeared quite robust against antibiotic treatment as well as osmotic stress conditions, which is relatively different from the diffusion of PbpH reacting to vancomycin and bacitracin strongly. Vancomycin is the only antibiotic having an effect on Pbp2a and leads to a change of roughly by 28% from 50% to 36%. It could mean that the stress conditions were still too mild to trigger a great reaction of Pbp2a, or perhaps the diffusion of Pbp2a is not as dependent on the lipid II localization as previously assumed in the research field, or that Pbp2a localizes by finding the structure of the bacterial cell wall, as already suggested for *E. coli* Pbp2 (Özbaykal et al., 2020).

Pbp2a demonstrated a similar behaviour in the context of the deletion/depletion as PbpH, and the molecules became approximately 24% more static. This leads to the identical assumptions made in the previous chapter/paragraph for PbpH. Surprisingly, comparing the reaction of PbpH to osmotic stress as well as antibiotic treatment in the absence of *pbpA*, and now the reaction of Pbp2a in the absence of *pbpH* to the same treatment, the effect on PbpH seems to be higher and the diffusion seems to be more susceptible to the stress conditions. This could in theory mean that PbpH is dealing with the stress factors while Pbp2a is keeping the normal function or behaviour up and needs to take over the function of PbpH when it is deleted. In both genetically modified backgrounds, fosfomycin is leading to an increase of the static population, so somehow the cytoplasmic

inhibition is slowing the diffusion of Pbp2a down, while by contrast, the other antibiotics which target processes in the periplasm make Pbp2a diffuse faster.

From the data shown, it is possible that Pbp2a diffusion and localization might be differently regulated than the one of PbpH, or also harbouring additional functions related to the cell cycle. The evidence for the different function in the cell cycle could be the interaction of *E. coli* Pbp2 with the division site. In *E. coli* it was shown that Pbp2 (corresponding to Pbp2a in *B. subtilis*) colocalizes with Pbp3, which is responsible for the construction of new poles, at the early division site (Van der Ploeg et al., 2013). Perhaps Pbp2a is also interacting with the division since the data presented in this thesis also show a localization to the division site. The idea of Pbp2a localizing to the division site is further supported by the knowledge that Pbp1 of *Bacillus subtilis* can shuttle between the elongasome and the divisome, having a function in both. Pbp1 is also known to interact with MreB, which is also an interaction partner of Pbp2a (Claessen et al., 2008; Kawai, Daniel, et al., 2009).

In the schematic figure below, a model for the effect of antibiotics on the PGEM is shown. While the untreated condition (left panel) is depicting the up-to-date knowledge on how the elongation of the cell wall synthesis works, while the antibiotic treatment panel is trying to summarize the findings of this thesis work together with the known influence of antibiotics on the proteins involved in the PGEM. Since all proteins´ diffusion could be explained by a two-population fit, the relatively small sized complexes arising from protein-protein interactions should indicate the slow-moving fraction, as already discussed before, there is still some interaction possible even though the substrate availability cannot support the localization of shown proteins, and therefore the single proteins might be the fast-moving molecule fraction. The lipid II level is depicted by small lipid II molecules under the cell and the effect of nisin is depicted by nisin pores. As the PGEM is a complex topic with several proteins involved, this is just a small insight into what is really happening and more details need to get discovered to shed full light on the full process.

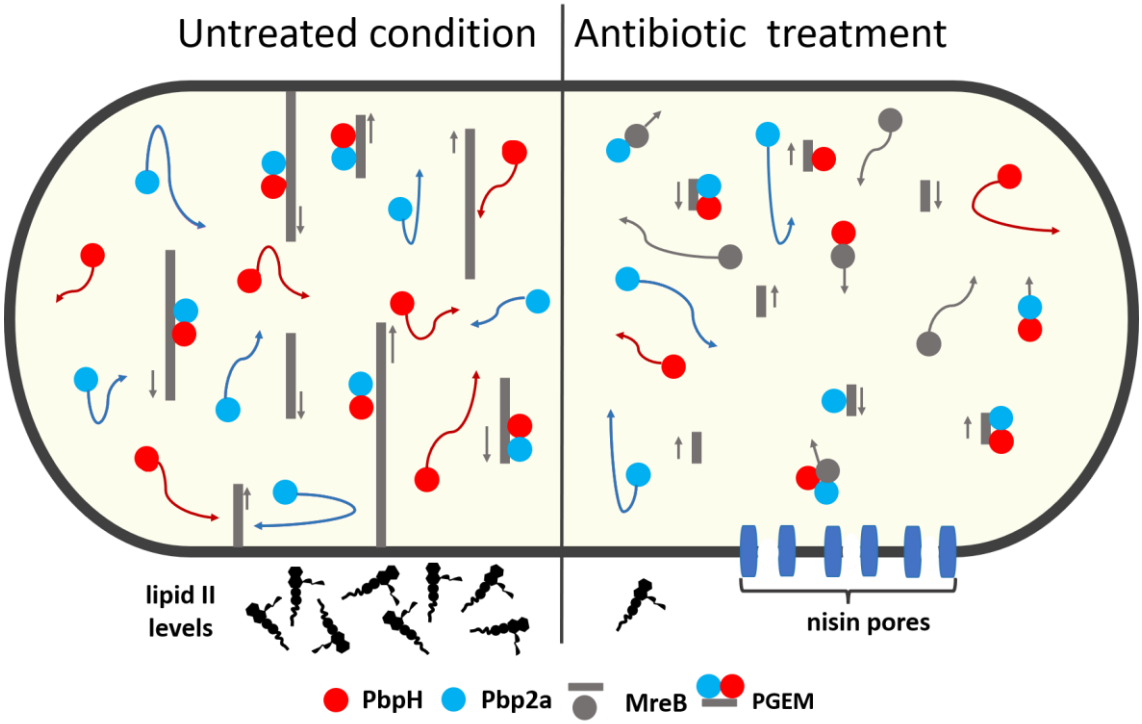

Figure 24: Schematic summary of the effect of antibiotics on PGEM proteins Arrows indicate direction of movement, vertical strands represent MreB filaments. Identities of depicted proteins explained in the figure legend. Left panel indicates dynamics pre-antibiotic treatment, right panel post-treatment.

4.5 Dynamics of additional PBPs and the adaptation to osmotic stress conditions or antibiotic treatment

The *Bacillus subtilis* genome codes for several PBPs, not all of them have a known function during in the cell cycle, but they are suggested to have a role in adaptation under unfavourable conditions. Recently, several studies were published dealing with specific functionalities during different adaptation processes mainly in *E. coli*. Mueller & Levin, 2020 summarized the adaptation not only of cell wall synthesis proteins to environmental changes, but also of the proteins involved in maturation and lysis of the bacterial cell wall. For example, the *E. coli* D,D-carboxypeptidase Pbp6b was found to have an important role in maintaining cell shape at low pH (Peters et al., 2016), showing that redundancy can strongly influence the adaptation to stress. Another interesting mechanism was found by Vigouroux et al., 2020, showing that the class A PBP Pbp1b in *E. coli* can repair small cell wall defects. The authors of this article suggest that a sensing of the cell wall structure is a potential mechanism of localization for PBPs as well. Additionally, more PBPs should have this ability to sense defects and repair them (Vigouroux et al., 2020). Since *E. coli* is the primarily studied organism when it comes to cell wall mechanisms, not as much is known for *Bacillus subtilis* yet. A recent study showed that the class A PBP Pbp1 also has a cell shape-regulating function as in *E. coli,*

and that it possesses the antagonistic function to the Rod-complex, leading to a normal width of the bacterial cell (Dion et al., 2019). This indicates that there must be some regulation and adaptation to environmental conditions taking place.

As already discussed for E. coli that the carboxypeptidase Pbp6b has a function in pH adaptation, the D,D,-endopeptidase Pbp4* has a regulatory function in high salt stress adaptation in *B. subtilis* (Palomino et al., 2009). In this thesis the dynamic adaptation of three additional PBPs, Pbp3, Pbp4 and Pbp4a, was examined under osmotic and antibiotic stress conditions as before the components of the PGEM. These proteins all have different enzymatic activities and thus belong to different classes of PBPs.

Pbp3 is another transpeptidase of *Bacillus subtilis* and it is known that it has a redundancy with the cell division-associated PBP Pbp2b (Sassine et al., 2017). Osmotic stress by sorbitol led to a pronounced change of the free diffusive population from 44.6% to 53.3% (overall by 15.9%). This could indicate that Pbp3 could be important for the coordination of cell shape maintenance under osmotic stress conditions, and that it is reacting to the higher turgor pressure. Since a more septal orientation of the Pbp3 molecules is visible with sorbitol stress, this might hint towards a function of the protein in stabilizing the cell division under osmotic stress. Interestingly, it is also reacting relatively strongly to all antibiotic treatments that were applied, with a bigger population of freely diffusing molecules and a higher proportion of them localizing at the division site, generally creating the picture of being involved in stabilizing the division site under different stress conditions. It would be interesting to follow up on this theory and perform additional experiments especially inhibiting the division site and have a look at the dynamics in a depletion or inactive Pbp2b background to see if a stronger reaction to stress conditions can be triggered.

Pbp4 was another examined member of the class A PBPs with both a transpeptidase and transglycosylase activity. *Bacillus subtilis* harbours four class A proteins, one of them being Pbp1, which is described to be part of the mechanism regulating the cell width together with the Rod complex (Dion et al., 2019). Additionally, keeping in mind that Pbp1b of *E. coli* is responsible for the repair of cell wall defects and also shows a more static diffusive fraction of molecules (Vigouroux et al., 2020), something similar can be seen for the slow diffusive population of Pbp4 in the data shown in this thesis for most of the applied stress conditions at a different intensity. This is leading to the idea that Pbp4 could also have a cell wall repair function, and that it is sensing cell wall defects mainly at the lateral cell wall, since it was not showing any strong tendency to have a division site affinity.

The last PBP that needs to get discussed is Pbp4a, a D,D-carboxypeptidase of *Bacillus subtilis* known to have an ability to bind D-Ala-D-Ala residues of PG (Sauvage et al., 2007). An *E. coli* carboxypeptidase Pbp6b is maintaining cell shape under low pH conditions (Peters et al., 2016) and a *B. subtilis* endopeptidase has a regulating function in high salt stress response (Palomino et al., 2009). Looking at the results of this thesis, slight changes in the behaviour of diffusion are visible, but stronger changes in the probability distribution of the Pbp4a molecules in the standardized heat map hint towards a relocalisation during stress response to mid-cell. Vancomycin and penicillin G are an exception to these observations. Molecules have a more diffuse distribution in the cell after the treatment with these antibiotics, which also lead to a somewhat higher increase in the mobile population. This could indicate that Pbp4a might be involved in the maturation of the cell wall and its diffusion is more dependent on the interaction with the PG strands of the cell wall and by the interaction with other PBPs or on the precursor lipid II availability. Additionally, the localisation also seems to be dependent on the site of strongest PG synthesis.

In general, there is still a lot that is unclear in the spatiotemporal organisation of the cell wall synthesis, as well as in the regulation and response to cell wall stress of *Bacillus subtilis*. Further studies need to be performed to cover the effect of cell wall stress on additional important proteins during PG synthesis, such as RodA, MurG, Mbl and some of the hydrolytic enzymes responsible for creating the space to insert newly synthesised PG strands. Another approach would be to determine the level of expression of PBPs during different stress conditions and find either up- or downregulations. Mutagenic studies inhibiting the enzymatic activities might be an option as well. This would allow better deeper insights into the regulation, and learning whether related proteins behave differently under such conditions.

References

Aarsman, M. E. G., Piette, A., Fraipont, C., Vinkenvleugel, T. M. F., Nguyen-Distèche, M., & Blaauwen, T. den. (2005). Maturation of the Escherichia coli divisome occurs in two steps. *Molecular Microbiology*, *55*(6), 1631–1645. https://doi.org/10.1111/J.1365-2958.2005.04502.X

Albertini, A., & Galizzi, A. (1999). The sequence of the trp operon of Bacillus subtilis 168 (trpC2) revisited. *Microbiology (Reading, England)*, *145 (Pt 1*(12), 3319–3320. https://doi.org/10.1099/00221287-145-12-3319

Angeles, D. M., & Scheffers, D. J. (2020). The cell wall of bacillus subtilis. *Current Issues in Molecular Biology*, *41*, 539–596. https://doi.org/10.21775/cimb.041.539

Barreteau, H., Kovač, A., Boniface, A., Sova, M., Gobec, S., & Blanot, D. (2008). Cytoplasmic steps of peptidoglycan biosynthesis. *FEMS Microbiology Reviews*, *32*(2), 168–207. https://doi.org/10.1111/j.1574-6976.2008.00104.x

Barrows, J. M., & Goley, E. D. (2021). FtsZ dynamics in bacterial division: What, how, and why? *Current Opinion in Cell Biology*, *68*, 163–172. https://doi.org/10.1016/j.ceb.2020.10.013

Beeby, M., Gumbart, J. C., Roux, B., & Jensen, G. J. (2013). Architecture and assembly of the Gram-positive cell wall. *Molecular Microbiology*, *88*(4), 664–672. https://doi.org/10.1111/MMI.12203

Bendezú, F. O., Hale, C. A., Bernhardt, T. G., & De Boer, P. A. J. (2009). RodZ (YfgA) is required for proper assembly of the MreB actin cytoskeleton and cell shape in E. coli. *EMBO Journal*, *28*(3), 193–204. https://doi.org/10.1038/emboj.2008.264

Bhavsar, A. P., & Brown, E. D. (2006). Cell wall assembly in Bacillus subtilis: How spirals and spaces challenge paradigms. *Molecular Microbiology*, *60*(5), 1077–1090. https://doi.org/10.1111/j.1365-2958.2006.05169.x

Billaudeau, C., Chastanet, A., Yao, Z., Cornilleau, C., Mirouze, N., Fromion, V., & Carballido-López, R. (2017). Contrasting mechanisms of growth in two model rod-shaped bacteria. *Nature Communications*, *8*. https://doi.org/10.1038/ncomms15370

Bisson-Filho, A. W., Hsu, Y. P., Squyres, G. R., Kuru, E., Wu, F., Jukes, C., Sun, Y., Dekker, C., Holden, S., VanNieuwenhze, M. S., Brun, Y. V., & Garner, E. C. (2017). Treadmilling by FtsZ filaments drives peptidoglycan synthesis and bacterial cell division. *Science*, *355*(6326), 739–743. https://doi.org/10.1126/science.aak9973

Botta, G. A., & Park, J. T. (1981). Evidence for involvement of penicillin-binding protein 3 in murein synthesis during septation but not during cell elongation. *Journal of Bacteriology*, *145*(1), 333–340. https://doi.org/10.1128/jb.145.1.333-340.1981

Bramkamp, M., Weston, L., Daniel, R. A., & Errington, J. (2006). Regulated intramembrane proteolysis of FtsL protein and the control of cell division in Bacillus subtilis. *Molecular Microbiology*, *62*(2), 580–591. https://doi.org/10.1111/J.1365-2958.2006.05402.X

Breukink, E., & de Kruijff, B. (2006). Lipid II as a target for antibiotics. *Nature Reviews Drug Discovery*, *5*(4), 321–323. https://doi.org/10.1038/nrd2004

Burkholder, P. R., & Giles, N. H. (1947). INDUCED BIOCHEMICAL MUTATIONS IN

BACILLUS SUBTILIS. *American Journal of Botany*, *34*(6), 345–348. https://doi.org/10.1002/J.1537-2197.1947.TB12999.X

Cho, H., Wivagg, C. N., Kapoor, M., Barry, Z., Rohs, P. D. A., Suh, H., Marto, J. A., Garner, E. C., & Bernhardt, T. G. (2016). Bacterial cell wall biogenesis is mediated by SEDS and PBP polymerase families functioning semi-Autonomously. *Nature Microbiology*, *1*(September). https://doi.org/10.1038/nmicrobiol.2016.172

Chung, K. M., Hsu, H. H., Govindan, S., & Chang, B. Y. (2004). Transcription regulation of ezrA and its effect on cell division of Bacillus subtilis. *Journal of Bacteriology*, *186*(17), 5926–5932. https://doi.org/10.1128/JB.186.17.5926-5932.2004

Claessen, D., Emmins, R., Hamoen, L. W., Daniel, R. A., Errington, J., & Edwards, D. H. (2008). Control of the cell elongation-division cycle by shuttling of PBP1 protein in Bacillus subtilis. *Molecular Microbiology*, *68*(4), 1029–1046. https://doi.org/10.1111/j.1365-2958.2008.06210.x

Csonka, L. N. (1989). Physiological and genetic responses of bacteria to osmotic stress. *Microbiological Reviews*, *53*(1), 121–147. https://doi.org/10.1128/mmbr.53.1.121-147.1989

Daniel, R. A., & Errington, J. (2000). Intrinsic instability of the essential cell division protein FtsL of Bacillus subtilis and a role for DivIB protein in FtsL turnover. *Molecular Microbiology*, *36*(2), 278–289. https://doi.org/10.1046/J.1365-2958.2000.01857.X

Daniel, R. A., & Errington, J. (2003). Control of cell morphogenesis in bacteria: Two distinct ways to make a rod-shaped cell. *Cell*, *113*(6), 767–776. https://doi.org/10.1016/S0092-8674(03)00421-5

Daniel, R. A., Williams, A. M., & Errington, J. (1996). A complex four-gene operon containing essential cell division gene pbpB in Bacillus subtilis. *Journal of Bacteriology*, *178*(8), 2343–2350. https://doi.org/10.1128/jb.178.8.2343-2350.1996

de Kruijff, B., van Dam, V., & Breukink, E. (2008). Lipid II: A central component in bacterial cell wall synthesis and a target for antibiotics. *Prostaglandins Leukotrienes and Essential Fatty Acids*, *79*(3–5), 117–121. https://doi.org/10.1016/j.plefa.2008.09.020

Defeu Soufo, H. J., & Graumann, P. L. (2004). Dynamic movement of actin-like proteins within bacterial cells. *EMBO Reports*, *5*(8), 789–794. https://doi.org/10.1038/sj.embor.7400209

Defeu Soufo, H. J., & Graumann, P. L. (2006). Dynamic localization and interaction with other Bacillus subtilis actin-like proteins are important for the function of MreB. *Molecular Microbiology*, *62*(5), 1340–1356. https://doi.org/10.1111/j.1365-2958.2006.05457.x

Defeu Soufo, H. J., & Graumann, P. L. (2010). Bacillus subtilis MreB paralogues have different filament architectures and lead to shape remodelling of a heterologous cell system. *Molecular Microbiology*, *78*(5), 1145–1158. https://doi.org/10.1111/j.1365-2958.2010.07395.x

Dersch, S., Mehl, J., Stuckenschneider, L., Mayer, B., Roth, J., Rohrbach, A., & Graumann, P. L. (2020). Super-Resolution Microscopy and Single-Molecule Tracking Reveal Distinct Adaptive Dynamics of MreB and of Cell Wall-Synthesis Enzymes. *Frontiers in Microbiology*, *11*(August), 1–19.

https://doi.org/10.3389/fmicb.2020.01946

Dion, M. F., Kapoor, M., Sun, Y., Wilson, S., Ryan, J., Vigouroux, A., van Teeffelen, S., Oldenbourg, R., & Garner, E. C. (2019). Bacillus subtilis cell diameter is determined by the opposing actions of two distinct cell wall synthetic systems. *Nature Microbiology*, *4*(8), 1294–1305. https://doi.org/10.1038/s41564-019-0439-0

Divakaruni, A. V., Baida, C., White, C. L., & Gober, J. W. (2007). The cell shape proteins MreB and MreC control cell morphogenesis by positioning cell wall synthetic complexes. *Molecular Microbiology*, *66*(1), 174–188. https://doi.org/10.1111/j.1365-2958.2007.05910.x

Divakaruni, A. V., Loo, R. R. O., Xie, Y., Loo, J. A., & Gober, J. W. (2005). The cell-shape protein MreC interacts with extracytoplasmic proteins including cell wall assembly complexes in Caulobacter crescentus. *Proceedings of the National Academy of Sciences of the United States of America*, *102*(51), 18602–18607. https://doi.org/10.1073/pnas.0507937102

Dominguez-Escobar, J., Chastanet, A., Crevenna, A. H., Fromion, V., Wedlich-Söldner, R., & Carballido-López, R. (2011). Processive Movement of MreB-Associated Cell Wall Biosynthethic Complexes in Bacteria. *Science*, *333*(July), 225–228.

Duez, C., Vanhove, M., Gallet, X., Bouillenne, F., Docquier, J. D., Brans, A., & Frère, J. M. (2001). Purification and characterization of PBP4a, a new low-molecular-weight penicillin-binding protein from Bacillus subtilis. *Journal of Bacteriology*, *183*(5), 1595–1599. https://doi.org/10.1128/JB.183.5.1595-1599.2001

Duman, R., Ishikawa, S., Celik, I., Strahl, H., Ogasawara, N., Troc, P., Löwe, J., & Hamoen, L. W. (2013). Structural and genetic analyses reveal the protein SepF as a new membrane anchor for the Z ring. *Proceedings of the National Academy of Sciences of the United States of America*, *110*(48). https://doi.org/10.1073/pnas.1313978110

Economou, N. J., Cocklin, S., & Loll, P. J. (2013). High-resolution crystal structure reveals molecular details of target recognition by bacitracin. *Proceedings of the National Academy of Sciences of the United States of America*, *110*(35), 14207–14212. https://doi.org/10.1073/pnas.1308268110

Edwards, D. H., & Errington, J. (1997). The Bacillus subtilis DivIVA protein targets to the division septum and controls the site specificity of cell division. *Molecular Microbiology*, *24*(5), 905–915. https://doi.org/10.1046/J.1365-2958.1997.3811764.X

Egan, A. J. F., Cleverley, R. M., Peters, K., Lewis, R. J., & Vollmer, W. (2017). Regulation of bacterial cell wall growth. In *FEBS Journal* (Vol. 284, Issue 6, pp. 851–867). https://doi.org/10.1111/febs.13959

Egan, A. J. F., Errington, J., & Vollmer, W. (2020). Regulation of peptidoglycan synthesis and remodelling. *Nature Reviews Microbiology*, *18*(8), 446–460. https://doi.org/10.1038/s41579-020-0366-3

Egan, A. J. F., & Vollmer, W. (2013). The physiology of bacterial cell division. *Annals of the New York Academy of Sciences*, *1277*(1), 8–28. https://doi.org/10.1111/J.1749-6632.2012.06818.X

Egan, A. J. F., & Vollmer, W. (2015). The stoichiometric divisome: A hypothesis. *Frontiers in Microbiology*, *6*(MAY), 1–6. https://doi.org/10.3389/fmicb.2015.00455

El Najjar, N., Van Teeseling, M. C. F., Mayer, B., Hermann, S., Thanbichler, M., & Graumann, P. L. (2020). Bacterial cell growth is arrested by violet and blue, but not yellow light excitation during fluorescence microscopy. *BMC Molecular and Cell Biology*, *21*(1), 1–12. https://doi.org/10.1186/s12860-020-00277-y

Emami, K., Guyet, A., Kawai, Y., Devi, J., Wu, L. J., Allenby, N., Daniel, R. A., & Errington, J. (2017). RodA as the missing glycosyltransferase in Bacillus subtilis and antibiotic discovery for the peptidoglycan polymerase pathway. *Nature Microbiology 2017 2:3*, *2*(3), 1–9. https://doi.org/10.1038/nmicrobiol.2016.253

Eswaramoorthy, P., Erb, M. L., Gregory, J. A., Silverman, J., Pogliano, K., Pogliano, J., & Ramamurthi, K. S. (2011). Cellular architecture mediates DivIVA ultrastructure and regulates min activity in Bacillus subtilis. *MBio*, *2*(6). https://doi.org/10.1128/MBIO.00257-11

Gamba, P., Veening, J. W., Saunders, N. J., Hamoen, L. W., & Daniel, R. A. (2009). Two-step assembly dynamics of the Bacillus subtilis divisome. *Journal of Bacteriology*, *191*(13), 4186–4194. https://doi.org/10.1128/JB.01758-08

Garner, E. C., Bernard, R., Wang, W., Zhuang, X., Rudner, D. Z., & Mitchison, T. (2011). Coupled, circumferential motions of the cell wall synthesis machinery and MreB filaments in B. subtilis. *Science*, *333*(6039), 222–225. https://doi.org/10.1126/science.1203285

Gibson, D. G., Young, L., Chuang, R.-Y., Venter, J. C., Hutchison, C. A., & Smith, H. O. (2009). Enzymatic assembly of DNA molecules up to several hundred kilobases. *Nature Methods 2009 6:5*, *6*(5), 343–345. https://doi.org/10.1038/nmeth.1318

Goffin, C., & Ghuysen, J.-M. (1998). Multimodular Penicillin-Binding Proteins: An Enigmatic Family of Orthologs and Paralogs. *Microbiology and Molecular Biology Reviews*, *62*(4), 1079–1093. https://doi.org/10.1128/mmbr.62.4.1079-1093.1998

Graumann, P. L. (2007). Cytoskeletal elements in bacteria. *Annual Review of Microbiology*, *61*, 589–618. https://doi.org/10.1146/annurev.micro.61.080706.093236

Graumann, P. L. (2009). Dynamics of bacterial cytoskeletal elements. *Cell Motility and the Cytoskeleton*, *66*(11), 909–914. https://doi.org/10.1002/cm.20381

Hayhurst, E. J., Kailas, L., Hobbs, J. K., & Foster, S. J. (2008). Cell wall peptidoglycan architecture in Bacillus subtilis. *Proceedings of the National Academy of Sciences of the United States of America*, *105*(38), 14603–14608. https://doi.org/10.1073/pnas.0804138105

Hoffmann, T., Wensing, A., Brosius, M., Steil, L., Völker, U., & Bremer, E. (2013). Osmotic control of opuA expression in Bacillus subtilis and its modulation in response to intracellular glycine betaine and proline pools. *Journal of Bacteriology*, *195*(3), 510–522. https://doi.org/10.1128/JB.01505-12

Höltje, J.-V. (1998). Growth of the Stress-Bearing and Shape-Maintaining Murein Sacculus of Escherichia coli. *Microbiology and Molecular Biology Reviews*, *62*(1), 181–203. https://doi.org/10.1128/mmbr.62.1.181-203.1998

Hussain, S., Wivagg, C. N., Szwedziak, P., Wong, F., Schaefer, K., Izoré, T., Renner, L. D., Holmes, M. J., Sun, Y., Bisson-Filho, A. W., Walker, S., Amir, A., Löwe, J., & Garner, E. C. (2018). MreB filaments align along greatest principal membrane curvature to orient cell wall synthesis. *ELife*, *7*, 1–45. https://doi.org/10.7554/eLife.32471

Jaqaman, K., Loerke, D., Mettlen, M., Kuwata, H., Grinstein, S., Schmid, S. L., & Danuser, G. (2008). Robust single-particle tracking in live-cell time-lapse sequences. *Nature Methods*, *5*(8), 695–702. https://doi.org/10.1038/nmeth.1237

Jensen, S. O., Thompson, L. S., & Harry, E. J. (2005). Cell division in Bacillus subtilis: FtsZ and FtsA association is Z-ring independent, and FtsA is required for efficient midcell Z-ring assembly. *Journal of Bacteriology*, *187*(18), 6536–6544. https://doi.org/10.1128/JB.187.18.6536-6544.2005

Jiang, C., Caccamo, P. D., & Brun, Y. V. (2015). Mechanisms of bacterial morphogenesis: Evolutionary cell biology approaches provide new insights. *BioEssays*, *37*(4), 413–425. https://doi.org/10.1002/bies.201400098

Jones, L. J. F., Carballido-López, R., & Errington, J. (2001). Control of cell shape in bacteria: Helical, actin-like filaments in Bacillus subtilis. *Cell*, *104*(6), 913–922. https://doi.org/10.1016/S0092-8674(01)00287-2

Jordan, S., Hutchings, M. I., & Mascher, T. (2008). Cell envelope stress response in Gram-positive bacteria. *FEMS Microbiology Reviews*, *32*(1), 107–146. https://doi.org/10.1111/j.1574-6976.2007.00091.x

Josephine, H. R., Charlier, P., Davies, C., Nicholas, R. A., & Pratt, R. F. (2006). Reactivity of penicillin-binding proteins with peptidoglycan-mimetic β-lactams: What's wrong with these enzymes? *Biochemistry*, *45*(51), 15873–15883. https://doi.org/10.1021/bi061804f

Josephine, H. R., Kumar, I., & Pratt, R. F. (2004). The perfect penicillin? Inhibition of a bacterial DD-peptidase by peptidoglycan-mimetic β-lactams. *Journal of the American Chemical Society*, *126*(26), 8122–8123. https://doi.org/10.1021/ja048850s

Kahan, F. M., Kahan, J. S., Cassidy, P. J., & Kropp, H. (1974a). THE MECHANISM OF ACTION OF FOSFOMYCIN (PHOSPHONOMYCIN). *Annals of the New York Academy of Sciences*, *235*(1), 364–386. https://doi.org/10.1111/j.1749-6632.1974.tb43277.x

Kahan, F. M., Kahan, J. S., Cassidy, P. J., & Kropp, H. (1974b). THE MECHANISM OF ACTION OF FOSFOMYCIN (PHOSPHONOMYCIN). *Annals of the New York Academy of Sciences*, *235*(1), 364–386. https://doi.org/10.1111/j.1749-6632.1974.tb43277.x

Kawai, Y., Asai, K., & Errington, J. (2009). Partial functional redundancy of MreB isoforms, MreB, Mbl and MreBHp in cell morphogenesis of Bacillus subtilis. *Molecular Microbiology*, *73*(4), 719–731. https://doi.org/10.1111/j.1365-2958.2009.06805.x

Kawai, Y., Daniel, R. A., & Errington, J. (2009). Regulation of cell wall morphogenesis in Bacillus subtilis by recruitment of PBP1 to the MreB helix. *Molecular Microbiology*, *71*(5), 1131–1144. https://doi.org/10.1111/j.1365-2958.2009.06601.x

Kawai, Y., Mercier, R., Mickiewicz, K., Serafini, A., Sório de Carvalho, L. P., & Errington, J. (2019). Crucial role for central carbon metabolism in the bacterial L-form switch and killing by β-lactam antibiotics. *Nature Microbiology*, *4*(10), 1716–1726. https://doi.org/10.1038/s41564-019-0497-3

Kocaoglu, O., & Carlson, E. E. (2013). Penicillin-binding protein imaging probes. *Current Protocols in Chemical Biology*, *5*(4), 239–250.

https://doi.org/10.1002/9780470559277.ch130102

Kohanski, M. A., Dwyer, D. J., & Collins, J. J. (2010). How antibiotics kill bacteria: From targets to networks. *Nature Reviews Microbiology*, *8*(6), 423–435. https://doi.org/10.1038/nrmicro2333

Koo, B.-M., Kritikos, G., Farelli, J. D., Todor, H., Tong, K., Kimsey, H., Wapinski, I., Galardini, M., Cabal, A., Peters, J. M., Hachmann, A.-B., Rudner, D. Z., Allen, K. N., Typas, A., & Gross, C. A. (2017). Construction and Analysis of Two Genome-Scale Deletion Libraries for Bacillus subtilis. *Cell Systems*, *4*(3), 291-305.e7. https://doi.org/10.1016/J.CELS.2016.12.013

Kuk, A. C. Y., Hao, A., Guan, Z., & Lee, S. Y. (2019). Visualizing conformation transitions of the Lipid II flippase MurJ. *Nature Communications*, *10*(1). https://doi.org/10.1038/s41467-019-09658-0

Kumar, S., Rubino, F. A., Mendoza, A. G., & Ruiz, N. (2019). The bacterial lipid II flippase MurJ functions by an alternating-access mechanism. *Journal of Biological Chemistry*, *294*(3), 981–990. https://doi.org/10.1074/jbc.RA118.006099

Laddomada, F., Miyachiro, M. M., & Dessen, A. (2016). Structural insights into protein-protein interactions involved in bacterial cell wall biogenesis. *Antibiotics*, *5*(2), 1–13. https://doi.org/10.3390/antibiotics5020014

Lages, M. C. A., Beilharz, K., Morales Angeles, D., Veening, J. W., & Scheffers, D. J. (2013). The localization of key Bacillus subtilis penicillin binding proteins during cell growth is determined by substrate availability. *Environmental Microbiology*, *15*(12), 3272–3281. https://doi.org/10.1111/1462-2920.12206

Leaver, M., & Errington, J. (2005). Roles for MreC and MreD proteins in helical growth of the cylindrical cell wall in Bacillus subtilis. *Molecular Microbiology*, *57*(5), 1196–1209. https://doi.org/10.1111/j.1365-2958.2005.04736.x

Leclercq, S., Derouaux, A., Olatunji, S., Fraipont, C., Egan, A. J. F., Vollmer, W., Breukink, E., & Terrak, M. (2017). Interplay between Penicillin-binding proteins and SEDS proteins promotes bacterial cell wall synthesis. *Scientific Reports*, *7*(January), 1–13. https://doi.org/10.1038/srep43306

Lee, T. K., Meng, K., Shi, H., & Huang, K. C. (2016). Single-molecule imaging reveals modulation of cell wall synthesis dynamics in live bacterial cells. *Nature Communications*, *7*, 1–9. https://doi.org/10.1038/ncomms13170

Liu, X., Biboy, J., Consoli, E., Vollmer, W., & den Blaauwen, T. (2020). MreC and MreD balance the interaction between the elongasome proteins PBP2 and RodA. *PLoS Genetics*, *16*(12 December), 1–23. https://doi.org/10.1371/journal.pgen.1009276

Lucena, D., Mauri, M., Schmidt, F., Eckhardt, B., & Graumann, P. L. (2018). Microdomain formation is a general property of bacterial membrane proteins and induces heterogeneity of diffusion patterns. *BMC Biology 2018 16:1*, *16*(1), 1–17. https://doi.org/10.1186/S12915-018-0561-0

Macheboeuf, P., Contreras-Martel, C., Job, V., Dideberg, O., & Dessen, A. (2006). Penicillin binding proteins: Key players in bacterial cell cycle and drug resistance processes. *FEMS Microbiology Reviews*, *30*(5), 673–691. https://doi.org/10.1111/j.1574-6976.2006.00024.x

McCausland, J. W., Yang, X., Squyres, G. R., Lyu, Z., Bruce, K. E., Lamanna, M. M., Söderström, B., Garner, E. C., Winkler, M. E., Xiao, J., & Liu, J. (2021).

Treadmilling FtsZ polymers drive the directional movement of sPG-synthesis enzymes via a Brownian ratchet mechanism. *Nature Communications*, *12*(1). https://doi.org/10.1038/s41467-020-20873-y

McPherson, D. C., & Popham, D. L. (2003). Peptidoglycan synthesis in the absence of class A penicillin-binding proteins in Bacillus subtilis. *Journal of Bacteriology*, *185*(4), 1423–1431. https://doi.org/10.1128/JB.185.4.1423-1431.2003

Meeske, A. J., Riley, E. P., Robins, W. P., Uehara, T., Mekalanos, J. J., Kahne, D., Walker, S., Kruse, A. C., Bernhardt, T. G., & Rudner, D. Z. (2016). SEDS proteins are a widespread family of bacterial cell wall polymerases. *Nature*, *537*(7622), 634–638. https://doi.org/10.1038/nature19331

Meeske, A. J., Sham, L. T., Kimsey, H., Koo, B. M., Gross, C. A., Bernhardt, T. G., & Rudner, D. Z. (2015). MurJ and a novel lipid II flippase are required for cell wall biogenesis in Bacillus subtilis. *Proceedings of the National Academy of Sciences of the United States of America*, *112*(20), 6437–6442. https://doi.org/10.1073/pnas.1504967112

Mohammadi, T., Van Dam, V., Sijbrandi, R., Vernet, T., Zapun, A., Bouhss, A., Diepeveen-De Bruin, M., Nguyen-Distéche, M., De Kruijff, B., & Breukink, E. (2011). Identification of FtsW as a transporter of lipid-linked cell wall precursors across the membrane. *EMBO Journal*, *30*(8), 1425–1432. https://doi.org/10.1038/emboj.2011.61

Morgenstein, R. M., Bratton, B. P., Nguyen, J. P., Ouzounov, N., Shaevitz, J. W., & Gitai, Z. (2015). RodZ links MreB to cell wall synthesis to mediate MreB rotation and robust morphogenesis. *Proceedings of the National Academy of Sciences of the United States of America*, *112*(40), 12510–12515. https://doi.org/10.1073/pnas.1509610112

Moyes, R. B., Reynolds, J., & Breakwell, D. P. (2009). Differential staining of bacteria: Gram stain. *Current Protocols in Microbiology*, *SUPPL. 15*, 1–8. https://doi.org/10.1002/9780471729259.mca03cs15

Mueller, E. A., & Levin, P. A. (2020). Bacterial cell wall quality control during environmental stress. *MBio*, *11*(5), 1–15. https://doi.org/10.1128/mBio.02456-20

Mullis, K., Faloona, F., Scharf, S., Saiki, R., & Horn, G. (1986). *Specific Enzymatic Amplification of DNA In Vitro: The Polymerase Chain Reaction*.

Münch, D., & Sahl, H. G. (2015). Structural variations of the cell wall precursor lipid II in Gram-positive bacteria - Impact on binding and efficacy of antimicrobial peptides. *Biochimica et Biophysica Acta - Biomembranes*, *1848*(11), 3062–3071. https://doi.org/10.1016/j.bbamem.2015.04.014

Murray, T., Popham, D. L., & Setlow, P. (1996). Identification and characterization of pbpC, the gene encoding Bacillus subtilis penicillin-binding protein 3. *Journal of Bacteriology*, *178*(20), 6001–6005. https://doi.org/10.1128/JB.178.20.6001-6005.1996

Murray, T., Popham, D. L., & Setlow, P. (1997). Identification and characterization of pbpA encoding Bacillus subtilis penicillin-binding protein 2A. *Journal of Bacteriology*, *179*(9), 3021–3029. https://doi.org/10.1128/JB.179.9.3021-3029.1997

Oppedijk, S. F., Martin, N. I., & Breukink, E. (2016). Hit ’em where it hurts: The growing and structurally diverse family of peptides that target lipid-II. *Biochimica et*

Biophysica Acta - Biomembranes, *1858*(5), 947–957. https://doi.org/10.1016/j.bbamem.2015.10.024

Otten, C., Brilli, M., Vollmer, W., Viollier, P. H., & Salje, J. (2018). Peptidoglycan in obligate intracellular bacteria. *Molecular Microbiology*, *107*(2), 142–163. https://doi.org/10.1111/MMI.13880

Oviedo-Bocanegra, L. M., Hinrichs, R., Rotter, D. A. O., Dersch, S., & Graumann, P. L. (2021). Single molecule/particle tracking analysis program SMTracker 2.0 reveals different dynamics of proteins within the RNA degradosome complex in Bacillus subtilis. *Nucleic Acids Research*. https://doi.org/10.1093/NAR/GKAB696

Özbaykal, G., Wollrab, E., Simon, F., Vigouroux, A., Cordier, B., Aristov, A., Chaze, T., Matondo, M., & van Teeffelen, S. (2020). The transpeptidase PBP2 governs initial localization and activity of the major cell-wall synthesis machinery in E. coli. *ELife*, *9*, 1–37. https://doi.org/10.7554/eLife.50629

Paintdakhi, A., Parry, B., Campos, M., Irnov, I., Elf, J., Surovtsev, I., & Jacobs-Wagner, C. (2016). Oufti: An integrated software package for high-accuracy, high-throughput quantitative microscopy analysis. *Molecular Microbiology*, *99*(4), 767–777. https://doi.org/10.1111/mmi.13264

Palomino, M. M., Sanchez-Rivas, C., & Ruzal, S. M. (2009). High salt stress in Bacillus subtilis: involvement of PBP4* as a peptidoglycan hydrolase. *Research in Microbiology*, *160*(2), 117–124. https://doi.org/10.1016/j.resmic.2008.10.011

Pasquina-Lemonche, L., Burns, J., Turner, R. D., Kumar, S., Tank, R., Mullin, N., Wilson, J. S., Chakrabarti, B., Bullough, P. A., Foster, S. J., & Hobbs, J. K. (2020). The architecture of the Gram-positive bacterial cell wall. *Nature*, *582*(7811), 294–297. https://doi.org/10.1038/s41586-020-2236-6

Pazos, M., Peters, K., & Vollmer, W. (2017). Robust peptidoglycan growth by dynamic and variable multi-protein complexes. *Current Opinion in Microbiology*, *36*, 55–61. https://doi.org/10.1016/j.mib.2017.01.006

Pedersen, L. B., Murray, T., Popham, D. L., & Setlow, P. (1998). Characterization of dacC, which encodes a new low-molecular- weight penicillin-binding protein in Bacillus subtilis. *Journal of Bacteriology*, *180*(18), 4967–4973. https://doi.org/10.1128/jb.180.18.4967-4973.1998

Peters, J. M., Colavin, A., Shi, H., Czarny, T. L., Larson, M. H., Wong, S., Hawkins, J. S., Lu, C. H. S., Koo, B. M., Marta, E., Shiver, A. L., Whitehead, E. H., Weissman, J. S., Brown, E. D., Qi, L. S., Huang, K. C., & Gross, C. A. (2016). A comprehensive, CRISPR-based functional analysis of essential genes in bacteria. *Cell*, *165*(6), 1493–1506. https://doi.org/10.1016/j.cell.2016.05.003

Peters, K., Kannan, S., Rao, V. A., Biboy, J., Vollmer, D., Erickson, S. W., Lewis, R. J., Young, K. D., & Vollmer, W. (2016). The redundancy of peptidoglycan carboxypeptidases ensures robust cell shape maintenance in Escherichia coli. *MBio*, *7*(3), 1–14. https://doi.org/10.1128/mBio.00819-16

Popham, D. L., & Setlow, P. (1995). Cloning, nucleotide sequence, and mutagenesis of the Bacillus subtilis ponA operon, which codes for penicillin-binding protein (PBP) 1 and a PBP- related factor. *Journal of Bacteriology*, *177*(2), 326–335. https://doi.org/10.1128/jb.177.2.326-335.1995

Popham, David L., & Setlow, P. (1996). Phenotypes of Bacillus subtilis mutants lacking multiple class a high-molecular-weight penicillin-binding proteins. *Journal of*

Bacteriology, *178*(7), 2079–2085. https://doi.org/10.1128/jb.178.7.2079-2085.1996

Radeck, J., Lautenschläger, N., & Mascher, T. (2017). The Essential UPP Phosphatase Pair BcrC and UppP Connects Cell Wall Homeostasis during Growth and Sporulation with Cell Envelope Stress Response in Bacillus subtilis. *Frontiers in Microbiology*, *0*(DEC), 2403. https://doi.org/10.3389/FMICB.2017.02403

Raynor, B. D. (1997). Penicillin and ampicillin. *Primary Care Update for Ob/Gyns*, *4*(4), 147–152. https://doi.org/10.1016/S1068-607X(97)00012-7

Reimold, C., Soufo, H. J. D., Dempwolff, F., & Graumann, P. L. (2013). Motion of variable-length MreB filaments at the bacterial cell membrane influences cell morphology. *Molecular Biology of the Cell*, *24*(15), 2340–2349. https://doi.org/10.1091/mbc.E12-10-0728

Reynolds, P. E. (1989). Structure, biochemistry and mechanism of action of glycopeptide antibiotics. *European Journal of Clinical Microbiology & Infectious Diseases*, *8*(11), 943–950. https://doi.org/10.1007/BF01967563

Rösch, T. C., Oviedo-Bocanegra, L. M., Fritz, G., & Graumann, P. L. (2018). SMTracker: a tool for quantitative analysis, exploration and visualization of single-molecule tracking data reveals highly dynamic binding of B. subtilis global repressor AbrB throughout the genome. *Scientific Reports*, *8*(1), 1–12. https://doi.org/10.1038/s41598-018-33842-9

Ruiz, N. (2016). Lipid Flippases for Bacterial Peptidoglycan Biosynthesis: *Https://Doi.Org/10.4137/LPI.S31783*, *2015*(8), 21–31. https://doi.org/10.4137/LPI.S31783

Sassine, J., Xu, M., Sidiq, K. R., Emmins, R., Errington, J., & Daniel, R. A. (2017). Functional redundancy of division specific penicillin-binding proteins in Bacillus subtilis. *Molecular Microbiology*, *106*(2), 304–318. https://doi.org/10.1111/mmi.13765

Sauvage, E., Duez, C., Herman, R., Kerff, F., Petrella, S., Anderson, J. W., Adediran, S. A., Pratt, R. F., Frère, J. M., & Charlier, P. (2007). Crystal Structure of the Bacillus subtilis Penicillin-binding Protein 4a, and its Complex with a Peptidoglycan Mimetic Peptide. *Journal of Molecular Biology*, *371*(2), 528–539. https://doi.org/10.1016/j.jmb.2007.05.071

Sauvage, E., Kerff, F., Terrak, M., Ayala, J. A., & Charlier, P. (2008). The penicillin-binding proteins: Structure and role in peptidoglycan biosynthesis. *FEMS Microbiology Reviews*, *32*(2), 234–258. https://doi.org/10.1111/j.1574-6976.2008.00105.x

Scheffers, D. J., Jones, L. J. F., & Errington, J. (2004). Several distinct localization patterns for penicillin-binding proteins in Bacillus subtilis. *Molecular Microbiology*, *51*(3), 749–764. https://doi.org/10.1046/j.1365-2958.2003.03854.x

Scherer, K. M., Spille, J. H., Sahl, H. G., Grein, F., & Kubitscheck, U. (2015). The lantibiotic nisin induces Lipid II aggregation, causing membrane instability and vesicle budding. *Biophysical Journal*, *108*(5), 1114–1124. https://doi.org/10.1016/j.bpj.2015.01.020

Schindelin, J., Arganda-Carreras, I., Frise, E., Kaynig, V., Longair, M., Pietzsch, T., Preibisch, S., Rueden, C., Saalfeld, S., Schmid, B., Tinevez, J. Y., White, D. J., Hartenstein, V., Eliceiri, K., Tomancak, P., & Cardona, A. (2012). Fiji: An open-source platform for biological-image analysis. *Nature Methods*, *9*(7), 676–682.

https://doi.org/10.1038/nmeth.2019

Schirner, K., Eun, Y. J., Dion, M., Luo, Y., Helmann, J. D., Garner, E. C., & Walker, S. (2015). Lipid-linked cell wall precursors regulate membrane association of bacterial actin MreB. *Nature Chemical Biology*, *11*(1), 38–45. https://doi.org/10.1038/nchembio.1689

Schroeder, J., & Simmons, L. (2013). Complete Genome Sequence of Bacillus subtilis Strain PY79. *Genome Announcements*, *1*(6). https://doi.org/10.1128/GENOMEA.01085-13

Sharifzadeh, S., Dempwolff, F., Kearns, D. B., & Carlson, E. E. (2020). Harnessing β-lactam antibiotics for illumination of the activity of penicillin-binding proteins in bacillus subtilis. *ACS Chemical Biology*, *15*(5), 1242–1251. https://doi.org/10.1021/acschembio.9b00977

Sheldrick, G. M., Jones, P. G., Kennard, O., Williams, D. H., & Smith, G. A. (1978). Structure of vancomycin and its complex with acetyl-D-alanyl-D-alanine. *Nature 1978 271:5642*, *271*(5642), 223–225. https://doi.org/10.1038/271223a0

Silver, L. L. (2017). Fosfomycin: Mechanism and resistance. *Cold Spring Harbor Perspectives in Medicine*, *7*(2), 1–11. https://doi.org/10.1101/cshperspect.a025262

Singh, J. K., Makde, R. D., Kumar, V., & Panda, D. (2007). A membrane protein, EzrA, regulates assembly dynamics of FtsZ by interacting with the C-terminal tail of FtSZ. *Biochemistry*, *46*(38), 11013–11022. https://doi.org/10.1021/bi700710j

Sjodt, M., Brock, K., Dobihal, G., Rohs, P. D. A., Green, A. G., Hopf, T. A., Meeske, A. J., Srisuknimit, V., Kahne, D., Walker, S., Marks, D. S., Bernhardt, T. G., Rudner, D. Z., & Kruse, A. C. (2018). Structure of the peptidoglycan polymerase RodA resolved by evolutionary coupling analysis. *Nature*, *556*(7699), 118–121. https://doi.org/10.1038/nature25985

Söderström, B., Badrutdinov, A., Chan, H., & Skoglund, U. (2018). Cell shape-independent FtsZ dynamics in synthetically remodeled bacterial cells. *Nature Communications*, *9*(1). https://doi.org/10.1038/s41467-018-06887-7

Soufo, H. J. D., & Graumann, P. L. (2005). Bacillus subtilis actin-like protein MreB influences the positioning of the replication machinery and requires membrane proteins MreC/D and other actin-like proteins for proper localization. *BMC Cell Biology*, *6*, 1–11. https://doi.org/10.1186/1471-2121-6-10

Spratt, B. G. (1975). Distinct penicillin binding proteins involved in the division, elongation, and shape of Escherichia coli K12. *Proceedings of the National Academy of Sciences*, *72*(8), 2999–3003.

Strahl, H., & Hamoen, L. W. (2010). Membrane potential is important for bacterial cell division. *Proceedings of the National Academy of Sciences of the United States of America*, *107*(27), 12281–12286. https://doi.org/10.1073/pnas.1005485107

Strominger, J. L., Blumberg, P. M., Suginaka, H., Umbreit, J., & Wickus, G. G. (1971). How penicillin kills bacteria: progress and problems. *Proceedings of the Royal Society of London. Series B. Biological Sciences*, *179*(57), 369–383. https://doi.org/10.1098/RSPB.1971.0103

Szwedziak, P., & Löwe, J. (2013). Do the divisome and elongasome share a common evolutionary past? *Current Opinion in Microbiology*, *16*(6), 745–751.

https://doi.org/10.1016/j.mib.2013.09.003

Typas, A., Banzhaf, M., Gross, C. A., & Vollmer, W. (2012). From the regulation of peptidoglycan synthesis to bacterial growth and morphology. *Nature Reviews Microbiology*, *10*(2), 123–136. https://doi.org/10.1038/nrmicro2677

Van Den Ent, F., Johnson, C. M., Persons, L., De Boer, P., & Löwe, J. (2010). Bacterial actin MreB assembles in complex with cell shape protein RodZ. *EMBO Journal*, *29*(6), 1081–1090. https://doi.org/10.1038/emboj.2010.9

Van Den Ent, F., Leaver, M., Bendezu, F., Errington, J., De Boer, P., & Löwe, J. (2006). Dimeric structure of the cell shape protein MreC and its functional implications. *Molecular Microbiology*, *62*(6), 1631–1642. https://doi.org/10.1111/j.1365-2958.2006.05485.x

Van der Ploeg, R., Verheul, J., Vischer, N. O. E., Alexeeva, S., Hoogendoorn, E., Postma, M., Banzhaf, M., Vollmer, W., & Den Blaauwen, T. (2013). Colocalization and interaction between elongasome and divisome during a preparative cell division phase in Escherichia coli. *Molecular Microbiology*, *87*(5), 1074–1087. https://doi.org/10.1111/mmi.12150

van Teeffelen, S., & Renner, L. D. (2018). Recent advances in understanding how rod-like bacteria stably maintain their cell shapes. *F1000Research*, *7*(0), 1–12. https://doi.org/10.12688/f1000research.12663.1

Van Teeffelen, S., Wang, S., Furchtgott, L., Huang, K. C., Wingreen, N. S., Shaevitz, J. W., & Gitai, Z. (2011). The bacterial actin MreB rotates, and rotation depends on cell-wall assembly. *Proceedings of the National Academy of Sciences of the United States of America*, *108*(38), 15822–15827. https://doi.org/10.1073/pnas.1108999108

Vigouroux, A., Cordier, B., Aristov, A., Alvarez, L., Özbaykal, G., Chaze, T., Oldewurtel, E. R., Matondo, M., Cava, F., Bikard, D., & van Teeffelen, S. (2020). Class-A penicillin binding proteins do not contribute to cell shape but repair cellwall defects. *ELife*, *9*, 1–26. https://doi.org/10.7554/eLife.51998

Vollmer, W., Blanot, D., & De Pedro, M. A. (2008). Peptidoglycan structure and architecture. *FEMS Microbiology Reviews*, *32*(2), 149–167. https://doi.org/10.1111/j.1574-6976.2007.00094.x

Vollmer, W., & Seligman, S. J. (2010). Architecture of peptidoglycan: more data and more models. *Trends in Microbiology*, *18*(2), 59–66. https://doi.org/10.1016/j.tim.2009.12.004

Wang, S., Furchtgott, L., Huang, K. C., & Shaevitz, J. W. (2012). Helical insertion of peptidoglycan produces chiral ordering of the bacterial cell wall. *Proceedings of the National Academy of Sciences of the United States of America*, *109*(10). https://doi.org/10.1073/pnas.1117132109

Wei, Y., Havasy, T., McPherson, D. C., & Popham, D. L. (2003). Rod shape determination by the Bacillus subtilis class B penicillin-binding proteins encoded by pbpA and pbpH. *Journal of Bacteriology*, *185*(16), 4717–4726. https://doi.org/10.1128/JB.185.16.4717-4726.2003

Wickstead, B., & Gull, K. (2011). The evolution of the cytoskeleton. *Journal of Cell Biology*, *194*(4), 513–525. https://doi.org/10.1083/JCB.201102065

Woodcock, D. M., Crowther, P. J., Doherty, J., Jefferson, S., Decruz, E., Noyer-

Weidner2, M., Smith3, S. S., Michael', M. Z., & Grahaml, M. W. (n.d.). *Quantitative evaluation of Escherichia coli host strains for tolerance to cytosine methylation in plasmid and phage recombinants*.

Young, K. D. (2007). Bacterial morphology: why have different shapes? *Current Opinion in Microbiology*, *10*(6), 596–600. https://doi.org/10.1016/j.mib.2007.09.009

Youngman, P., Perkins, J. B., & Losick, R. (1984). A novel method for the rapid cloning in Escherichia coli of Bacillus subtilis chromosomal DNA adjacent to Tn 917 insertions. *MGG Molecular & General Genetics*, *195*(3), 424–433. https://doi.org/10.1007/BF00341443

Yousif, S. Y., Broome-Smith, J. K., & Spratt, B. G. (1985). Lysis of Escherichia coli by β-lactam antibiotics: Deletion analysis of the role of penicillin-binding proteins 1A and 1B. *Journal of General Microbiology*, *131*(10), 2839–2847. https://doi.org/10.1099/00221287-131-10-2839

Zeigler, D. R., Prágai, Z., Rodriguez, S., Chevreux, B., Muffler, A., Albert, T., Bai, R., Wyss, M., & Perkins, J. B. (2008). The origins of 168, W23, and other Bacillus subtilis legacy strains. *Journal of Bacteriology*, *190*(21), 6983–6995. https://doi.org/10.1128/JB.00722-08

Zhao, H., Patel, V., Helmann, J. D., & Dörr, T. (2017). Don't let sleeping dogmas lie: new views of peptidoglycan synthesis and its regulation. *Molecular Microbiology*, *106*(6), 847–860. https://doi.org/10.1111/mmi.13853

Appendix

Supplementary tables

Table S1:Plasmid list

Plasmids	Features	Host organisms
pHJDS	GFP, amp and cm resistance cassette	*E. coli* DH5α
pHJDS-mVenus	mVenus, amp and cm resistance cassette	*E. coli* DH5α
pHJDS-pbpA	PbpA from B.subtilis, mVenus, amp and cm resistance cassette	*E. coli* DH5α
pHJDS-pbpH	PbpH from B.subtilis, mVenus, amp and cm resistance cassette	*E. coli* DH5α
pHJDS-pbpD	PbpD from B.subtilis, mVenus, amp and cm resistance cassette	*E. coli* DH5α
pHJDS-pbpC	PbpC from B.subtilis, mVenus, amp and cm resistance cassette	*E. coli* DH5α
pHJDS-dacC	dacC from B.subtilis, mVenus, amp and cm resistance cassette	*E. coli* DH5α
RL1849	Cm::tet, to exchange the cm resistance cassette with a tet resistance cassette	*E. coli* DH5α
pDR244	Cre/lox mediated loop-out of resistance cassettes, for deletion strains of the BGSC, spec resistance	*E. coli*

Table S2: List of oligonucleotides used to amplify gene subsequently used to create plasmids and original locus integration of mVenus fusion into the Bacillus subtilis genome

Name	Oligonucleotide 5' to 3'
GA_pbpA_nt_fwd	CACTGCGGATCCACGGGCCCATGAGGAGAAATAAACCAAAAAAG
GA_pbpA_nt_rev	ACTCTAGAACTAGTGAATTCAATCCGTTTTAGCTGAAGCT
GA_pbpD_nt_fwd	CACTGCGGATCCACGGGCCCGTGACCATGTTACGAAAAATAA
GA_pbpD_nt_rev	ACTCTAGAACTAGTGAATTCATTTTTCGTATATTTTTTCTCC
GA_dacC_nt_fwd	CACTGCGGATCCACGGGCCCATGAAAAAAAGCATAAAGCT
GA_dacC_nt_rev	ACTCTAGAACTAGTGAATTCTGATAATCGCATGTCATCAT
GA_pbpC_nt_fwd	CACTGCGGATCCACGGGCCCATGTTAAAAAAGTGTATTCT
GA_pbpC_nt_rev	ACTCTAGAACTAGTGAATTCCCATTTTTATCGTAAATTTG
GA_mVenus_fwd	GAGATTCCTAGGATGGGTACCCTGCAGATGGTGAGCAAGGGCGAGGA
GA_mVenusNewLinker_rev	AGGGGGGGCCCGTGGATCCGCAGTGATCCTCCTCCTCCTCCCAGGCCAGATAGGCCCTTGTACAGCTCGTCCATGC

Table S3: Strain list used to perform the experiments in this work

Strain	**Konstrukt**	**Resistance cassette**
E. coli DH5α	F^- endA1 glnV44 thi-1 recA1 relA1 gyrA96 deoR nupG purB20 φ80dlacZΔM15 Δ(lacZYA-argF)U169, hsdR17($r_K^-m_K^+$), λ^-	/
Bacillus subtilis PY79		
Bacillus subtilis 168		
E. coli DH5α pHJDS-mVevnus	To create N-Terminal fusion	Amp/cm
E. coli DH5α pHJDS-mV-pbpA (mV-Pbp2a)	n-terminal fusion of mVenus to the first 500 bp of pbpA	Amp/cm
E. coli DH5α pHJDS-mV-pbpH (mV-PbpH)	n-terminal fusion of mVenus to the first 500 bp of pbpH	Amp/cm
E. coli DH5α pHJDS-mV-pbpD(mV-Pbp4)	n-terminal fusion of mVenus to the first 500 bp of pbpD	Amp/cm

E. coli DH5α pHJDS-mV-pbpC(mV-Pbp3)	n-terminal fusion of mVenus to the first 500 bp of pbpC	Amp/cm
E. coli DH5α pHJDS-mV-dacC(mV-Pbp4a)	n-terminal fusion of mVenus to the first 500 bp of dacC	Amp/cm
Bacillus subtilis PY79 mVenus-Pbp2a	Original locus integration of mVenus-pbpA, P_{Xyl} controlled	Chloramphenicol (cm)
Bacillus subtilis PY79 mVenus-PbpH	Original locus integration of mVenus-pbpH, P_{Xyl} controlled	Cm
Bacillus subtilis PY79 mVenus-Pbp4	Original locus integration of mVenus-pbpD, P_{Xyl} controlled	Cm
Bacillus subtilis PY79 mVenus-Pbp3	Original locus integration of mVenus-pbpC, P_{Xyl} controlled	Cm
Bacillus subtilis PY79 mVenus-Pbp4a	Original locus integration of mVenus-dacC, P_{Xyl} controlled	Cm
Bacillus subtilis PY79 ∆*pbpH mVenus-pbpA*	Original locus integration of mVenus-pbpA, deletion of pbpH gene	Cm, kan
Bacillus subtilis PY79 ∆*pbpA mVenus-pbpH*	Original locus integration of mVenus-pbpH, deletion of pbpA gene	Cm, kan
Bacillus subtilis 168 d*epletion mreB mVenus-pbpA*	Original locus integration of mVenus-pbpA, depletion of *mreB* gene using a Cas9	Cm, ery, tet
Bacillus subtilis 168 depletion mreB mVenus-pbpH	Original locus integration of mVenus-pbpH, depletion of *mreB* gene using a Cas9	Cm, ery, tet

Table S4: software used for the data obtaining and analysis in this thesis

Software	Company
Fiji	Open-source platform for analysing of biological pictures (Schindelin et al., 2012)
MatLab (different versions)	The MatWorks, Inc., Natick, Massachusetts, USA
VisiView	Visitron System, Germany
Oufti	Jacobs Wagner Lab, University of Yale, New Haven, USA (Paintdakhi et al., 2016)
SMTracker (Version 2.0)	Copyright © Thomas Rösch (Oviedo-Bocanegra et al., 2021; Rösch et al., 2018)
UTrack	Danuser Lab, UT Southwestern medical center, Dallas, Texas, USA (Jaqaman et al., 2008)

Table S5: mV-MreB treated with different antibiotics

Condition of strain YFP-mreB	unstressed	vancomycin	penicillin G	nisin	fosfomycin	bacitracin
# movies	20	30	20	20	20	30
# cells	185	304	228	186	158	351
av. cell length [µm]	3.1700	3.3000	2.9000	2.7500	2.9800	3.2000
# tracks	25837	42856	32659	10270	23360	43722
#tracks/cell	149.7251	140.0506	157.0084	62.7386	153.7283	123.6997
dwell time radius [nm]	120	120	120	120	120	120
static tracks [%]	7.7000	6.8000	6	6.7000	8.4000	7.5000
mobile tracks [%]	92.3000	93.2000	94	93.3000	91.6000	92.5000
free [%]	80.6000	83.7000	83.6000	80.6000	78.6000	83.1000
mixed behaviour [%]	11.8000	9.5000	10.3000	12.7000	13	9.4000
Diffusion constants from GMM						
Static D ± sd [µm² s^{-1}]	0.043 ± 4.1e-09	0.043 ± 4.1e-09	0.043 ± 4.1e-09	0.043 ± 4.1e-09	0.043 ± 4.1e-09	0.043 ± 4.1e-09
Mobile D ± sd [µm² s^{-1}]	0.44 ± 4.1e-08	0.44 ± 4.1e-08	0.44 ± 4.1e-08	0.44 ± 4.1e-08	0.44 ± 4.1e-08	0.44 ± 4.1e-08
Static fraction ± sd [%]	50 ± 4e-06	47 ± 3.6e-06	47 ± 3.7e-06	51 ± 3.2e-06	56 ± 4.5e-06	46 ± 3.8e-06
Mobile fraction ± sd [%]	50 ± 4e-06	53 ± 3.6e-06	53 ± 3.7e-06	49 ± 3.2e-06	44 ± 4.5e-06	54 ± 3.8e-06

Dwell times						
ƈ (1-comp.) ± sd [ms]	0.32 ± 0.0029 s	0.31 ± 0.0023 s	0.36 ± 0.0034 s	0.35 ± 0.0047 s	0.36 ± 0.0027 s	0.29 ± 0.0015 s
stars / p-value	unstressed	vancomycin	penicillin G	nisin	fosfomycin	bacitracin
unstressed	-	(lv) *** / 0.00057876	(lv) *** / 3.4338e-28	(lv) *** / 6.7779e-11	(lv) *** / 1.2965e-18	(lv) *** / 8.1396e-09
vancomycin	-	-	(lv) *** / 2.5842e-15	(lv) ** / 0.011635	(lv) *** / 5.7162e-08	(lv) *** / 8.5165e-18
penicillin G	-	-	-	(lv) *** / 0.0005609	(lv) ** / 0.020823	(lv) *** / 9.063e-59
nisin	-	-	-	-	(lv)* / 0.084825	(lv) *** / 1.4126e-25
fosfomycin	-	-	-	-	-	(lv) *** / 1.697e-43
bacitracin	-	-	-	-	-	-

Table S6: mV-PbpH treated with different antibiotics

Condition of strain mVenus-PbpH	unstressed	vancomycin	penicillin G	nisin	fosfomycin	bacitracin
# movies	33	36	37	46	45	52
# cells	205	200	268	279	314	608
av. cell length [µm]	2.9700	3.0500	3.3100	3.0600	3.2800	2.3500
# tracks	2542	4316	1812	22977	3959	5931
#tracks/cell	13.8297	24.9251	7.7553	86.3055	13.4433	12.4793
dwell time radius [nm]	120	120	120	120	120	120
static tracks [%]	3	1.5000	4.8000	3.5000	4	1.2000
mobile tracks [%]	97	98.5000	95.2000	96.5000	96	98.8000
free [%]	93.7000	96.5000	90.9000	91.7000	92.4000	96.8000
mixed behaviour [%]	3.2000	1.9000	4.2000	4.8000	3.6000	2
Diffusion constants from GMM						
Static D ± sd [µm² s^{-1}]	0.063 ± 1.3e-07	0.063 ± 1.3e-07	0.063 ± 1.3e-07	0.063 ± 1.3e-07	0.063 ± 1.3e-07	0.063 ± 1.3e-07
Mobile D ± sd [µm² s^{-1}]	0.61 ± 5.7e-07	0.61 ± 5.7e-07	0.61 ± 5.7e-07	0.61 ± 5.7e-07	0.61 ± 5.7e-07	0.61 ± 5.7e-07
Static fraction ± sd [%]	43 ± 8e-05	18 ± 4.9e-05	43 ± 0.00011	42 ± 4.8e-05	52 ± 5.8e-05	19 ± 4.5e-05
Mobile fraction ± sd [%]	57 ± 8e-05	82 ± 4.9e-05	57 ± 0.00011	58 ± 4.8e-05	48 ± 5.8e-05	81 ± 4.5e-05
Dwell times						

ƈ (1-comp.) ± sd [ms]	0.24 ± 0.0041 s	0.25 ± 0.0023 s	0.28 ± 0.0059 s	0.28 ± 0.0042 s	0.25 ± 0.0053 s	0.27 ± 0.0046 s
stars / p-value	unstressed	vancomycin	penicillin G	nisin	fosfomycin	bacitracin
unstressed	-	(tt) ns / 0.44989	(lv) *** / 0.0058799	(lv) *** / 0.00024225	(lv) ** / 0.039216	(lv) *** / 0.0055941
vancomycin	-	-	(lv) *** / 0.0042506	(lv) *** / 0.0002394	(lv) ** / 0.032773	(lv) *** / 0.004916
penicillin G	-	-	-	(tt) ns / 0.49726	(tt) ns / 0.17995	(tt) ns / 0.93288
nisin	-	-	-	-	(lv) *** / 0.0064668	(tt) ns / 0.52689
fosfomycin	-	-	-	-	-	(tt) ns / 0.183
bacitracin	-	-	-	-	-	-

Table S7: comparison between the unstressed diffusion behaviour of PbpH in different genetic background

Condition of strain mVenus-PbpH	mVenus-PbpH	ΔpbpA mVenus-PbpH	ΔmreB mVenus-PbpH
# movies	33	30	30
# cells	205	221	236
av. cell length [µm]	2.9700	3	2.9800
# tracks	2542	1509	4027
#tracks/cell	13.8297	7.0177	17.8410
dwell time radius [nm]	120	120	120
static tracks [%]	3	4.2000	4.4000
mobile tracks [%]	97	95.8000	95.6000
free [%]	93.7000	91.8000	89
mixed behaviour [%]	3.2000	4	6.6000
Diffusion constants from GMM			
Static D ± sd [µm² s^{-1}]	0.058 ± 3.9e-07	0.058 ± 3.9e-07	0.058 ± 3.9e-07
Mobile D ± sd [µm² s^{-1}]	0.6 ± 4.4e-06	0.6 ± 4.4e-06	0.6 ± 4.4e-06
Static fraction ± sd [%]	42 ± 0.00026	46 ± 0.00022	54 ± 0.00026
Mobile fraction ± sd [%]	58 ± 0.00026	54 ± 0.00022	46 ± 0.00026

Dwell times			
ƈ (1-comp.) ± sd [ms]	0.24 ± 0.0041 s	0.25 ± 0.0033 s	0.28 ± 0.004 s
stars / p-value	mVenusPbpH	ΔpbpA mVenus-PbpH	ΔmreB mVenus-PbpH
mVenus-PbpH	-	(tt) ns / 0.26975	(lv) *** / 0.0026769
ΔpbpA mVenus-PbpH	-	-	(lv)* / 0.075989
ΔmreB mVenus-PbpH	-	-	-

Table S8: mV-PbpH in a deletion pbpA background stressed with osmotic reagents

Condition of strain Δ*pbpA* mVenus-PbpH	unstressed	NaCl	sorbitol
# movies	30	30	30
# cells	221	237	241
av. cell length [µm]	3	3.1600	3.0400
# tracks	1509	1551	1284
#tracks/cell	7.0177	7.0909	6.3835
dwell time radius [nm]	120	120	120
static tracks [%]	4.2000	3.5000	3.4000
mobile tracks [%]	95.8000	96.5000	96.6000
free [%]	91.8000	91.9000	93.5000
mixed behaviour [%]	4	4.6000	3
Diffusion constants from GMM			
Static D ± sd [µm² s^{-1}]	0.056 ± 5.5e-07	0.056 ± 5.5e-07	0.056 ± 5.5e-07
Mobile D ± sd [µm² s^{-1}]	0.59 ± 6.3e-06	0.59 ± 6.3e-06	0.59 ± 6.3e-06
Static fraction ± sd [%]	45 ± 0.00042	42 ± 0.00037	40 ± 0.0005
Mobile fraction ± sd [%]	55 ± 0.00042	58 ± 0.00037	60 ± 0.0005

Dwell times			
ƈ (1-comp.) ± sd [ms]	0.25 ± 0.0033 s	0.25 ± 0.0019 s	0.26 ± 0.0039 s
stars / p-value	unstressed	NaCl	sorbitol
unstressed	-	(tt) ns / 0.70577	(tt) ns / 0.76294
NaCl	-	-	(tt) ns / 0.54922
sorbitol	-	-	-

Table S9: mV-PbpH in a Δ*pbpA* background and antibiotic treatment

Condition of strain Δ*pbpA* mVenus-PbpH	unstressed	vancomycin	penicillin G	nisin	fosfomycin	bacitracin
# movies	30	30	30	30	30	30
# cells	221	216	263	228	194	195
av. cell length [µm]	3	3.0800	3.0700	3.0300	3.1800	3.2500
# tracks	1509	2421	1871	6236	873	1945
#tracks/cell	7.0177	13.5358	8.6740	31.4226	5.3466	10.8810
dwell time radius [nm]	120	120	120	120	120	120
static tracks [%]	4.2000	2	3.8000	2.2000	3	3
mobile tracks [%]	95.8000	98	96.2000	97.8000	97	97
free [%]	91.8000	96.1000	93.2000	94.7000	93.8000	93.9000
mixed behaviour [%]	4	1.9000	3	3.1000	3.2000	3.1000
Diffusion constants from GMM						
Static D ± sd [µm² s^{-1}]	0.059 ± 2.2e-07	0.059 ± 2.2e-07	0.059 ± 2.2e-07	0.059 ± 2.2e-07	0.059 ± 2.2e-07	0.059 ± 2.2e-07
Mobile D ± sd [µm² s^{-1}]	0.64 ± 1.7e-06	0.64 ± 1.7e-06	0.64 ± 1.7e-06	0.64 ± 1.7e-06	0.64 ± 1.7e-06	0.64 ± 1.7e-06
Static fraction ± sd [%]	48 ± 0.00015	17 ± 0.00012	40 ± 0.00011	31 ± 9.3e-05	41 ± 0.00025	38 ± 0.00011
Mobile fraction ± sd [%]	52 ± 0.00015	83 ± 0.00012	60 ± 0.00011	69 ± 9.3e-05	59 ± 0.00025	62 ± 0.00011

Dwell times						
ƈ (1-comp.) ± sd [ms]	0.25 ± 0.0033 s	0.26 ± 0.0038 s	0.29 ± 0.0078 s	0.25 ± 0.0051 s	0.25 ± 0.0048 s	0.31 ± 0.0076 s
stars / p-value	unstressed	vancomycin	penicillin G	nisin	fosfomycin	bacitracin
unstressed	-	(tt) ns / 0.32615	(lv)* / 0.073224	(tt) ns / 0.90018	(tt) ns / 0.92793	(lv) *** / 0.0041206
vancomycin	-	-	(tt) ns / 0.94619	(lv) ** / 0.035111	(tt) ns / 0.46845	(tt) ns / 0.45385
penicillin G	-	-	-	(lv) ** / 0.01173	(tt) ns / 0.22565	(tt) ns / 0.32678
nisin	-	-	-	-	(tt) ns / 0.98176	(lv) *** / 7.0819e-05
fosfomycin	-	-	-	-	-	(lv) ** / 0.035695
bacitracin	-	-	-	-	-	-

Table S10: mV-PbpH in a depletion MreB background and osmotic stress conditions

Condition of strain ΔMreB mVenus-PbpH	unstressed	NaCl	sorbitol
# movies	30	30	31
# cells	236	227	257
av. cell length [µm]	2.9800	3.1400	2.9600
# tracks	4027	4728	7258
#tracks/cell	17.8410	22.9011	30.6970
dwell time radius [nm]	120	120	120
static tracks [%]	4.4000	2.9000	2.7000
mobile tracks [%]	95.6000	97.1000	97.3000
free [%]	89	93.1000	94.1000
mixed behaviour [%]	6.6000	4	3.1000
Diffusion constants from GMM			
Static D ± sd [µm² s^{-1}]	0.061 ± 1.4e-07	0.061 ± 1.4e-07	0.061 ± 1.4e-07
Mobile D ± sd [µm² s^{-1}]	0.7 ± 9.9e-07	0.7 ± 9.9e-07	0.7 ± 9.9e-07
Static fraction ± sd [%]	57 ± 7.6e-05	43 ± 7.5e-05	37 ± 6.5e-05
Mobile fraction ± sd [%]	43 ± 7.6e-05	57 ± 7.5e-05	63 ± 6.5e-05

Dwell times			
ƈ (1-comp.) ± sd [ms]	0.28 ± 0.004 s	0.27 ± 0.0039 s	0.28 ± 0.0068 s
stars / p-value	unstressed	NaCl	sorbitol
unstressed	-	(tt) ns / 0.9259	(lv) ** / 0.037981
NaCl	-	-	(tt) ns / 0.50792
sorbitol	-	-	-

Table S11: mV-PbpH in a depletion MreB background and antibiotic treatment

Condition of strain ΔMreB mVenus-PbpH	unstressed	vancomycin	penicillin	nisin	fosfomycin	bacitracin
# movies	30	30	30	30	30	29
# cells	236	246	229	271	253	364
av. cell length [µm]	2.9800	3.0100	3.0300	3.0800	3.1300	3.1200
# tracks	4027	7179	4677	9984	6962	10561
#tracks/cell	17.8410	34.3516	20.8604	41.0199	32.4900	36.0598
dwell time radius [nm]	120	120	120	120	120	120
static tracks [%]	4.4000	2.6000	3.7000	3	2.1000	4
mobile tracks [%]	95.6000	97.4000	96.3000	97	97.9000	96
free [%]	89	94.6000	92.8000	93.2000	94.4000	92.7000
mixed behaviour [%]	6.6000	2.8000	3.4000	3.8000	3.5000	3.4000
Diffusion constants from GMM						
Static D ± sd [µm² s^{-1}]	0.059 ± 9e-08	0.059 ± 9e-08	0.059 ± 9e-08	0.059 ± 9e-08	0.059 ± 9e-08	0.059 ± 9e-08
Mobile D ± sd [µm² s^{-1}]	0.73 ± 5.2e-07	0.73 ± 5.2e-07	0.73 ± 5.2e-07	0.73 ± 5.2e-07	0.73 ± 5.2e-07	0.73 ± 5.2e-07
Static fraction ± sd [%]	57 ± 4.6e-05	32 ± 4.2e-05	43 ± 3.5e-05	40 ± 3.8e-05	32 ± 4.4e-05	39 ± 3.4e-05
Mobile fraction ± sd [%]	43 ± 4.6e-05	68 ± 4.2e-05	57 ± 3.5e-05	60 ± 3.8e-05	68 ± 4.4e-05	61 ± 3.4e-05

Dwell times						
ƈ (1-comp.) ± sd [ms]	0.28 ± 0.004 s	0.27 ± 0.0033 s	0.28 ± 0.0034 s	0.29 ± 0.0053 s	0.28 ± 0.0039 s	0.29 ± 0.0044 s
stars / p-value	unstressed	vancomycin	penicillin G	nisin	fosfomycin	bacitracin
unstressed	-	(tt) ns / 0.41643	(tt) ns / 0.96144	(lv) ** / 0.012948	(tt) ns / 0.98809	(tt) ns / 0.63408
vancomycin	-	-	(tt) ns / 0.47377	(lv) *** / 0.0050672	(tt) ns / 0.44867	(tt) ns / 0.18502
penicillin G	-	-	-	(lv) ** / 0.017278	(tt) ns / 0.97447	(tt) ns / 0.62643
nisin	-	-	-	-	(lv) ** / 0.029835	(lv) ** / 0.022914
fosfomycin	-	-	-	-	-	(tt) ns / 0.64094
bacitracin	-	-	-	-	-	-

Table S12: mV-Pbp2a treated with additional three antibiotics

Condition of strain mVenus-Pbp2a	unstressed	nisin	fosfomycin	bacitracin
# movies	33	22	22	22
# cells	232	149	163	185
av. cell length [µm]	2.8200	2.9000	3.1800	3.1700
# tracks	2030	7468	2162	2968
#tracks/cell	10.1400	50.4876	12.5955	17.0127
dwell time radius [nm]	120	120	120	120
static tracks [%]	1.9000	3.9000	2.8000	3.1000
mobile tracks [%]	98.1000	96.1000	97.2000	96.9000
free [%]	94.9000	91.6000	94.5000	93.6000
mixed behaviour [%]	3.2000	4.5000	2.7000	3.2000
Diffusion constants from GMM				
Static D ± sd [µm² s⁻¹]	0.056 ± 2.3e-07	0.056 ± 2.3e-07	0.056 ± 2.3e-07	0.056 ± 2.3e-07
Mobile D ± sd [µm² s⁻¹]	0.57 ± 1.3e-06	0.57 ± 1.3e-06	0.57 ± 1.3e-06	0.57 ± 1.3e-06
Static fraction ± sd [%]	39 ± 0.00013	39 ± 9.5e-05	39 ± 0.00013	34 ± 9.4e-05
Mobile fraction ± sd [%]	61 ± 0.00013	61 ± 9.5e-05	61 ± 0.00013	66 ± 9.4e-05

Dwell times				
ƈ (1-comp.) ± sd [ms]	0.26 ± 0.0066 s	0.3 ± 0.0036 s	0.26 ± 0.0039 s	0.28 ± 0.0023 s
stars / p-value	unstressed	nisin	fosfomycin	bacitracin
unstressed	-	(lv)* / 0.052058	(tt) ns / 0.59615	(tt) ns / 0.55563
nisin	-	-	(lv) *** / 0.0038984	(lv) ** / 0.02019
fosfomycin	-	-	-	(tt) ns / 0.26045
bacitracin	-	-	-	-

Table S13: comparison of mV-Pbp2a in different genetic backgrounds

Condition of strain mVenus-Pbp2a	mVenusPbp2a	Δ*pbpH* mVenus-Pbp2a	Δ*mreB* mVenus-Pbp2a
# movies	33	32	30
# cells	232	214	292
av. cell length [µm]	2.8200	2.9500	2.9500
# tracks	2030	3194	4836
#tracks/cell	10.1400	16.0985	19.7031
dwell time radius [nm]	120	120	120
static tracks [%]	1.9000	3.5000	5
mobile tracks [%]	98.1000	96.5000	95
free [%]	94.9000	93	89.6000
mixed behaviour [%]	3.2000	3.5000	5.3000
Diffusion constants from GMM			
Static D ± sd [µm² s^{-1}]	0.052 ± 1.5e-07	0.052 ± 1.5e-07	0.052 ± 1.5e-07
Mobile D ± sd [µm² s^{-1}]	0.59 ± 2.3e-06	0.59 ± 2.3e-06	0.59 ± 2.3e-06
Static fraction ± sd [%]	39 ± 0.00023	42 ± 0.0001	54 ± 0.00012
Mobile fraction ± sd [%]	61 ± 0.00023	58 ± 0.0001	46 ± 0.00012

Dwell times			
ƈ (1-comp.) ± sd [ms]	0.26 ± 0.0066 s	0.26 ± 0.0054 s	0.27 ± 0.0043 s
stars / p-value	mVenusPbp2a	Δ*pbpH* mVenus-Pbp2a	Δ*mreB* mVenus-Pbp2a
unstressed	-	(tt) ns / 0.95192	(tt) ns / 0.35801
NaCl	-	-	(lv)* / 0.059993
sorbitol	-	-	-

Table S14: mV-Pbp2a delta *pbpH* genetic backgrounds stressed with osmotic reagents

Condition of strain Δ*pbpH* mVenus-Pbp2a	unstressed	NaCl	sorbitol
# movies	32	30	30
# cells	214	168	186
av. cell length [µm]	2.9500	3.0200	3.0200
# tracks	3194	4680	2175
#tracks/cell	16.0985	26.8085	13.2848
dwell time radius [nm]	120	120	120
static tracks [%]	3.5000	1.9000	4.6000
mobile tracks [%]	96.5000	98.1000	95.4000
free [%]	93	94.8000	92.5000
mixed behaviour [%]	3.5000	3.2000	2.9000
Diffusion constants from GMM			
Static D ± sd [µm² s^{-1}]	0.06 ± 4.2e-07	0.06 ± 4.2e-07	0.06 ± 4.2e-07
Mobile D ± sd [µm² s^{-1}]	0.73 ± 3.1e-06	0.73 ± 3.1e-06	0.73 ± 3.1e-06
Static fraction ± sd [%]	48 ± 0.00019	34 ± 0.00019	42 ± 0.00022
Mobile fraction ± sd [%]	52 ± 0.00019	66 ± 0.00019	58 ± 0.00022

Dwell times			
ƈ (1-comp.) ± sd [ms]	0.26 ± 0.0054 s	0.27 ± 0.0036 s	0.29 ± 0.0053 s
stars / p-value	unstressed	NaCl	sorbitol
unstressed	-	(tt) ns / 0.34291	(lv) ** / 0.014294
NaCl	-	-	(tt) ns / 0.48089
sorbitol	-	-	-

Table S15: mV-Pbp2a delta *pbpH* genetic backgrounds antibiotic stress

Condition of strain Δ*pbpH* mVenus-Pbp2a	unstressed	vancomycin	penicillin	nisin	fosfomycin	bacitracin
# movies	32	29	30	28	31	30
# cells	214	189	212	179	254	200
av. cell length [µm]	2.9500	3.0500	2.9600	2.8600	3.0200	3.0200
# tracks	3194	2159	2622	5947	2084	2836
#tracks/cell	16.0985	12.0423	13.6762	35.7597	9.8568	17.0750
dwell time radius [nm]	120	120	120	120	120	120
static tracks [%]	3.5000	3.2000	2.8000	3.5000	5.1000	3.8000
mobile tracks [%]	96.5000	96.8000	97.2000	96.5000	94.9000	96.2000
free [%]	93	93.6000	94.8000	92	90.1000	94.2000
mixed behaviour [%]	3.5000	3.2000	2.4000	4.4000	4.8000	2
Diffusion constants from GMM						
Static D ± sd [µm² s^{-1}]	0.055 ± 1.6e-07	0.055 ± 1.6e-07	0.055 ± 1.6e-07	0.055 ± 1.6e-07	0.055 ± 1.6e-07	0.055 ± 1.6e-07
Mobile D ± sd [µm² s^{-1}]	0.7 ± 1.6e-06	0.7 ± 1.6e-06	0.7 ± 1.6e-06	0.7 ± 1.6e-06	0.7 ± 1.6e-06	0.7 ± 1.6e-06
Static fraction ± sd [%]	46 ± 9.4e-05	38 ± 6.3e-05	32 ± 8.1e-05	42 ± 8e-05	54 ± 0.00016	35 ± 9.4e-05
Mobile fraction ± sd [%]	54 ± 9.4e-05	62 ± 6.3e-05	68 ± 8.1e-05	58 ± 8e-05	46 ± 0.00016	65 ± 9.4e-05

Dwell times						
ƈ (1-comp.) ± sd [ms]	0.26 ± 0.0054 s	0.26 ± 0.0054 s	0.26 ± 0.006 s	0.29 ± 0.0049 s	0.27 ± 0.0046 s	0.3 ± 0.0057 s
stars / p-value	unstressed	vancomycin	penicillin G	nisin	fosfomycin	bacitracin
unstressed	-	(lv) ** / 0.013041	(tt) ns / 0.51069	(lv) *** / 0.0018165	(tt) ns / 0.3484	(lv) *** / 0.0019837
vancomycin	-	-	(tt) ns / 0.5595	(tt) ns / 0.69248	(tt) ns / 0.60566	(tt) ns / 0.61733
penicillin G	-	-	-	(tt) ns / 0.22996	(tt) ns / 0.86536	(tt) ns / 0.20771
nisin	-	-	-	-	(tt) ns / 0.22589	(tt) ns / 0.80569
fosfomycin	-	-	-	-	-	(tt) ns / 0.21266
bacitracin						

Table S16: mV-Pbp2a depletion MreB genetic backgrounds and osmotic stress conditions

Condition of strain ΔMreB mVenus-Pbp2a	unstressed	NaCl	sorbitol
# movies	30	30	30
# cells	292	271	287
av. cell length [µm]	2.9500	2.9500	2.9900
# tracks	4836	4166	6863
#tracks/cell	19.7031	17.6536	25.5838
dwell time radius [nm]	120	120	120
static tracks [%]	5	4.8000	4.7000
mobile tracks [%]	95	95.2000	95.3000
free [%]	89.6000	90.1000	90.1000
mixed behaviour [%]	5.3000	5.1000	5.2000
Diffusion constants from GMM			
Static D ± sd [µm² s^{-1}]	0.052 ± 1.6e-07	0.052 ± 1.6e-07	0.052 ± 1.6e-07
Mobile D ± sd [µm² s^{-1}]	0.65 ± 2.9e-06	0.65 ± 2.9e-06	0.65 ± 2.9e-06
Static fraction ± sd [%]	55 ± 0.00012	52 ± 0.00012	51 ± 0.00014
Mobile fraction ± sd [%]	45 ± 0.00012	48 ± 0.00012	49 ± 0.00014

Dwell times			
ƈ (1-comp.) ± sd [ms]	0.27 ± 0.0043 s	0.28 ± 0.0045 s	0.29 ± 0.0057 s
stars / p-value	unstressed	NaCl	sorbitol
unstressed	-	(tt) ns / 0.39472	(lv) *** / 0.0019886
NaCl	-	-	(tt) ns / 0.34437
sorbitol	-	-	-

Table S17: mV-Pbp2a depletion MreB genetic backgrounds and antibiotic stress

Condition of strain ΔMreB mVenus-Pbp2a	unstressed	vancomycin	penicillin	nisin	fosfomycin	bacitracin
# movies	30	30	29	30	30	30
# cells	292	282	207	191	318	293
av. cell length [µm]	2.9500	2.8500	3.0200	3.0200	2.9700	2.9500
# tracks	4836	3326	2444	2868	3172	6844
#tracks/cell	19.7031	12.3853	12.8825	15.6780	10.9991	25.6508
dwell time radius [nm]	120	120	120	120	120	120
static tracks [%]	5	5.7000	4.7000	4.6000	7.1000	3.6000
mobile tracks [%]	95	94.3000	95.3000	95.4000	92.9000	96.4000
free [%]	89.6000	90.6000	90.3000	90.9000	88.2000	92.7000
mixed behaviour [%]	5.3000	3.7000	5	4.5000	4.7000	3.7000
Diffusion constants from GMM						
Static D ± sd [µm² s^{-1}]	0.053 ± 1e-07	0.053 ± 1e-07	0.053 ± 1e-07	0.053 ± 1e-07	0.053 ± 1e-07	0.053 ± 1e-07
Mobile D ± sd [µm² s^{-1}]	0.73 ± 8.9e-07	0.73 ± 8.9e-07	0.73 ± 8.9e-07	0.73 ± 8.9e-07	0.73 ± 8.9e-07	0.73 ± 8.9e-07
Static fraction ± sd [%]	57 ± 5.3e-05	52 ± 6.2e-05	54 ± 6.3e-05	51 ± 8.8e-05	62 ± 6e-05	41 ± 4.7e-05
Mobile fraction ± sd [%]	43 ± 5.3e-05	48 ± 6.2e-05	46 ± 6.3e-05	49 ± 8.8e-05	38 ± 6e-05	59 ± 4.7e-05

Dwell times						
ƈ (1-comp.) ± sd [ms]	0.27 ± 0.0043 s	0.29 ± 0.0032 s	0.28 ± 0.0061 s	0.28 ± 0.0048 s	0.27 ± 0.0029 s	0.3 ± 0.0046 s
stars / p-value	unstressed	vancomycin	penicillin G	nisin	fosfomycin	bacitracin
unstressed	-	(tt) ns / 0.97025	(tt) ns / 0.93556	(tt) ns / 0.63432	(tt) ns / 0.7648	(lv) ** / 0.021572
vancoymcin	-	-	(tt) ns / 0.90327	(lv)* / 0.093568	(tt) ns / 0.79457	(lv) *** / 0.0016889
penicillin G	-	-	-	(tt) ns / 0.72261	(tt) ns / 0.72836	(lv) ** / 0.049524
nisin	-	-	-	-	(lv)* / 0.096307	(tt) ns / 0.31822
fosfomycin	-	-	-	-	-	(lv) *** / 0.0013391
bacitracin	-	-	-	-	-	-

Table S18: mV-Pbp3 with additional antibiotic treatments

Condition of strain mVenus-Pbp3	unstressed	nisin	fosfomycin	bacitracin
# movies	29	35	34	34
# cells	277	289	275	291
av. cell length [µm]	3.1400	2.9400	33200	3.2300
# tracks	943	12503	5696	5509
#tracks/cell	4.2130	52.1592	24.2452	21.9586
dwell time radius [nm]	120	120	120	120
static tracks [%]	4.1000	3.9000	2.1000	2.8000
mobile tracks [%]	95.9000	96.1000	97.9000	97.2000
free [%]	91.5000	90.9000	95.3000	94.3000
mixed behaviour [%]	4.3000	5.2000	2.6000	2.8000
Diffusion constants from GMM				
Static D ± sd [µm² s⁻¹]	0.063 ± 1.9e-07	0.063 ± 1.9e-07	0.063 ± 1.9e-07	0.063 ± 1.9e-07
Mobile D ± sd [µm² s⁻¹]	0.65 ± 1.1e-06	0.65 ± 1.1e-06	0.65 ± 1.1e-06	0.65 ± 1.1e-06
Static fraction ± sd [%]	53 ± 0.00026	47 ± 8.8e-05	30 ± 7.3e-05	36 ± 8.8e-05
Mobile fraction ± sd [%]	47 ± 0.00026	53 ± 8.8e-05	70 ± 7.3e-05	64 ± 8.8e-05

Dwell times				
ζ (1-comp.) ± sd [ms]	0.25 ± 0.0037 s	0.28 ± 0.0041 s	0.27 ± 0.0073 s	0.28 ± 0.0033 s
stars / p-value	unstressed	nisin	fosfomycin	bacitracin
unstressed	-	(lv) *** / 0.005622	(lv) *** / 0.0041713	(lv) ** / 0.028244
nisin	-	-	(tt) ns / 0.19575	(tt) ns / 0.99518
fosfomycin	-	-	-	(tt) ns / 0.27405
bacitracin	-	-	-	-

Table S19: mV-Pbp4 and antibiotic treatments

Condition of strain mVenus-Pbp4	unstressed	nisin	fosfomycin	bacitracin
# movies	24	34	31	33
# cells	256	313	318	372
av. cell length [µm]	3.0600	3.0400	3.1200	3.2300
# tracks	2969	9540	3423	7426
#tracks/cell	17.7866	35.6575	14.7302	30.1867
dwell time radius [nm]	120	120	120	120
static tracks [%]	2	3.8000	4.2000	2.6000
mobile tracks [%]	98	96.2000	95.8000	97.4000
free [%]	94.2000	91.3000	91.4000	94.2000
mixed behaviour [%]	3.8000	4.9000	4.5000	3.2000
Diffusion constants from GMM				
Static D ± sd [µm² s⁻¹]	0.059 ± 1.3e-07	0.059 ± 1.3e-07	0.059 ± 1.3e-07	0.059 ± 1.3e-07
Mobile D ± sd [µm² s⁻¹]	0.59 ± 1.1e-06	0.59 ± 1.1e-06	0.59 ± 1.1e-06	0.59 ± 1.1e-06
Static fraction ± sd [%]	33 ± 0.0001	42 ± 7.5e-05	49 ± 6.9e-05	34 ± 6.8e-05
Mobile fraction ± sd [%]	67 ± 0.0001	58 ± 7.5e-05	51 ± 6.9e-05	66 ± 6.8e-05

Dwell times				
ƈ (1-comp.) ± sd [ms]	0.3 ± 0.0061 s	0.28 ± 0.004 s	0.3 ± 0.005 s	0.3 ± 0.0057 s
stars / p-value	unstressed	nisin	fosfomycin	bacitracin
unstressed	-	(tt) ns / 0.79746	(tt) ns / 0.6769	(tt) ns / 0.44557
nisin	-	-	(tt) ns / 0.43637	(tt) ns / 0.1791
fosfomycin	-	-	-	(tt) ns / 0.73059
bacitracin	-	-	-	-

Table S20: mV-Pbp4a and addition of antibiotic treatments

Condition of strain mVenus-Pbp4a	unstressed	nisin	fosfomycin	bacitracin
# movies	32	34	34	34
# cells	322	275	225	303
av. cell length [µm]	2.6500	3	3.2400	3.2000
# tracks	1844	9614	3588	4334
#tracks/cell	7.1800	34.2444	15.6056	13.4482
dwell time radius [nm]	120	120	120	120
static tracks [%]	3.3000	3.5000	3.8000	3.9000
mobile tracks [%]	96.7000	96.5000	96.2000	96.1000
free [%]	93.4000	91.9000	92.7000	91.7000
mixed behaviour [%]	3.3000	4.6000	3.5000	4.5000
Diffusion constants from GMM				
Static D ± sd [µm² s⁻¹]	0.054 ± 2e-07	0.054 ± 2e-07	0.054 ± 2e-07	0.054 ± 2e-07
Mobile D ± sd [µm² s⁻¹]	0.58 ± 1.8e-06	0.58 ± 1.8e-06	0.58 ± 1.8e-06	0.58 ± 1.8e-06
Static fraction ± sd [%]	46 ± 0.00016	42 ± 0.00012	36 ± 0.0001	48 ± 0.00012
Mobile fraction ± sd [%]	54 ± 0.00016	58 ± 0.00012	64 ± 0.0001	52 ± 0.00012

Dwell times				
ƈ (1-comp.) ± sd [ms]	0.3 ± 0.011 s	0.3 ± 0.0058 s	0.28 ± 0.0039 s	0.29 ± 0.0039 s
stars / p-value	unstressed	nisin	fosfomycin	bacitracin
unstressed	-	(tt) ns / 0.65193	(lv) *** / 3.1915e-06	(lv) *** / 3.2441e-05
nisin	-	-	(lv) *** / 4.1896e-05	(lv) *** / 0.00019755
fosfomycin	-	-	-	(tt) ns / 0.32506
bacitracin	-	-	-	-

Supplementary figures

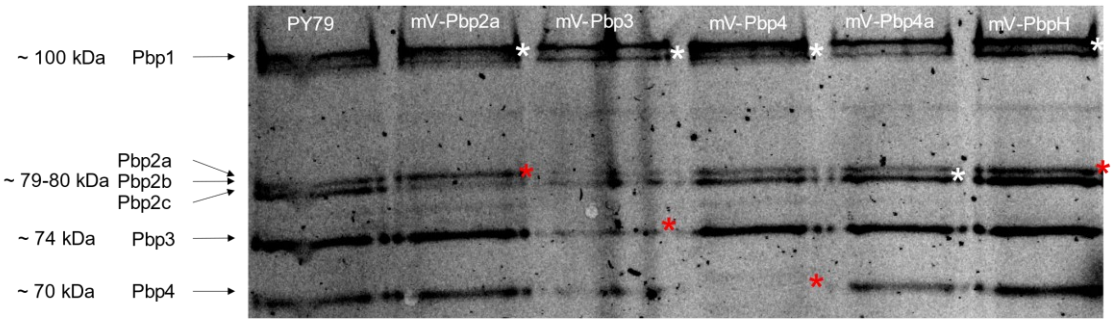

Fig. S1: Bocillin-FL binding assay. Showing six different strains of *Bacillus subtilis* PY79 with different fluorophore tagged PBPs. The red star is indicating the loss or weakening of the corresponding band and the white star is indicating the strengthening of the corresponding PBP band.

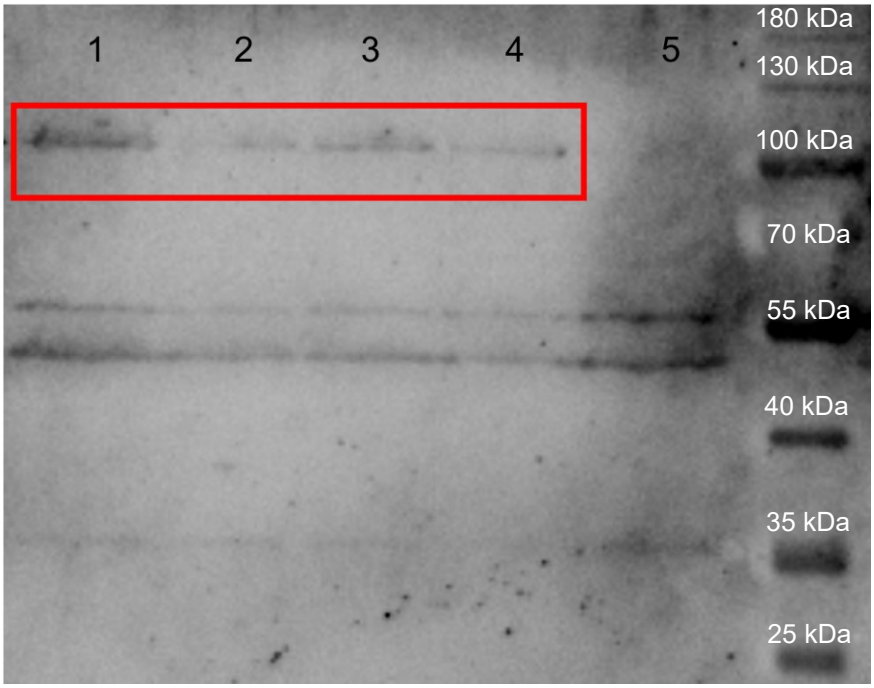

Fig. S2: Western blot with an anti GFP antibody. Showing band for the fusion PBP mVenus-PbpH in a genetically modified background. 1 is showing PbpH in the depletion MreB strain and lanes 2-5 are showing different clones of mVenus-PbpH in a deletion *pbpA* background.

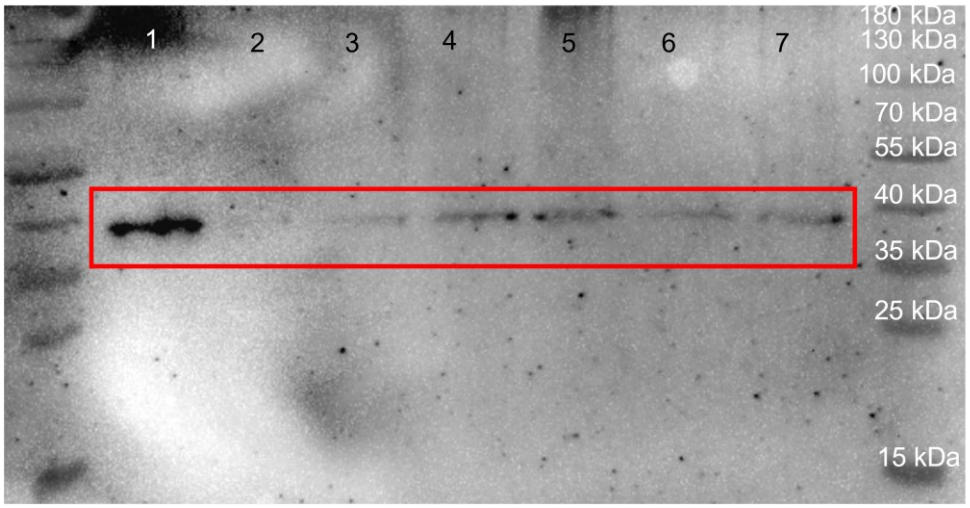

Fig. S3: Western blot showing the depletion of MreB of the mV-PbpH strain. Different Xylose levels (0.01%,0.05%, 0.1%, 0.5%,1% and 5%) were tested to show the level of depletion of MreB in the *B. subtilis* strain. The xylose is inducing the Cas9 from an ectopic site to reduce the amount of mreB RNA in the cell and by that reducing the level of MreB. In lane 1 the level of MreB is indicated with no additional induction by xylose, but fructose as a component in the minimal media leading to a basal induction of Cas9 starting to deplete MreB.

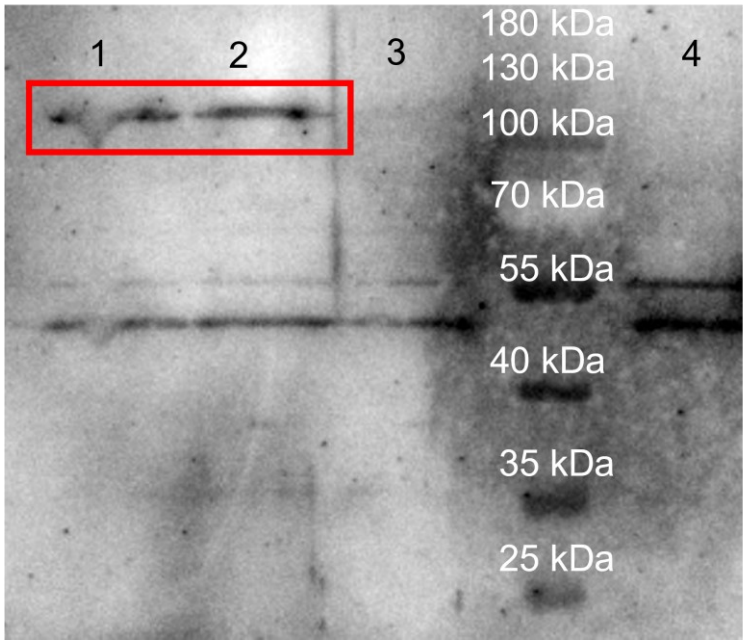

Fig.S4: Western blot with an anti GFP antibody. Showing band for the fusion PBP mVenus-Pbp2a in a genetically modified background. 1 is showing Pbp2a in the depletion MreB strain and lanes 2 and 3 are showing two different clones for mVenus-Pbp2a in a deletion *pbpH* background. Lane 4 is showing a negative control of an unmodified *Bacillus subtilis* PY79

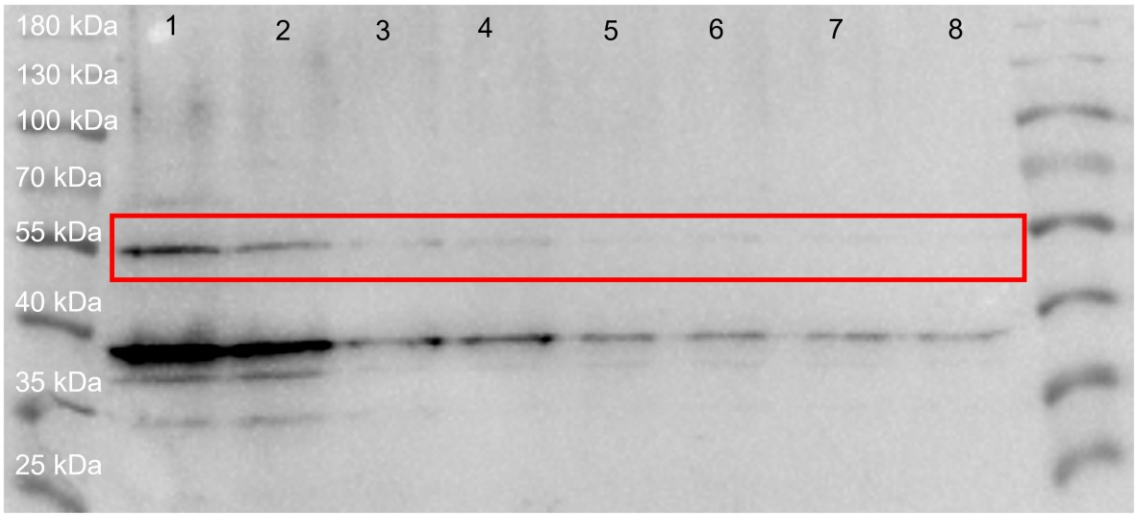

Fig.S5: Western blot showing the depletion of MreB of the mV-Pbp2a strain. Different xylose levels (0.01%,0.05%, 0.1%, 0.5%,1% and 5% in lane 3 - 8) were tested to show the level of depletion of MreB in the *B. subtilis* strain. In lane 1 the normal level of MreB in Bacillus subtilis PY79 is shown and in lane 2 the level of MreB is indicated with no additional induction by xylose, but fructose as a component in the minimal media leading to a basal induction of Cas9 starting to deplete MreB.

CURRICULUM VITAE

	Lisa Stuckenschneider
	Place of birth: Hamburg, Germany
Apr. 2017 – Sep. 2021	Philipps-Universität Marburg
	PhD thesis in Microbiology/ Biochemistry under the supervision of Prof. Dr. Peter L. Graumann Zentrum für Synthetische Mikrobiologie and Department of Chemistry
Apr. 2014 – Oct. 2016	Christian-Albrechts-Universität zu Kiel
	Master of Science in Biology
Sep. 2010- Mar. 2014	Universität Rostock
	Bachelor of Science in biological sciences (Biowissenschaften)
2001 – 2010	Abitur, Helene-Lange Gymnasium, Hamburg

Danksagung